SISSA

Scuola
Internazionale
Superiore di
Studi Avanzati

Neuroscience Area – PhD course in

Functional and Structural Genomics

RT-QuIC analyses of peripheral tissues and body fluids collected from patients with primary and secondary tauopathies

Candidate:

Martina Rossi

Advisor:

Prof. Giuseppe Legname

Co-advisor:

Dott. Fabio Moda

Academic Year 2018-19

Abstract

Neurodegenerative diseases (NDs) are fatal and incurable conditions characterized by the progressive accumulation in specific brain regions of abnormally folded (misfolded) proteins, which are considered disease-specific biomarkers (DSB). These misfolded proteins are able to spread through neuroanatomical connected regions and to accelerate the conformational conversion of native monomers (seeding), thus progressively amplifying the pathological process. Primary tauopathies are NDs associated with the accumulation of misfolded tau and include Corticobasal degeneration (CBD), Progressive supranuclear palsy (PSP), Frontotemporal dementia and parkinsonism linked to chromosome 17 (FTDP-17) and other cases of Frontotemporal dementia (FTD). Alzheimer's disease (AD) can be considered a secondary tauopathy as it is characterized by tau misfolding in addition to amyloid-β (Aβ) protein deposition. Synucleinopathies comprise a group of NDs associated with the accumulation of misfolded α-synuclein (αS), including Parkinson's disease (PD) and other atypical parkinsonisms known as Multiple system atrophy (MSA) and Dementia with Lewy bodies (DLB). Given the overlap between clinical symptoms among NDs and the lack of sensitive and specific diagnostic tests, the definite diagnosis of NDs lay on neuropathological detection of these misfolded proteins in *post-mortem* brain tissues. However, recent findings have raised the possibility that trace-amount of DSB might circulate in peripheral tissues and body fluids of affected individuals, thus constituting easily accessible biomarkers. For this reason, in my PhD project we evaluated the ability of an extremely sensitive technique, named Real-Time Quaking Induced Conversion (RT-QuIC), to detect seeding activity of misfolded tau eventually present in peripheral tissues, such as olfactory mucosa (OM), and body fluids (urine and cerebrospinal fluid) collected from patients with clinical diagnosis of primary (FTDP-17, FTD, PSP, CBD) and secondary (AD) tauopathies. RT-QuIC assay was optimized using a recombinant tau protein fragment named tauK18 (4R-tau) as substrate, whose aggregation was efficiently triggered (seeded) by the addition of minute amount (attograms) of tauK18 pre-formed fibrils (PFFs) previously generated *in vitro*. We demonstrated that tauK18 RT-QuIC assay was able to

detect seeding activity of misfolded tau contained in brain samples of neuropathologically confirmed cases of FTDP-17, PSP, and AD. Thus, we performed RT-QuIC analysis of (i) OM, (ii) CSF and (iii) exosomes extracted from urine samples collected from patients with different primary and secondary tauopathies. As a comparison, we included in the analysis samples belonging to patients with different synucleinopathies (PD, MSA, and DLB), Multiple sclerosis (MS), Non-demented patients (NDP) and healthy controls (HC). Results showed that tauK18 RT-QuIC assay was able to detect tau seeding activity in CBD and PSP OM samples, but also in some PD, MSA, DLB and MS cases. Similarly, RT-QuIC analysis of CSF samples displayed small differences in tau seeding activity between AD and NDP cases. On the other hand, RT-QuIC analysis of urinary exosomes revealed that AD, FTD and CBD samples triggered tauK18 aggregation with higher efficiency if compared to HC, thus potentially discriminating between tauopathies and healthy subjects. We investigated the ability of PFFs generated *in vitro* from other NDs-associated proteins (3R-tau fragment named tauK19, αS, A$\beta_{1-40,}$ and Aβ_{1-42}) to influence tauK18 aggregation (cross-seeding) and we found that some conformational variants of αS PFFs were able to cross-seed tauK18 aggregation, thus representing a potential issue for our assay and possibly explaining results obtained with the analysis of OM samples. Moreover, preliminary structural analysis showed that final reaction products were characterized by different morphologies when seeded by different (i) OM samples or by (ii) PFFs generated *in vitro* from tauK19, αS, A$\beta_{1-40,}$ and A$\beta_{1-42,}$ suggesting that biophysical assessments might help in discriminating between different seeding-competent samples. Although further retrospective analysis is required to confirm results obtained with our tauK18 RT-QuIC assay, this preliminary study might lay the basis for the development of a new diagnostic approach which combines RT-QuIC and biophysical techniques to detect tau seeding activity in peripheral tissues and body fluids of patients with tauopathies and to discriminate between different pathological conditions.

List of publications

Gandini A, Bartolini M, Tedesco, Martinez-Gonzalez L, Roca C, Campillo NE, Zaldivar-Diez J, Perez C, Zuccheri G, Miti A, Feoli A, Castellano S, Petralla S, Monti B, **Rossi M**, Moda F, Legname G, Martinez A, Bolognesi ML. *Tau-Centric Multitarget Approach for Alzheimer's Disease: Development of First-in-Class Dual Glycogen Synthase Kinase 3β and Tau Aggregation Inhibitors.* J Med Chem. 2018 Sep 13;61(17):7640-7656. doi:10.1021/acs.jmedchem.8b00610.

Author contribution: performed RT-QuIC experiments.

De Luca CMG, Elia AE, Portaleone SM, Cazzaniga FA, **Rossi M**, Bistaffa E, De Cecco E, Narkiewicz J, Salzano G, Carletta O, Romito L, Devigili G, Soliveri P, Tiraboschi P, Legname G, Tagliavini F, Eleopra R, Giaccone G, Moda F. *Efficient RT-QuIC seeding activity for α-synuclein in olfactory mucosa samples of patients with Parkinson's disease and multiple system atrophy.* Transl Neurodegener. 2019 Aug 8;8:24. doi: 10.1186/s40035-019-0164-x.

Author contribution: performed most of biochemical and TEM experiments and analyzed the data.

Others pubblications not cited here

Redaelli V, Bistaffa E, Zanusso G, Salzano G, Sacchetto L, **Rossi M**, De Luca CMG, Di Bari M, Portaleone SM, Agrimi U, Legname G, Roiter I, Forloni G, Tagliavini F, Moda F. *Detection of prion seeding activity in the olfactory mucosa of patients with Fatal Familial Insomnia.* Sci Rep. 2017 Apr 7;7:46269. doi: 10.1038/srep46269

Author contribution: performed part of the RT-QuIC analysis and Western blot experiments.

Vanni S, Moda F, Zattoni M, Bistaffa E, De Cecco E, **Rossi M**, Giaccone G, Tagliavini F, Haïk S, Deslys JP, Zanusso G, Ironside JW, Ferrer I, Kovacs GG, Legname G. *Differential overexpression of SERPINA3 in human prion diseases.* Sci Rep. 2017 Nov 15;7(1):15637. doi: 10.1038/s41598-017-15778-8.

Author contribution: contributed to the acquisition of samples and analysis of data.

Bistaffa E, Moda F, Virgilio T, Campagnani I, De Luca CMG, **Rossi M**, Salzano G, Giaccone G, Tagliavini F, Legname G. *Synthetic Prion Selection and Adaptation*. Mol Neurobiol. 2018 Aug 3. doi: 10.1007/s12035-018-1279-2.

Author contribution: performed the practical work.

Bistaffa E, **Rossi M**, De Luca CMG, Cazzaniga F, Carletta O, Campagnani I, Tagliavini F, Legname G, Giaccone G, Moda F. *Prion Efficiently Replicates in α-Synuclein Knockout Mice*. Mol Neurobiol. 2019 Apr 30. doi: 10.1007/s12035-019-1602-6.

Author contribution: performed part of the biochemical analysis.

Book chapter

Bistaffa E, Rossi M, De Luca CMG, Moda F. *Biosafety of prions*. In: Progress in Molecular Biology and Translational Science. Editors: Giuseppe Legname and Silvia Vanni. Assistant editor: Helene Kabes; Elsevier.

Author contribution: contributed to writing the chapter.

Table of contents

INTRODUCTION

1.1. Neurodegenerative diseases as protein misfolding disorders

Neurodegenerative disorders (NDs) comprise a wide range of incurable and debilitating conditions which primarily affect the central nervous system (CNS) and sometimes the peripheral nervous system (PNS) [1]. They include Alzheimer's disease (AD)[2], Dementia with Lewy bodies (DLB) [3], Frontotemporal dementia (FTD) [4, 5], Parkinson's disease (PD) [6, 7] and a series of atypical parkinsonisms comprising Multiple system atrophy (MSA), Corticobasal degeneration (CBD) and Progressive supranuclear palsy (PSP) [8]. Currently, NDs affect almost 50 million people worldwide [9] and this number will increase substantially as the world population rapidly ages. Indeed, aging and particular genetic polymorphisms are the most important risk factors for these disorders [10]. Most of the NDs are sporadic, however, they can be inherited in 10-20% of cases [11].

Although comprising a wide spectrum of disorders and presenting phenotypic heterogeneity [12], they share several clinical, pathological and molecular features [13]. Indeed, they are characterized by synaptic impairment and neuronal loss, which progressively lead to cognitive impairment (dementia) and movement disability (ataxia) [14]. Moreover, these disorders usually arise in late adulthood and show a slowly progressive clinical course [15]. Finally, NDs are characterized by neuropathological changes that affect specific brain areas and involve the deposition of aggregates made up of abnormally folded (misfolded) proteins, whose secondary conformation is enriched in β-sheet structures. These protein aggregates are disease-specific and, therefore, they are considered important biomarkers of the disease [16]. Indeed, neurodegenerative diseases are also known as "protein misfolding disorders" [12, 17-19]. Thus, the molecular classification of NDs is mainly protein-based by evaluating the presence of protein deposits, their distribution in the brain and their correlation to clinical symptoms [20].

NDs have a severe impact on patients and their families' quality of life, with a huge economic burden [21]. Diagnosis of dementia is extremely challenging, especially in the early stages of the disease, and relies on clinical evaluations and laboratory tests. Therefore, its accuracy is not absolute and definite diagnosis can be formulated only at the neuropathological level [22]. Moreover, although several efforts have been made to develop disease-modifying therapies, none of them efficiently blocked disease progression and no cure is currently available for such devastating disorders.

1.1.1. Classification

Classification of NDs is quite challenging and is based on clinical and neuropathological evaluations [23-25]. In recent years, leading experts in the field of neurodegeneration have refined consensus criteria [26] for disease classification and highlighted the importance of the identification of these protein aggregates as specific "molecular signature" for each disease (Fig.1.1).
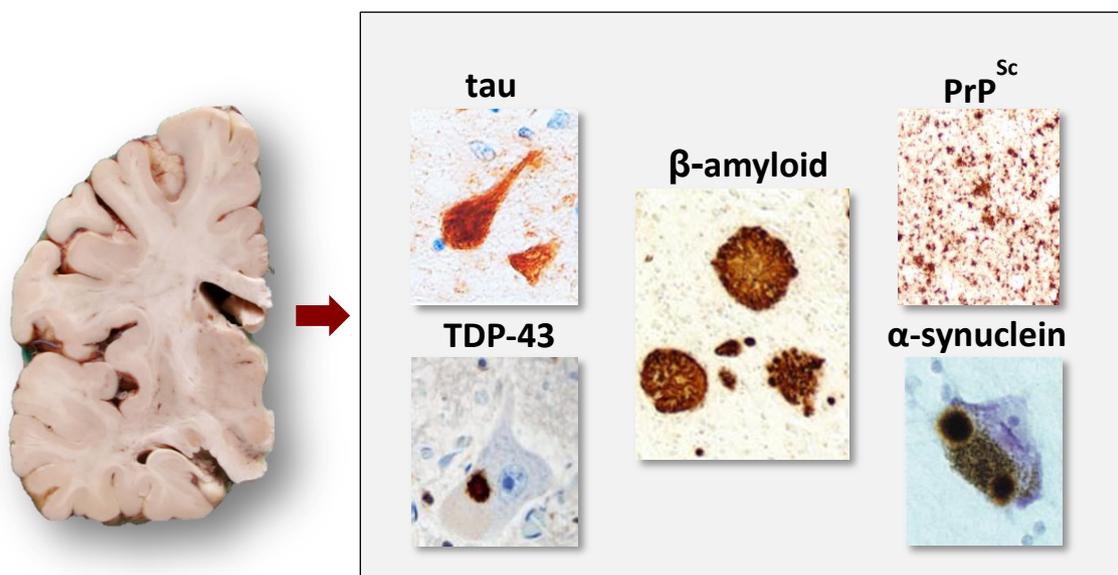
Figure 1.1 Main abnormally folded proteins found to aggregate in the CNS of patients with neurodegenerative diseases.
Immunoreactive protein deposits found in NDs are associated with the aggregation of misfolded proteins, such as tau, β-amyloid (Aβ), PrP^{Sc}, α-synuclein and TAR DNA-binding protein 43 (TDP-43).

Protein deposits found to accumulate in NDs are associated with the aggregation of different misfolded proteins, such as tau, β-amyloid (Aβ), PrP^{Sc}, α-synuclein and TAR DNA-binding protein 43 (TDP-43). Thus, current NDs classification is based on the combination of the molecular characterization of the conformationally altered proteins, anatomical regions and cell types affected, clinical presentation (symptoms, motor signs) and etiology if known (e.g. gene mutations) [12]. Based on the abnormally folded proteins found to aggregate in CNS [20], neurodegenerative diseases can be classified as follows (summarized in Table 1.1):

- **Tauopathies**: heterogeneous group of conditions characterized by intracellular deposition of abnormally folded forms of the **microtubule-associated protein tau (MAPT)**, accumulating in neurofibrillary tangles (NFTs) mainly in its hyperphosphorylated form [27]; tau is important for the assembly and stabilization of neuronal microtubules and can also interact with other cellular components participating in many neuronal physiological processes [28]. Depending on the nature of tau pathology, they can be further divided into primary or secondary:

    ⇒ **Primary tauopathies**: group of diseases where tau is thought to be the major player of the pathological processes and include Pick's disease (PiD), Progressive supranuclear palsy (PSP) [4] Corticobasal degeneration (CBD) [5], Argyrophilic grain disease (AGD), Globular glial tauopathy (GGT) [29], behavioral-variant FTD (bvFTD) [30] and Primary progressive aphasia (PPA) [31]. Mutations in the tau MAPT gene can cause a hereditary primary tauopathy known as Frontotemporal dementia and parkinsonism linked to chromosome 17 (FTDP-17) [32].

    ⇒ **Secondary tauopathies**: diseases in which tau pathology is considered as having another driving force or is combined with other molecular alterations [29]. For instance, Alzheimer's disease (AD) can be considered a secondary tauopathy since it is characterized by the accumulation of **amyloid-β (Aβ) protein** (in the form of amyloid plaques) in addition to misfolded tau [27]. Another example of secondary tauopathy is represented by the Chronic

traumatic encephalopathy (CTE), in which tau pathology is thought to be induced by repeated mild head injuries [33].

- **Synucleinopathies:** conditions characterized by intracellular deposition of abnormally folded **α-synuclein**, a protein shown to be localized at presynaptic terminal of neuronal axons and to bind membranes [34], but whose physiological function has still not been completely understood. Aggregates of α-synuclein are found in different pathologies, including Parkinson's disease (PD), Dementia with Lewy bodies (DLB), Multiple system atrophy (MSA) [35] and Pure autonomic failure (PAF) [36].

- **TDP-43 proteinopathies:** diseases that show intra-nuclear deposition of **TAR DNA-binding protein 43 (TDP-43)**, a member of the heterogeneous nuclear ribonucleoproteins (hnRNPs) family able to bind both mRNA and DNA, thereby regulating mRNA splicing, stability, and translation as well as gene transcription [37]. Hyperphosphorylated, ubiquitinated and cleaved forms of TDP-43 are found in the majority of cases of Frontotemporal dementia (FTLD-TDP) [38] and in Amyotrophic lateral sclerosis (ALS/MND-TDP) [37].

- **Prion diseases:** diseases characterized by the presence of aggregates of the misfolded form of the cellular prion protein (PrP^C), called **scrapie prion protein (PrP^{Sc})** or **prion** [39, 40]. The most common form of human prion diseases is the Creutzfeldt–Jakob disease (CJD), followed by sporadic Familial insomnia (sFI) and Variably protease-sensitive prionopathy (VPSPr). Prion diseases occurs also in animals. For instance, scrapie affects sheep, goats, and mouflons, Bovine Spongiform Encephalopathy (BSE) occurs in cattle, Chronic Wasting Disease (CWD) in cervids and Transmissible Mink Encephalopathy (TME) in mink [41].

- **FUS/FET proteinopathies:** conditions characterized by intra-nuclear and intra-cytoplasmatic deposition of **RNA-binding proteins belonging to the FET (FUS/TLS, EWS or TAF15) family.** Fused in sarcoma (FUS) is the most represented FET member and is a DNA/RNA binding protein that regulates various aspects of RNA metabolism, including splicing, mRNA processing and microRNA (miRNA)

biogenesis [42], showing several similarities with TDP-43 [38]. FUS pathology characterizes familial ALS cases (ALS/MND-FUS) and a rare group of FTLD (FTLD-FUS), known as Basophilic inclusion body disease (BIBD), atypical FTLD-U (aFTLD-U) and Neuronal intermediate filament inclusion disease (NIFID) [43, 44].

- **Trinucleotide repeat expansion disorder:** conditions characterized by pathological expansion of unstable trinucleotide repeats in certain genes or introns exceeding the normal stable threshold and promoting the aggregation of their gene products, such as **huntingtin**, **fragile X mental retardation protein (FMRP)** and **frataxin** [45]; repeats expansion in non-coding sequences are responsible for the development of Fragile X syndrome (FXS), Friedreich ataxia (FRDA), Spinocerebellar ataxia type 8 (SCA8) and type 12 (SCA12), and Myotonic dystrophy (DM); exonic $(CAG)_n$ repeats expansions that code for polyglutamine (poly-Q) tracts give rise to a group of diseases named polyglutamine diseases and comprises Hungtington's disease (HD), Spinal and bulbar muscular atrophy (SBMA), the majority of Spinocerebellar ataxia (SCA) cases and few other rare conditions [45].

- **Neuroserpinopathies:** Serpinopathies result from point mutations in members of the serpin superfamily, a group of serine protease inhibitors. In the brain, they are characterized by the presence of inclusion bodies composed of **neuroserpin** (α1-antitrypsin), which have a central role in many biological pathways, such as inflammation, complement system, coagulation, fibrinolytic cascade and chromatin [46]. The accumulation of neuroserpin was found to cause an autosomal-dominant form of dementia named Familial encephalopathy with neuroserpin inclusion bodies (FENIB) [47].

Table 1.1 Summary of the most relevant neurodegenerative diseases with their classification based on the peculiar aggregated proteins found to accumulate in those conditions.

Classification	Protein	Disease Type
Primary Tauopathies	Tau	Pick's disease (PiD) Corticobasal degeneration (CBD) Progressive supranuclear palsy (PSP) Frontotemporal lobar degeneration (FTLD-tau) NFT-dementia/PART Frontotemporal dementia and parkinsonisms linked to chromosome 17 (FTDP-17)
Secondary Tauopathies	Tau, Aβ Tau	Alzheimer's disease (AD) Chronic traumatic encephalopathy (CTE)
TDP-43 proteinopathies	TDP-43	Frontotemporal lobar degeneration (FTLD-TDP) Amyotrophic lateral sclerosis (ALS/MND-TDP) FTLD/MND-TDP
FUS/FET-proteinopathies	FUS/FET	Frontotemporal lobar degeneration (FTLD-FUS) Amyotrophic lateral sclerosis (ALS/MND-FUS)
Synucleinopathies	αS	Parkinson's disease (PD) Dementia with Lewy bodies (DLB) Multiple system atrophy (MSA)
Prion diseases	PrP	Sporadic Creutzfeldt-Jakob disease (sCJD) Genetic Creutzfeldt-Jakob disease (gCJD) Iatrogenic Creutzfeldt-Jakob disease (iCJD) Variant Creutzfeldt-Jakob disease (vCJD) Kuru Variably protease-sensitive prionopathy (VPSPr) Gerstmann-Sträussler-Scheinker disease (GSS) Fatal familial insomnia (FFI)
Trinucleotide repeat expansion disorders (TRD)	Htt Ataxin, FMRP ARP	Huntington's disease (HD) Spinocerebellar ataxia (SCA) Fragile X syndrome (FXS) Spinal and bulbar muscular atrophy (SBMA)
Neuroserpinopathy	Neuroserpin	Familial encephalopathy with neuroserpin inclusion bodies (FENIB)

1.1.2. Aggregation of misfolded proteins

The correct conformation of a protein is usually fundamental for its biologically functions. Protein structure depends on its amino acid sequence and local, low-energy chemical bonds between atoms in both the polypeptide backbone and in amino acid side chains [48]. It is possible to recognize four levels of protein structure by the degree of complexity in the polypeptide chain conformation:

⇒ **primary structure** is the conformation driven by the amino acid sequence of the protein;

⇒ **secondary structure** depends on local interactions between stretches of a polypeptide chain which can acquire α-helix and β-sheet structures (Fig. 1.2);

⇒ **tertiary structure** is the overall three-dimension folding driven largely by interactions between side chains;

⇒ **quaternary** structure is the orientation and arrangement of subunits in a multi-subunit protein.
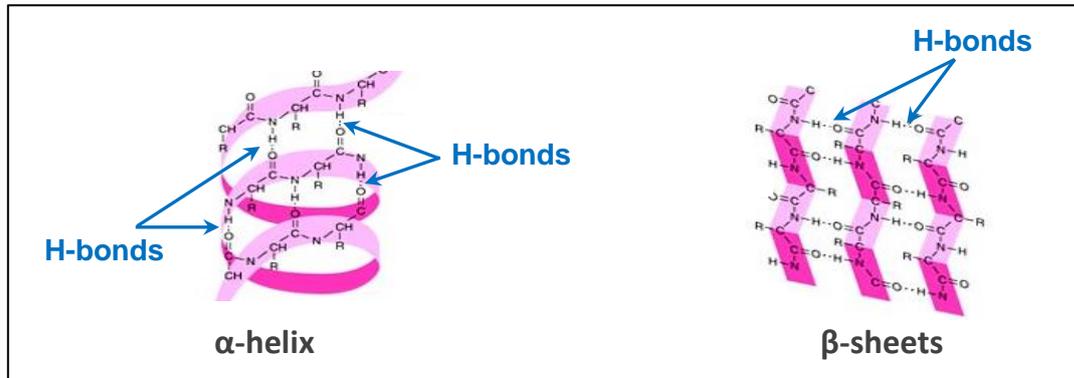
Figure 1.2 Secondary structure of proteins showing α-helix and β-sheets conformations. Protein secondary structure, showing that α-helix is formed when polypeptide chains twist into a spiral, whereas in β-sheets polypeptide chains run alongside each other. Both structures are mainly driven by the formation of hydrogen bonds between amino acids.

Some of the key proteins that cause neurodegeneration, such as tau, α-synuclein, and Aβ, have been shown to contain intrinsically disordered regions (IDRs), as they lack stable tertiary and/or secondary structure under physiological conditions, presumably to interact with a broad range of binding partners [49]. The flexibility of IDRs is thought to be

important for the conformational rearrangements which drive the formation of amyloid structures [50]. Normally folded proteins are generally characterized by higher content of α-helix structures (Fig. 2) [51]. Misfolded proteins show a prevalence of β-sheet structures (Fig. 1.2) and are usually either degraded by the ubiquitin-proteasome system (UPS) or refolded correctly by chaperone proteins [52]. However, sometimes these systems fail and, as a consequence, misfolded proteins start to aggregate and form oligomers. Oligomers are a heterogeneous group of species ranging from dimers to larger protofibrillar structures, likely composed of hundreds of monomers (Fig. 1.3) [53]. Oligomers and protofibrils are then packaged into longer amyloid aggregates, ranging from 100–200 Ångström (Å) in diameter [54]. Once formed, these amyloids are deposited as intra- or extra-cellular aggregates into the CNS causing cell death and neurodegeneration.

Protein misfolding can be due to mutations in protein-encoding genes (causing familial forms of NDs) [55] or can be caused by several factors (e.g. proteotoxic stress, cellular aging) responsible of sporadic forms of NDs. At present, the exact molecular mechanism which leads to protein misfolding and aggregation remains still elusive [49].
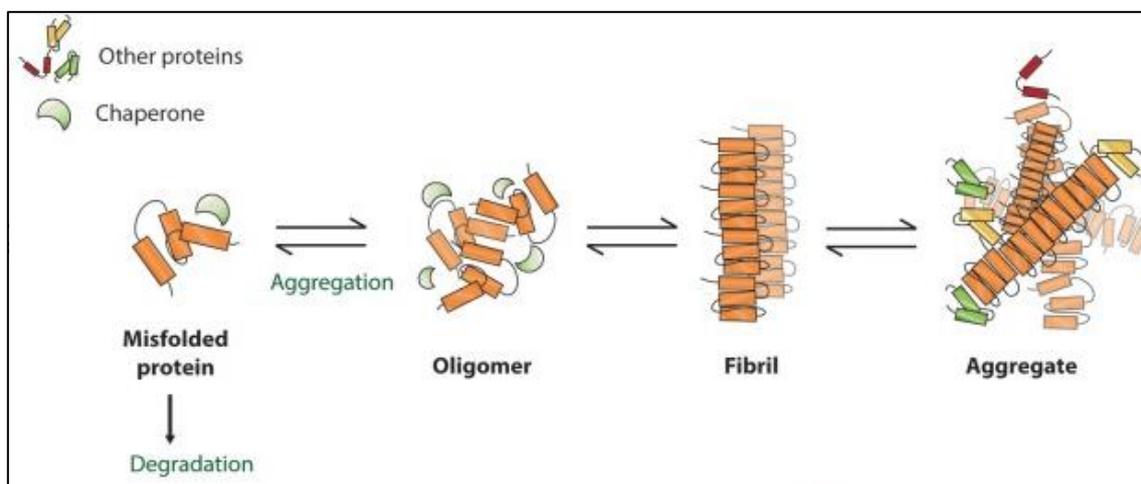
Figure 1.3 Proposed mechanism for amyloid formation.
A misfolded protein that escapes protein control systems might undergo the aggregation pathway, involving the formation of oligomers and large aggregates through the elongation of the fibrils, finally sequestering other proteins or cellular factors. (Adapted from [53])

It was originally thought that amyloids in the form of large fibrils and aggregates were neurotoxic, however now it is widely accepted that oligomers are the most neurotoxic species and fibrils formation may actually be a way for the cell to minimize their deleterious effects [54]. Indeed, toxicity of oligomers may arise from the abnormal exposition of hydrophobic groups on their surface [56], resulting in inappropriate interactions with many functional cellular components like membranes and organelles [57]. Intracellular aggregates might damage cell integrity, segregate essential factors for cell viability, bind to organelles deregulating their function and might disrupt cell membranes, resulting in depolarization and alteration of ion homeostasis [58]. Extracellular oligomers might interact with cellular receptors and activate undesirable signal transduction pathways leading to apoptosis or might interfere with the cellular and tissue network [16]. Finally, they could induce cellular oxidative stress by producing free radical species, resulting in protein and lipid oxidation and mitochondrial dysfunctions [59]. Thus, neurons containing protein aggregates show transcriptional alteration, mitochondrial dysfunction, and an impaired protein/RNA quality control system that might critically contribute to the initiation and progression of neurodegeneration [60].

1.1.3. Propagation and transmission of misfolded proteins

Since NDs are characterized by the presence of many protein aggregates, it is of fundamental importance to understand the mechanisms through which they are generated and how they accumulate in different cells. One of the most puzzling aspects of misfolded protein is their ability to interact with their physiological counterparts and force them to adopt similar structural alterations (Fig. 1.4) [16]. This phenomenon was initially observed in prion diseases, where PrP^{Sc} was found to propagate the disease by acting as seed for the conformational conversion of the normal protein PrP^{C} to the pathological isoform. By seeding misfolding of the PrP^{C} into PrP^{Sc}, prions spread in the CNS (and sometimes to the periphery) and can be transmitted (more or less efficiently) between individuals of the same or different species. Similarly, recent findings showed that tau, α-

synuclein, and Aβ can also transmit their abnormal conformation to their normally folded isoforms [16].
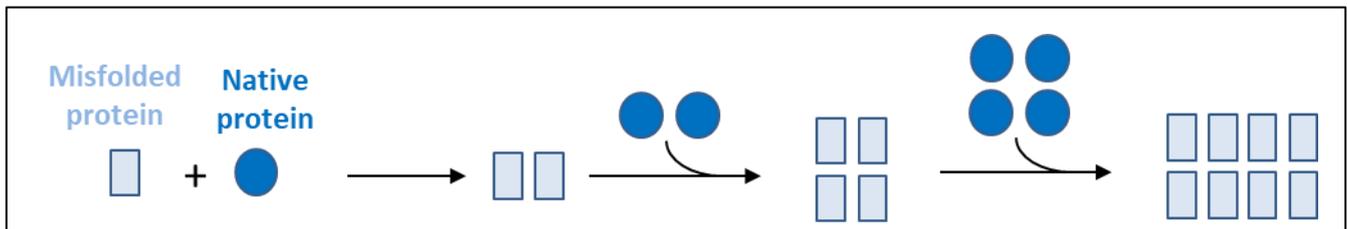
Figure 1.4 Proposed model for protein misfolding propagation.
A misfolded protein is able to interact with its physiological counterpart (native protein) and force it to adopt similar abnormal conformations, leading to the progression of the misfolding process.

This process seems to sustain the pathological process associated with many NDs and can be reproduced *in vitro* [61]. In the seeding-nucleation model of protein misfolding propagation (Fig. 1.5A), a slow and thermodynamically unfavorable nucleation phase (lag phase) induce the formation of a stable nucleus of polymerized protein, called seed, followed by a rapid elongation stage in which seeds rapidly grow by incorporating monomeric proteins into the polymer (elongation phase) [61]. The kinetics of protein aggregation may be graphically represented by plotting amyloid formation against time, showing a sigmoidal curve characterized by a slow lag phase and a rapid elongation phase as depicted in Fig. 1.5A (blue line).

A typical feature of the seeding–nucleation model is the ability of pre-formed fibrils (PFFs) to greatly accelerate the aggregation process by recruiting the soluble normal protein into the growing aggregate [62]. Thus, the aggregation kinetics of the protein is efficiently accelerated by the addition of pre-formed seeds, showing a reduction in lag phase as in Fig. 1.5A (red line). This process seems to occur *in vivo* and drives disease progression along routes of neuronal connectivity on the basis of trans-cellular propagation of protein seeds [63].

It is fundamental that misfolded proteins interact with their physiological counterparts. Therefore, they need to spread from cell to cell by mechanisms that are still not well understood (Fig. 1.5B). Different hypotheses have been postulated so far. For instance, cellular endocytic mechanisms can be involved in the release and uptake of protein aggregates and in their trans-cellular spreading [64]. Aggregates might bind to heparan sulfate proteoglycans (HSPGs) on the cell surface and trigger the formation of large endocytic vesicles (macropinosomes) that bring aggregates into cells [65]. Receptor-mediated endocytosis may also occur through the binding of aggregates to specific proteins at the cell surface [66]. Moreover, a growing body of evidence proposes that exosomes play important roles in the cell-to-cell transmission of pathogenic protein aggregates, thereby contributing to the pathological and clinical progression of NDs [67].
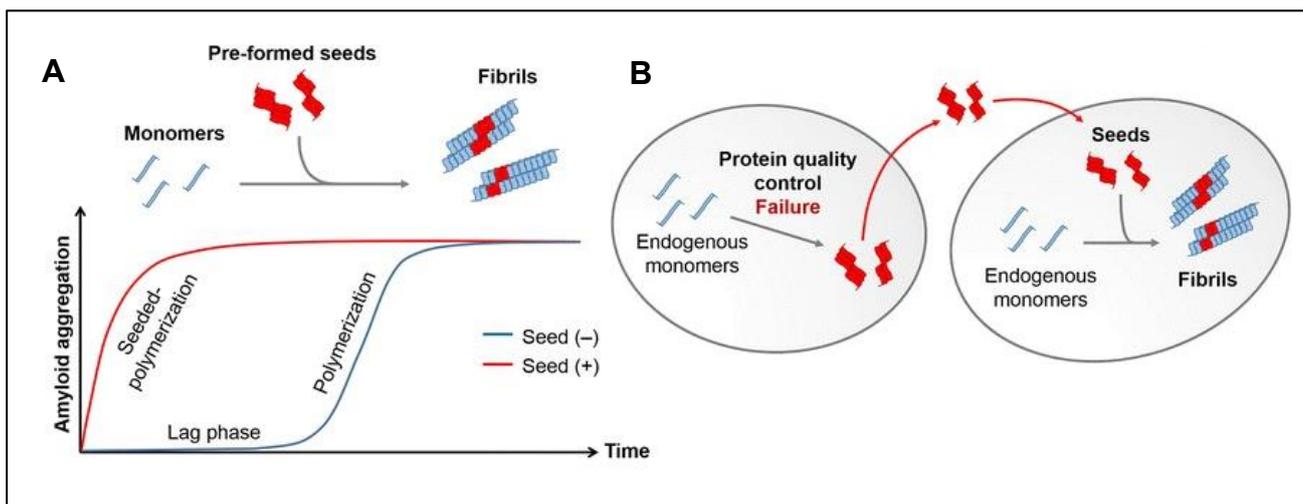
Figure 1.5 Kinetic principle of protein aggregation and inter-cellular aggregates transmission.
A) Simplified scheme illustrating the kinetics of protein fibrillation (blue line) and seeded polymerization (red line). The addition of pre-formed fibrils (PFFs) as 'seeds' drastically reduced the lag phase and accelerate protein aggregation (red line). B) Illustration of the seeded polymerization principle in cell-to-cell aggregates transmission. When protein aggregates are transferred from one cell to another, the transferred aggregates could act as 'seeds' in the recipient cells. (Adapted from [66])

Protein misfolding can occur between cells of the same organism but, in some cases and with low efficiency, can occur between different organisms, thus highlighting the pathological features of such misfolded proteins [62].

This feature has been extensively described for prion diseases, which can be easily transmitted within hosts belonging to the same species while the efficiency of this transmission is almost abolished between hosts belonging to different species. This is due to the so-called species barrier, where differences in the aminoacidic sequence of the host vs donor proteins drastically reduced the ability of the misfolded protein (PrP^{Sc}) to drive the conformational conversion of PrP^{C} [40].

However, in particular conditions (e.g. high sequence homology, intrinsically unfolding and high flexibility of proteins) the species barrier might be over-crossed allowing protein misfolding transmission between different species [68]. Indeed, natural transmission of prion diseases, such as the BSE epidemic in Great Britain in the 1980s in cattle which cause the variant Creautzfeldt-Jakob Disease (vCJD) in humans due to cattle food consumption, have raised important health questions. Thus, the potential intra- and inter-species transmissibility of other misfolded proteins (Aβ, tau, and α-synuclein) is under investigation [69].

The self-propagation ability of misfolded Aβ was proposed decades ago from *in vitro* studies [61] and from inoculation experiments with non-human primates [70]. Recently, it has been shown that the intracerebral injection of Aβ amyloid-rich brain extracts from Alzheimer's disease (AD) patients accelerate the formation of Aβ plaques in genetically modified mouse models of AD pathology, showing that Aβ can be induced to deposit *in vivo* through a prion-like mechanism [71]

In vitro tau preformed fibrils (PFFs) can act as seeds in a templated fibrillization reaction in which misfolded tau recruits and corrupts normal, soluble tau into a fibrillar conformation. This process has been demonstrated *in vitro* and *in vivo* with recombinant tau proteins assembled into PFFs under different conditions and shown to propagate misfolded conformations that are capable of further seeding tau fibrillization in cell-culture models and tau transgenic mice [72, 73].

Similarly, the intracerebral injection of tauopathy brain extracts induced tau deposition in transgenic [74, 75] and wild-type mice [76]. When young transgenic mice expressing tau with the human pathological mutation P301S were inoculated with old mice brain extracts containing tau aggregates, they showed tau assembly into filaments and its spreading to distant brain regions [74]. Propagation of tau pathology from the injection site to connected areas suggested the potential neuronal uptake and transport of tau aggregates. Lee and colleagues showed that intracerebral inoculation of tau fibrils purified from AD brains resulted in the formation of abundant tau inclusions in wild-type mice, both in the site of injection and anatomically connected brain regions [72]. Interestingly, brain extracts from various human tauopathies, such as AD, TD, PiD, AGD, PSP, and CBD, have induced different tau lesions in wild-type mice who resemble those in the relative human diseases [77].

The same mechanism has been proposed for α-synuclein propagation, as the intracerebral injection of brain extracts containing pathological α-synuclein into transgenic mice stimulated the formation of α-synuclein lesions [78, 79]. The progression of α-synuclein pathology along neuronal routes leads to progressive neurodegeneration and signs of motor dysfunction resembling those found in Parkinson's disease (PD) [79]. Surprisingly, αS displayed prion-like characteristics when PD patients received fetal nigral dopaminergic nerve cells grafts into the brain as part of a clinical trial. Investigation at autopsy revealed the presence of αS deposits in the transplanted cells suggesting that transmission occurred from the host to the grafted tissue in the 11–16 years post-surgery. Moreover, intracerebral injections of *in vitro* α-synuclein PFFs or autopsy-derived brain extracts from patients affected by Dementia with Lewy bodies (DLB) induced the formation of Lewy bodies composed of aggregated α-synuclein and neuronal loss in wild-type mice [79]. Interestingly, some α-synuclein PFFs were able to induce tauopathy [80], possibly due to α-synuclein acting as seed for tau aggregation. This phenomenon is known as cross-seeding or heterologous seeding (Fig. 1.6) and involves the ability of pre-formed seeds from one protein (e.g. αS) to greatly accelerate the aggregation process of other proteins (e.g. tau).

Several *in vitro* and *in vivo* studies suggested that misfolded proteins associated with different NDs can promote their mutual aggregation, potentiating pathological mechanisms and accelerating disease progression [81]. *In vitro* interaction between Aβ and αS has been reported [82], as well as the binding between Aβ and tau forming soluble complexes that promote the aggregation of both proteins [83].
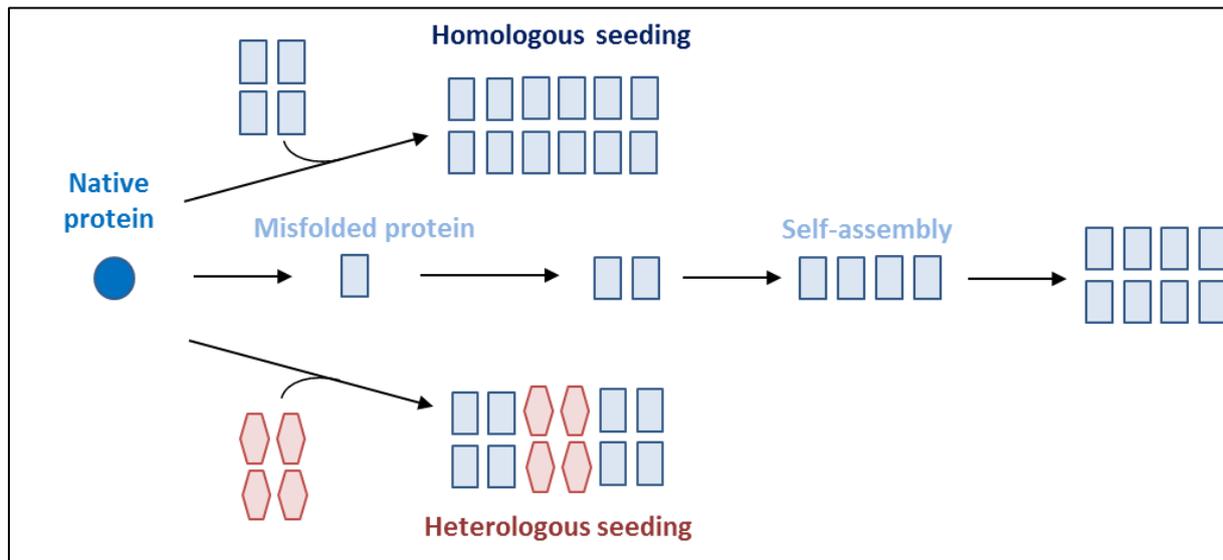
Figure 1.6. The heterologous seeding phenomenon, also known as cross-seeding.
Homologous seeding occurs when preformed seeds (light blue squares) are able to facilitate and speed up the polymerization process of the same monomeric protein (light blue square). In the heterologous seeding, seeds composed of one misfolded protein can promote the polymerization of a different protein.

Transgenic mice developing both Aβ, α-synuclein and tau deposits displayed an accelerated cognitive decline which positively correlates with the deposition of all three amyloidogenic proteins [84]. Moreover, neuropathological studies confirmed the presence of αS aggregates in approximately 50% of the AD patients and its deposition was associated with more severe pathological outcomes [85].

As reported in this chapter, several studies give strong support for conformationally altered proteins as the agent driving the transmission and propagation of neurodegeneration in protein misfolding diseases and support the concept that these misfolded proteins may propagate as prions.

1.1.4. Conformational variants of misfolded proteins

We have previously described that protein aggregates can be efficiently propagated in cell culture and animal models. There is now increasing evidence that distinct conformational variants of the same protein, also known as strains, might account for different neurodegenerative diseases (or even distinct phenotypes of the same pathology) and might propagate their aberrant conformations in a templated-assisted mechanism (Fig. 1.7).

Indeed, it has been shown that tau aggregates propagate distinct strains in cell culture and induce different pathological patterns in mice [86]. The tau inclusions-containing cell lysates were able to induce the same inclusion pattern into new cells, suggesting a process of templated conformational conversion for tau strikingly similar to that characterized for prion strains [87]. Moreover, these clones displayed distinct biochemical features, seeding activity and toxicity *in vitro*. Similarly, after injecting these lysates into the hippocampus of transgenic mice (P301S), some lysates induced inclusions *in vivo* that were morphologically and biochemically similar to what produced in cells, supporting the idea that distinct strains of misfolded tau might be propagated and could produce distinct pathologies. They also demonstrated that brain homogenates from a range of tauopathies, including AD, AgD, CBD, PiD and PSP would give rise to distinct patterns of tau deposition and different pathologies in tau cell culture model [86].

Interestingly, the intracerebral injection of brain homogenates from humans with pathologically confirmed cases of AD, TD, PiD, AgD, PSP, and CBD led to the formation of neuronal and glial tau inclusions in transgenic mice expressing human tau, producing tau lesions similar to those of the human disorders [77]. Indeed, injection of PSP brain homogenate gave rise to silver-positive neuronal and glial tau aggregates similar to tufted astrocytes, the hallmark lesion of PSP. The injection of CBD homogenates produced neuronal inclusions and silver-positive structures reminiscent of astrocytic plaques. After AGD brain homogenates inoculation, argyrophilic grains and silver-negative astrocytic tau inclusions were present [77]. Similar inclusions, but fewer in number, were induced after

the intracerebral injection of brain homogenates from human tauopathies into non-transgenic mice [88, 89].

The presence of different Aβ strains have been also suggested by the finding that different genetic cases of AD are associated to different clinical phenotypes, distinct Aβ deposition pattern and unique biochemical profiles of Aβ species [90]. Interestingly, transgenic AD mouse models inoculated with human brain from patients affected by distinct AD phenotypes generate distinct profiles of pathological Aβ species that reflect the human condition and these strain-specific features were conserved following serial passage in mice [90]. Consistent with these observations, different recombinant Aβ fibrils were produced by *in vitro* fibrillization in the absence or in the presence of detergent that induced differential plaque characteristics and Aβ peptide ratios in mouse brain [91]. Hence, the conformation of the Aβ species appears to be a contributing factor to the clinical and pathological heterogeneity of the disease.

Similarly, recombinant αS monomers can assemble into *in vitro* PFFs with distinct conformations and biological activities [80]. Indeed, through repetitive seeded fibrillization *in vitro,* Guo and colleagues were able to generate two different conformational variants of αS (strain A and B). Strain B was found to be less potent in seeding αS aggregation than strain A, however, efficiently induced the aggregation of tau in both primary neurons and transgenic mice. This finding not only demonstrates the possibility to generate αS strains *in vitro* but also illustrates that some conformational variants of αS are able to influence the aggregation propensity of tau *in vivo* (cross-seeding). Morphological differences in αS deposits have been also observed in distinct human synucleinopathies. Differential proteinase-K cleavage of α-synuclein aggregates was observed in the brains of PD patients, indicative of alternative α-synuclein conformations [80].
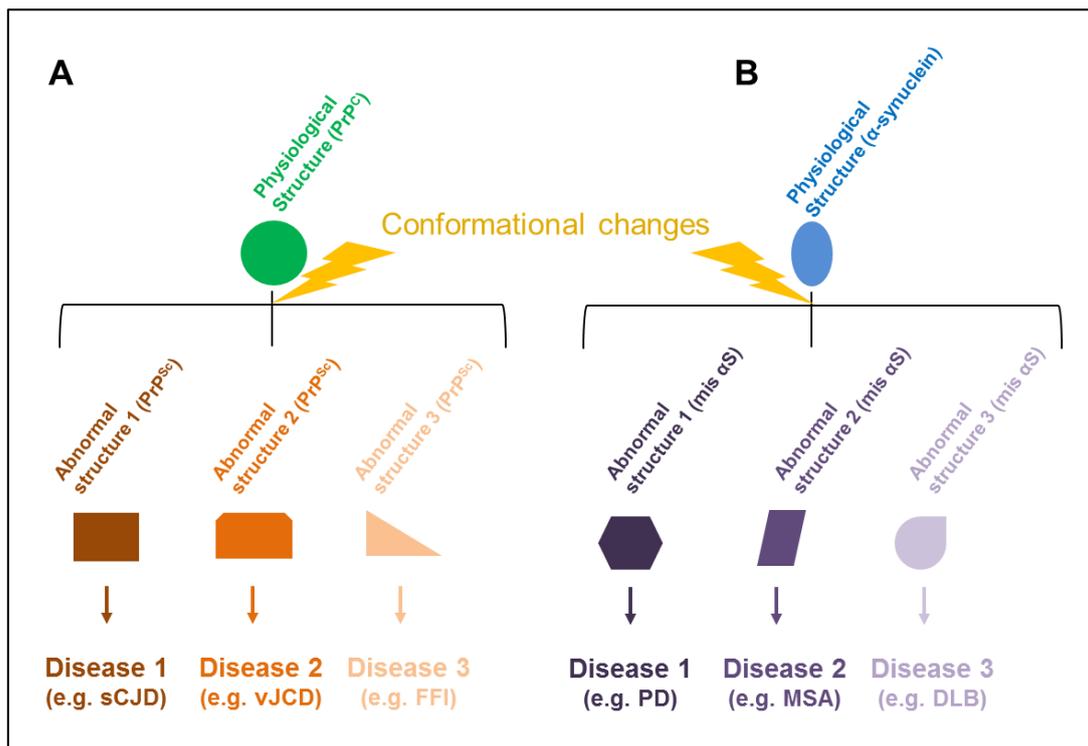
Figure 7. Conformational strains and their implications for the spectrum of NDs.
Conformational variants of the same misfolded proteins (strains) may account for the large heterogeneity of NDs and may provide a molecular explanation for distinct diseases associated with the deposition of the same misfolded protein, such as (A) PrP^{Sc} in prion diseases and (B) misfolded α-synuclein (mis αS) in synucleinopathies.

Insoluble αS fraction extracted from the brain of a patient with Dementia with Lewy bodies (DLB) was able to induce αS aggregation in wild type mice [92], which resemble LBs pathology. In a particular form of Parkinson's disease (PD), named PD with dementia (PDD), Lewy bodies (LBs) in the substantia nigra showed biochemical dissimilarities from LBs in neocortical areas of these patients, therefore different abnormal conformations may be also acquired among the same condition. Interestingly, MSA patients but not PD or DLB patients induced αS aggregation in a mouse model expressing A53T mutant αS [93, 94]. These results suggest that potential conformational differences between pathological αS might drive the diversity of clinical manifestations observed in synucleinopathies.

1.1.5.   Misfolded proteins structural polymorphisms

Due to the low solubility nature of amyloid species, few structures were determined at high resolution. However, recent advances in solid-state Nuclear Magnetic Resonance (NMR) and in cryo Electron Microscopy (cryo-EM) have generated substantial advances in atomic-level structural information of physiologically relevant amyloid proteins including yeast prions [95], α-synuclein [96], Aβ [97] and tau [98] [99], the latter extracted from post mortem human brain tissue (Fig. 1.8).

These structures have elucidated that different protein strains are associated with different diseases, as it has been described for tau, whose cores in paired helical (PHFs) and straight filaments (SFs) in AD were found to be significantly different from those found in Pick's disease [100].
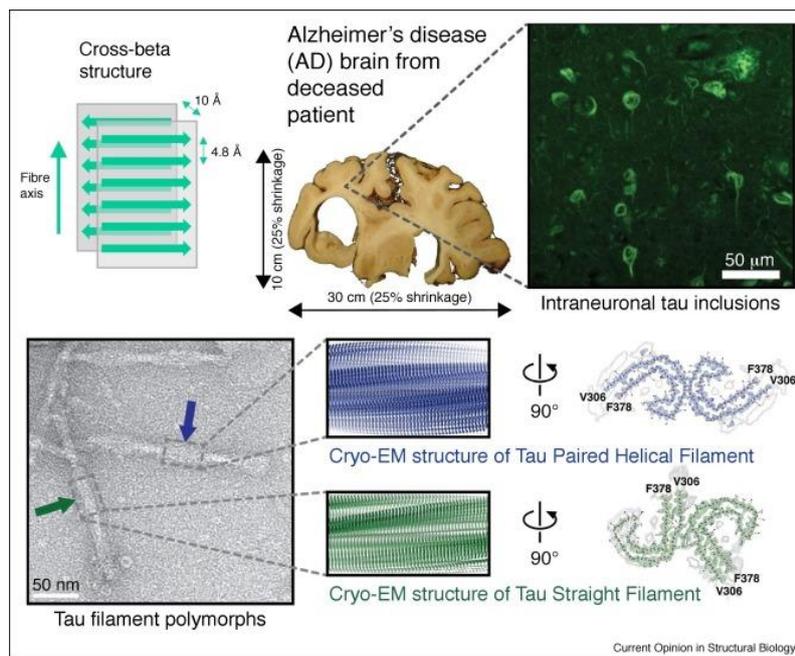
Figure 1.8 Cross-β structure and tau deposits in Alzheimer's disease brain.
From left to right, the upper panels show a schematic of the β-strand arrangement in the cross-β core of an amyloid fibril; the AD brain used for cryo-EM; and a Thioflavin-S stained light microscopy image showing abundant neurofibrillary tangles in temporal cortex. Lower panels, an electron micrograph of negatively stained filaments with a blue arrow indicating a paired helical filament (PHF) and a green arrow indicating a straight filament (SF); cryo-EM reconstructions of PHFs (blue) and SFs (green) with detailed cross-sections; and *de novo* atomic models of filaments showing C-shaped subunits stacked to form each protofilament, with protofilaments paired into twisted polymorphic fibrils (adapted from [99])

Based on these observations, two all-β structural motifs have been proposed to be associated with amyloid and prion structure: cross-β packing and β-helices or solenoid [101]. The generic cross-β structure is a polypeptide scaffold characterized by arrays of continuous β-sheets, separated by an inter-sheet distance of 8–12 Å running parallel to the long axis of the fibrils (Fig. 1.9A). The importance of sequence-independent hydrogen bonding in defining the cross-β fold is highlighted by the observation that polar, non-polar and even homopolymeric sequences of amino acids can form cross-β amyloid fibrils [102], making this structure widely accessible to peptides and proteins of varying lengths with unrelated amino acid sequence similarity. On the other hand, β-solenoids (Fig. 1.9B) are intricate structures composed of three β-sheets arranged in a triangular fashion, mediated by specific interactions that are not accessible to most amino acid sequences [103]. Moreover, the promiscuity of the cross-β fold allows this structural scaffold to template dissimilar protein molecules and cross-seed the aggregation of proteins with at least 70% of sequence homology [104].

Atomical evaluation of tau protofilament extracted from human AD brain displayed the presence of both sidechain-specific β-helical and generic cross-β structural elements (Fig. 1.9C). The core of the paired helical filaments and straight filaments are composed of eight β-sheets along the length of the protofilament, adopting a C-shaped architecture. Each C consists of a β-helix region with three β-sheets are arranged in a triangular fashion, and two regions with a cross-β architecture characterized by pairs of β-sheets that pack anti-parallel to each other. Significant differences in the lateral contacts formed between two C-shaped fold structures might give rise to the ultrastructural polymorphism [105] displayed by tau paired helical filaments and straight filaments in AD. Moreover, the different fold of tau filaments in human Pick's disease and AD brains, despite having many β-structure residues in common [100], can be explained by the discovery that tau residues 337–357 can adopt both a canonical β-helix structure in AD and cross-β packing in Pick's disease. This finding highlights the importance of molecular polymorphism [106] in generating disease-specific conformations of tau filaments.
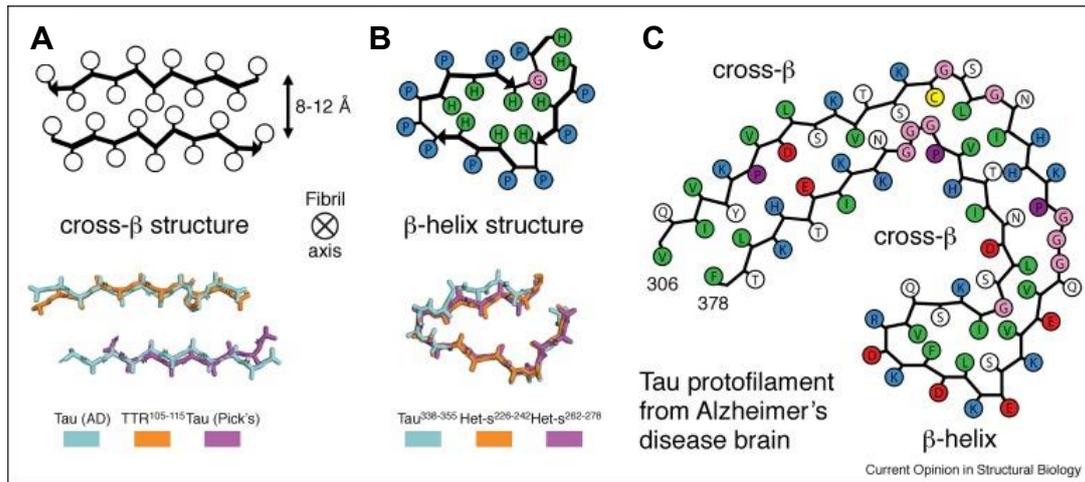
Figure 1.9 Atomic structures of amyloid fibrils, viewed down the fibril axis, showing the cross-β structure, β-helices and a combination of cross-β and β-helical structural motifs.

A) The cross-β packing between laminated β-sheets is generic and can be formed by any amino acid sequence (open circles). Backbones of cross-β structures from AD, PiD and another amyloidogenic fragment (TTR[105-115]) showed a high level of overlay. B) β-helices require a specific pattern of hydrophobic residues (green-filled circles), polar residues (blue-filled circles) and a glycine (pink-filled circle) closing the triangular motif. Overlay of the backbones of the β-helix in AD tau filaments and in the [HET-s] prion. C) Schematic view of the C-shaped protofilament core formed by the tau protein in human Alzheimer's disease brain. Each C-shaped protofilament consists of a β-helix region, where three β-sheets are arranged in a triangular fashion, and two regions with a cross-β architecture, where pairs of β-sheets pack anti-parallel to each other (Adapted from [99]).

Different amyloid fibril polymorphisms have been shown to possess distinct biophysical properties, such as surface hydrophobicity [98], fibrillization kinetics [107], thermodynamic stability [108] and *in vivo* pathogenicity [109]. Thus, the sequential, structural and physical determinants of fibril polymorphisms might lead to a variety of behaviors *in vivo*, possibly resulting in a broad spectrum of disease phenotypes.

1.2. Tauopathies

Human tau is encoded by the microtubule-associated protein tau gene (MAPT), a long and unique gene (134 kb) containing 16 exons located on chromosome 17 in position 17q21 [110]. Its sequence is well conserved among mammals, with some regions characterized by high sequence homology (97 to 100 %) [111], especially those located in the microtubule-binding domain.

In humans, tau is expressed mainly in neurons, where it localizes to axons [112] promoting axonal transport and neuronal integrity [113] and, to a lesser extent, to dendrites, where interacts with factors able to modulate post-synaptic receptor activity [114]. However, tau protein can be also found in other cell types, such as glial cells [115, 116]. Moreover, tau mRNA and protein are present in several peripheral tissues, such as heart, kidney, lung, muscle, pancreas, testis, as well as fibroblasts [117].

Tau expression is developmentally regulated by alternative splicing of exons 2, 3 and 10, producing six different isoforms in the human adult brain (Fig. 1.10) accordingly to the variable number of N-terminal insertions (0,1 or 2) and C-terminal repeated regions (3 or 4), ranging from 352 to 441 amino acids [118]. Exon 2 (E2) and 3 (E3) encode for insertions located at the N-terminal which might be totally excluded (0N isoforms), partially retained (1N) or completely translated (2N). Exons 9-12 (E9-12) encode 31/32-aminoacids imperfect repeats which, together with flanking regions, compose the microtubules (MTs)-binding domain [119]. Alternative splicing of exon 10 (E10) gives rise to tau isoforms with three (3R) or four (4R) MTs-binding repeats, found in equal amounts in the normal adult human brain [120]. Interestingly, in fetal rodent and human brain, E2, E3, and E10 are excluded and a single isoform is produced (0N3R), whereas in adult rodent brain only the three E10+ single isoforms are expressed producing only 4R tau isoforms [121]. Differences in tau isoforms ability to bind MTs have been observed, with 4R tau being able to bind MTs three-fold more strongly and assembling MTs more efficiently than 3R tau [122].
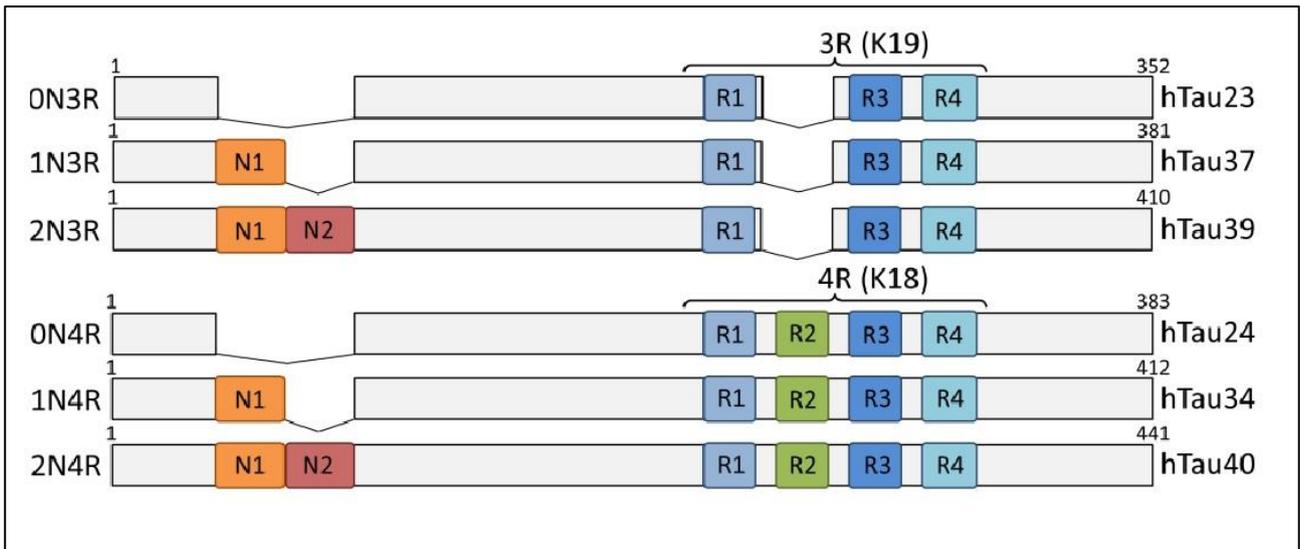
Figure 1.10 Alternative splicing variant isoforms of tau.
The six different isoforms of tau generated by alternative splicing of exons 2 and 3 for the N-terminal region, which encode the N1 and N2 segments of the protein (labeled here in orange and red, respectively), and of exon 10 in the microtubule-binding region, which encodes the second repeat sequence (R2, shown in green). The microtubule-binding domain is composed of 3 or 4 repeat sequences (blue and green). These domains form the core of tau fibrils, and when expressed recombinantly as truncated protein products, they are referred to as 3R and 4R or alternatively as K19 and K18, respectively. (From McHugh, K.P., Morozova, O.A., & Colby, D.W. (2015). Tau strains and their propagation in experimental disease models. Book: The Prion Phenomena in Neurodegenerative Diseases. Edited by Nova Science Publishers, Inc ISBN: 978-1-63483-399-8)

Tau binding to MTs through its MTs-binding domain increases the rate of polymerization, decreases the rate of transit into the shrinking phase (catastrophe) and inhibits the rate of depolymerization of MTs [123]. Biophysical studies have revealed the natively unfolded nature of tau, which maintains a highly flexible conformation and overall has a low content of secondary structures [124]. The N-terminal part is referred to as the projection domain since it projects from the microtubule surface where it may interact with other cytoskeletal elements, with the plasma and organelles membranes or with proteins involved in signal transduction pathways, such as PLC-γ and Src-kinases [125]. The C-terminal part is also able to participate in other cellular functions and to regulate tau phosphorylation state through its binding to protein phosphatase 2A (PP2A) [126] or presenilin 1 (PS1) [127].

In order to study tau aggregation process *in vitro*, recombinant tau purified from E. Coli was generated, however, it shows very little intrinsic tendency to aggregate

presumably due to the lack of a series of post-translational modifications required for its aggregation [128]. Indeed, truncated tau constructs that include the 3R and 4R domain alone, named K19 and K18 respectively (Fig. 9), aggregates much faster than full-length tau in *in vitro* fibrillation studies. Thus, they are often used to study tau aggregation *in vitro* and to represent aggregation properties of the two major classes of tau isoforms [129].

The developmental expression of different tau isoforms and their differential affinity to MTs suggests the presence of particular isoform-associated functions required for tau–MT interactions in modulating the extent and rate of microtubule assembly and in maintaining the dynamic stability of the neuronal cytoskeletal architecture [130]. Since tau is the major microtubule-associated protein of a mature neuron [131], its functions are of particular importance for the maintenance of fundamental brain functions, such as cellular integrity and morphology, axons and dendrites formation and neuronal trafficking and signaling [132].

There is preferential accumulation of 3R or 4R tau in various tauopathies, thus giving the possibility to further classify these pathologies (Table 1.2): in AD, 3R and 4R tau accumulate with a 1:1 ratio, 4R tau accumulates preferentially in PSP and CBD, while 3R tau accumulates in Pick's Disease [133]. In FTDP-17, there is often a two- to six-fold increase in the 4R/3R ratio. Indeed, cases associated with P301L tau mutation usually display a predominant 4R tau isoform deposition. However, such aggregates composition strictly depends on the localization and the effect of MAPT mutation. [133].

Table 1.2 Classification of the most common tauopathies based on the major tau isoforms found to accumulate in each condition.

Tau isoform	Tauopathy
3R	Pick's Disease (PiD)
4R	Progressive supranuclear palsy (PSP)
	Corticobasal degeneration (CBD)
	Frontotemporal dementia-P301L mutation (FTDP-P301L)
3R + 4R	Alzheimer's disease (AD)

Interestingly, the electrophoretic profile of insoluble tau purified from brain of patients with different tauopathies correspond to the specific isoforms that accumulate together with their phosphorylation levels, thus it is often disease-specific [134]. As described in Fig. 1.11, biochemical characterization of insoluble tau extracted from AD brain reveals the presence of three main bands (tau60, 64 and 69), also referred to as PHF-tau, corresponding to the molecular weight of 3R and 4R isoforms and relative phosphorylation levels. Sometimes a 72–74 kDa faint band is also present and corresponds to the longest tau isoform.
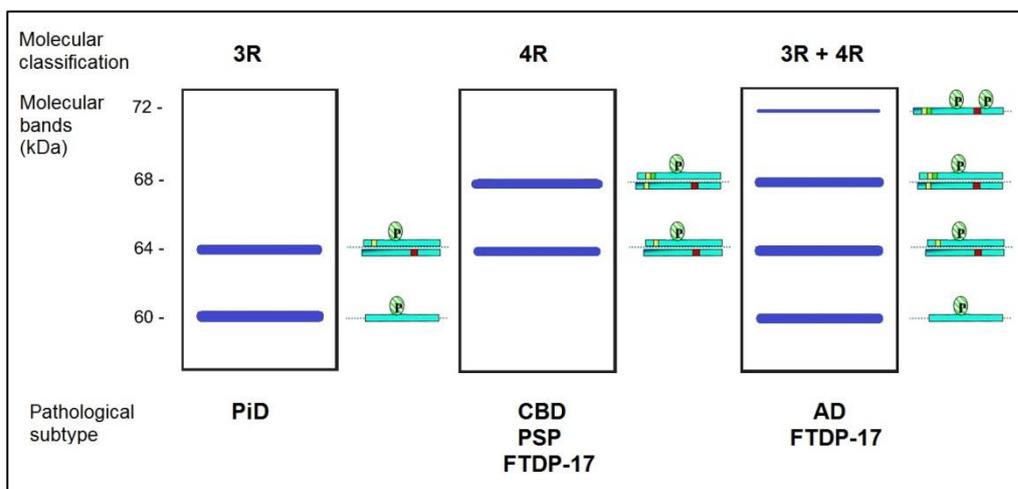
Figure 1.11 Biochemical profiles of abnormal tau found in different tauopathies.
Schematic representation of electrophoretic bands pattern and the relative isoforms composition (right of each frame). The six tau isoforms are involved in the formation of the typical AD-triplet tau60, 64 and 69 with the minor tau74 variant. The typical PSP/CBD doublet tau64 and tau69 is related to the aggregation of hyperphosphorylated tau isoforms with exon 10. The FTDP-17 families with mutations in exon 10 or intron 10 exhibit profiles depending on the associated mutation (middle panel). Hyperphosphorylated tau proteins without exon 10 aggregated in PiD are detected as a tau60, 64 doublets (right panel).

Using AD PHF-tau preparations, Goedert and colleagues showed that dephosphorylated PHF-tau proteins have a similar electrophoretic mobility than the six recombinant tau isoforms [135]. Thus, it was possible to identify the following scheme (Fig. 11): tau60 results from the phosphorylation of 0N3R isoform, tau 64 from the phosphorylation of 1N3R and 0N4R tau variants and tau69 from the phosphorylation of 2N3R and 1N4R tau variants. Phosphorylation of the longest tau isoform (2N4R) induces

the formation of the additional hyperphosphorylated tau band with molecular weights ranging from 68 to 72 kDa according to its degree of phosphorylation. PSP and CBD showed distinct biochemical profiles from that of AD (corresponding to the aggregation of the 4R isoforms) and that of PiD (corresponding to the aggregation of 3R tau). Indeed, PSP and CBD insoluble tau present two main bands corresponding to tau64 and 69, whereas PiD tau bands possess a molecular weight (MW) of 60 and 64 kDa. In FTDP-17 immunoblot tau bands depend on the class and the effect of the mutation associated with the disease: P301L, the most common tau mutation, and others located in the proximity of exon 10 or in the intronic region, are associated with the formation of 4R insoluble tau presenting MW of 64 and 69 kDa. Other mutations, however, may promote the aggregation of both isoforms thus producing insoluble tau with MW of 60, 64 and 69 kDa. (Fig. 1.11) [136].

1.2.1. Alzheimer's disease

Alzheimer's disease (AD) is the most frequent cause of dementia [137] and is characterized by extracellular deposition of β-amyloid plaques and the intracellular accumulation of tau in neurofibrillary tangles (NFTs). The vast majority of AD occurs from an apparently sporadic origin (sAD) and is characterized by a typical late-onset (80–90 years of age) with an average duration of illness of 8–10 years [138]. sAD seems to be driven by a complex interplay between genetic and environmental factors, in which genetics accounts for 70% of AD risk [139]. Mutations in three genes, which are amyloid precursor protein (APP), presenilin 1 (PSEN1) and presenilin 2 (PSEN2), are causative of rare familial forms of AD (fAD) characterized by early disease onset (30-50 years of age) [140].

The typical presentation of AD is centered on episodic memory deficits, starting from amnestic mild cognitive impairment (MCI) [141]. Subsequently, difficulties in the simultaneous execution of multiple tasks and loss of confidence may emerge, together with more profound cognitive impairments as the condition progresses, starting to interfere with activities of daily living [142]. In the late stages of the disease, behavioral change, impaired mobility, hallucinations, and seizures may also be present, finally leading to death [143].

Amyloid plaques are extracellular accumulations composed of abnormally folded Aβ with 40 or 42 amino acids (Aβ$_{40}$ and Aβ$_{42}$), two products of APP metabolism [144]. Aβ$_{42}$ is more abundant than Aβ$_{40}$ within plaques due to its higher rate of fibrillization and insolubility [145]. Amyloid deposition does not always follow a stereotypical pattern of progression but seems to broadly develop in the isocortex and only latterly affects subcortical structures. Entorhinal cortex and hippocampal formations are less involved in Aβ pathology [146].

NFTs are mainly composed of paired helical filaments (PHFs) built up by hyperphosphorylated tau (Fig. 1.12d) [144]. Tau pathology typically begins in the entorhinal cortex and hippocampus before spreading to the isocortex, whereas primary sensory, motor, and visual areas are not normally involved [141]. Neuronal and synapse loss typically correspond to tangle formation, indeed it has been shown that AD clinical features and severity are better correlated with NFT pathology than β-amyloid deposition [146]. Typical changes accompanying NFTs are the neutrophil threads (Fig. 1.12e), which are thought to result from the breakdown of dendrites and axons of the tangle-bearing neurons [99].

Ultrastructural studies on AD brain specimens revealed that NFTs are primarily made of paired helical filaments (PHFs) of 3R and 4R tau fibrils (ratio 1:1), which are tau fibrils of ≈10 nm in diameter that form pairs with a helical tridimensional conformation at a regular periodicity of ≈65 nm [144]. A small proportion of fibrils within the NFTs do not form pairs but give the appearance of straight filaments (SFs) although sharing the same structural core of PHFs [147], as shown in Paragraph 1.1.5.

Three NFTs morphological stages have been identified: (1) pre-NFTs or diffuse NFTs are diffuse tau staining within the cytoplasm of otherwise normal-looking neurons, with well-preserved dendrites and a centered nucleus; (2) mature or fibrillar intraneuronal NFTs (iNFTs) consist of cytoplasmic filamentous aggregates of tau that displace the nucleus toward the periphery of the soma causing distorted-appearing dendrites; (3) extraneuronal "ghost" NFTs (eNFTs) result from the death of the tangle-bearing neurons and are identifiable by the absence of nucleus and stainable cytoplasm in their proximity [148].

1.2.2.   Progressive supranuclear palsy (PSP)

Progressive supranuclear palsy is an atypical parkinsonism characterized by axial rigidity, postural instability, and unexplained falls, with most patients, also developing progressive vertical gaze palsy, dysarthria, and dysphagia [149]. Five clinical variants have been described: one classical PSP (Richardson's syndrome) and four atypical variants of PSP including PSP-Parkinsonism (PSP-P), PSP-Pure akinesia with gait freezing (PSP-PAGF), PSP-corticobasal syndrome (PSP-CBS) and PSP-progressive non-fluent aphasia (PSP-PNFA) [133]. Richardson's syndrome is the most common clinical variant and manifests with a lurching gait, falls due to postural instability, cognitive impairment and slowing of vertical saccadic eye movements. Progressively patients may develop other problems such as speech deficits, supranuclear gaze palsy, and difficulties in swallowing. PSP-P is characterized by prominent early parkinsonism, including tremor, limb bradykinesia, axial and limb rigidity [150]. PSP-PAGF shows progressive freezing of gait, speech and writing early in the course of the disease, whereas axial rigidity and supranuclear downgaze paresis may emerge after a decade. PSP-corticobasal syndrome (PSP-CBS) has asymmetric cortical atrophy and can clinically mimic CBD manifestations. PSP-PNFA patients firstly show the presence of speech anomalies (apraxia of speech, agrammatism, phonemic errors) and motor symptoms appear later in the course of the disease.

The typical neuroanatomical regions affected in all PSP cases include basal ganglia, subthalamic nucleus, and substantia nigra [151]. Pathology of the cerebellar dentate nucleus and the cerebellar outflow pathway (dentato-rubro-thalamic pathway) is usually severe and associated with profound atrophy of the superior cerebellar peduncle [152]. Neuropathological evaluation of PSP brain lesions reveal the presence of 4R tau-associated NFTs in neurons and glia of the basal ganglia, diencephalon, brainstem, and spinal cord; however, the hallmark lesion is the presence of tuft-shaped astrocyte, which are usually abundant in the motor cortex and the corpus striatum [153]. Tufted astrocytes are distinct and differ from astrocytic lesions in other neurodegenerative disorders (Fig. 1.12h), such as astrocytic plaques that are typically found in Corticobasal degeneration (CBD) [154].

Oligodendroglial lesions are also present in PSP and appear as argyrophilic and tau-positive globose tangle (Fig. 1.12g), so-called coiled bodies, and they are usually accompanied by thread-like processes in the white matter, especially in the diencephalon, brainstem and cerebellum [155].

From a neuropathological point of view, microscopic changes are similar in the different PSP variants, however, the distribution of tau pathology determines the particular clinical presentation, as some cases have severe brainstem involvement (e.g., PSP-PAGF) and others important cortical involvement (e.g., PSP-CBS and PSP-PNFA) [156]. The basis for anatomical selective vulnerability to tau pathology in PSP and its variants remains to be determined.

1.2.3. Corticobasal degeneration (CBD)

Corticobasal degeneration (CBD) is an atypical parkinsonism which presents a range of clinical presentations mainly associated with the region involved by focal cortical degeneration [157]. The classic clinical presentation of CBD, which is referred to as the corticobasal syndrome (CBS), is associated with asymmetrical rigidity and apraxia, often with dystonia and alien limb sign, accompanied by asymmetrical cortical degeneration of the superior frontal gyrus and superior parietal lobe [158]. Atypical presentations are common, including clinical manifestations similar to behavioral variant-FTD (CBD-bvFTD) with focal atrophy in the frontal lobes [159] or to Progressive non-fluent aphasia (CBD-PNFA) with focal degeneration in perisylvian areas (Fig. 1.12c) [160].

The characteristic pathological sign in CBD is 4R tau accumulation in cell processes of neurons and glia in the cortex, basal ganglia, thalamus and brainstem [161]. Particularly, CBD specific histopathological lesion consists of astrocytic plaques, which are not present in other disorders [154] and are visible as blurry outgrowths from the astrocyte (Fig. 1.12I) [162]. In the affected areas, ballooned neurons (BN) are present as swollen and vacuolated cortical neurons [163]. Abnormal tau-positive, thread-like processes are present in both gray and white matter of cortical and subcortical regions and are typical CBD

neuropathological signs, accompanied by variable, sometimes sparse, oligodendroglial inclusions [161].

1.2.4. Frontotemporal dementia and parkinsonism (FTDP-17)

Frontotemporal dementia and parkinsonism linked to chromosome 17 (FTDP-17) is a rare familial disorder with autosomal dominant inheritance [164]. Its three major clinical features include behavioral disturbances, cognitive impairment and parkinsonism, however, clinical heterogeneity could be described between and within families with FTDP-17 [125]. Molecular genetic studies have identified 38 unique tau mutations in families affected by FTDP-17, with approximately 60% of known cases associated with P301L, N279K and a splice site mutation (exon 10 +16) [165].

Mutations in tau gene associated with FTDP-17 can be divided in two groups. The first comprises missense mutations and deletions that have been shown to disrupt the binding of tau to microtubules and to accelerate its aggregation [166]. The proposed mechanisms involve both an increase in the proportion of tau that is unbound to microtubules and available for aggregation and also tau increased propensity to form filaments. The second group of tau mutations appears to interfere with the alternative splicing of exon 10 thus altering the ratio of 4R: 3R tau [167]. These mutations comprise a mixture of coding changes within exon 10 (e.g. N279K, P301L, P301S, N296N) and intronic mutations close to the 5' splice site of exon 10. Almost all of these mutations have been demonstrated to increase the splicing of exon 10 and consequently the proportion of 4R tau [125].

Clinical features of FTDP-17 vary considerably among affected individuals, even if they inherit the same mutation. Indeed, members within the same family might present different clinical manifestations [32]. The behavioral and personality abnormalities can include disinhibition, apathy, defective judgment, compulsive behavior, hyper-religiosity, neglect of personal hygiene, alcoholism, illicit drug addiction, verbal and physical aggressiveness. Cognitive disturbances may impair memory, orientation, and visuospatial functions, progressively leading to dementia and finally mutism. Motor signs are

represented by parkinsonism usually characterized by symmetrical bradykinesia, postural instability, rigidity and absence of resting tremor. They can manifest early or late in the course of the disease, sometimes misdiagnosed as Parkinson's disease (PD) or Progressive supranuclear palsy (PSP), or they might not be present. Up to date, no significant correlation between specific tau mutations and different phenotypes have been found [168].

Neuropathologically, FTDP-17 patients present atrophy of frontal and temporal cortex, basal ganglia and substantia nigra. In the majority of cases, these features are accompanied by neuronal loss, gliosis and tau inclusions in both neurons and glial cells (Fig. 1.12l) [164]. Different tau pathologies have been observed in different FTDP-17 families or within the same family [169]. In some cases tau deposits are found mainly in neurons and contain filaments indistinguishable from AD PHFs and SFs, appearing on immunoblots as major bands of 60, 64, 68 kDa and a minor band of 72 kDa. However, tau pathology of these FTDP-17 patients differs from AD in the regional and cellular distribution of NFTs and NTs and by the absence of NPs [170]. Tau pathology may also appear on immunoblots as 2 major bands of 64 and 68 kDa and a minor band of 72 kDa, mainly composed of 4R tau similarly to PSP and CBD. However, tau pathology is more diffuse in FTDP-17 as compared to PSP and no astrocytic plaques typical of CBD have been observed. Therefore, the distribution of tau deposits and their structural and biochemical characteristics in FTDP-17 patients are different from those present in AD, PSP, CBD and PiD [171].
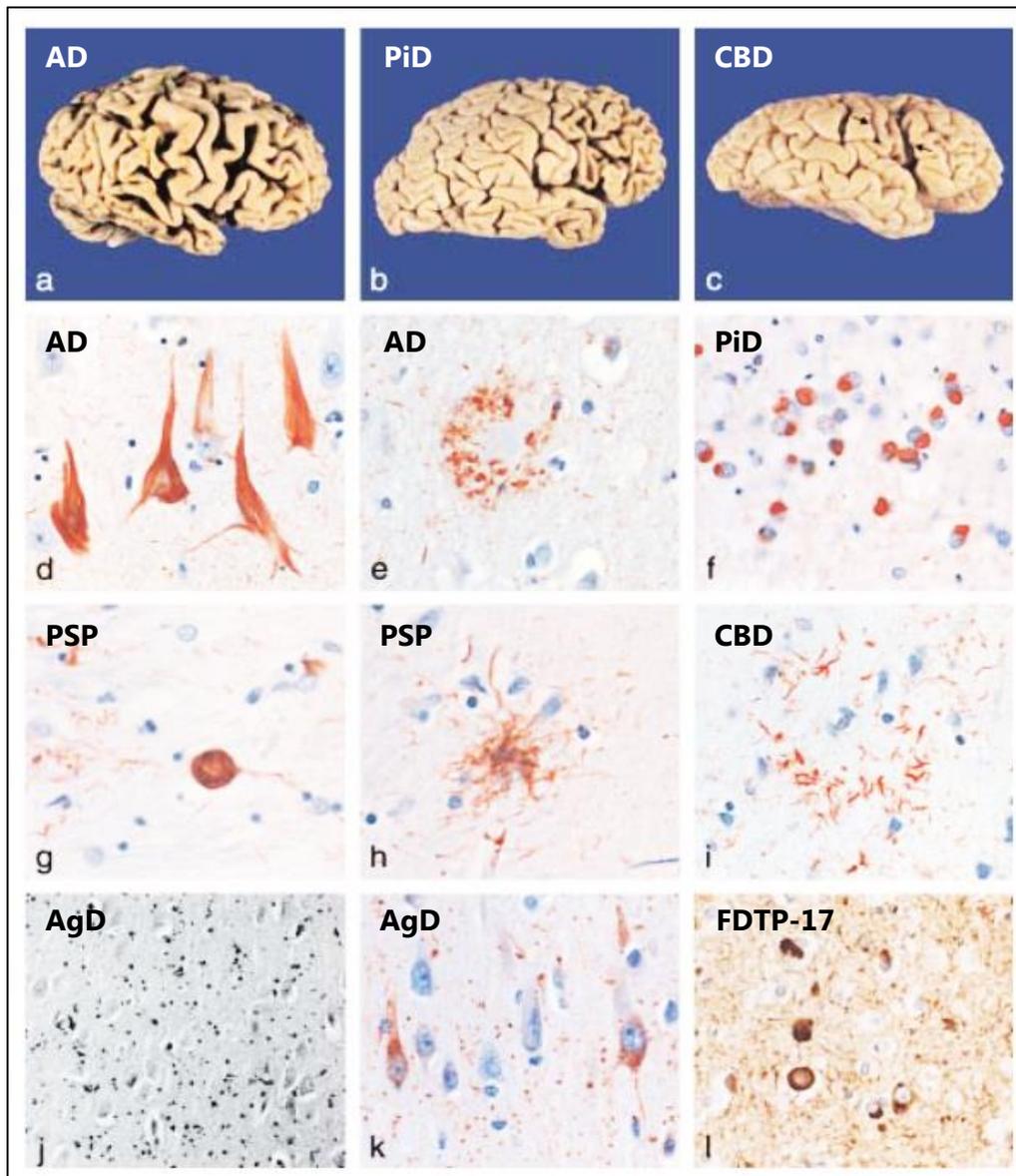
Figure 1.12 Neuropathological evaluation of different tauopathies showing distinct macroscopic and microscopic lesions.

a) Diffuse convolutional atrophy of the frontal, parietal and temporal lobes in AD is in contrast to b) a severe shrinkage of circumscribed parts of the brain in PiD, with a 'knife-edge' appearance of the frontal and anterior temporal gyri. c) CBD is characterized by atrophy of the pre- and post-central gyri (black arrows). d) Hippocampal AD brain section showing several flame-shaped neurofibrillary lesions (tangles) and neuropil threads, as well as: e) dystrophic neurites surrounding a senile plaque (neuritic plaque). (f) PiD granule cell layer of the dentate gyrus showing abundant intracellular Pick bodies. g) PSP subthalamic nucleus showing globose tangle next to several neuropil threads. h) PSP, tufted astrocyte in the striatum. i) CBD, cingulate gyrus showing astrocytic plaques that differs from tufted astrocytes. j) AgD hippocampal section showing abundant silver-stained grains. k) Next to argyrophilic grains there is also tau-immunoreactivity in some pyramidal cells (pre-tangled neurons). l) Frontal cortex of a case of Frontotemporal dementia and parkinsonism linked to chromosome 17 due to an intron 10 mutation of the tau gene (P301L), showing numerous tau filamentous inclusions in nerve cells and glial cells. Tau immunostaining also reveals a dense network of neuropil threads.

1.3. Synucleinopathies

In humans, α-synuclein (αS) is encoded by SNCA gene on chromosome 4 and belongs to synucleins, a protein family which also include β-synuclein and γ-synuclein [172]. α-synuclein is a small protein comprising 140 amino acids and three domains: an N-terminal domain (aa 1–65), a non-amyloid-β component of plaques (NAC) domain (aa 66–95), and a C-terminal domain (aa 96–140) (Fig. 1.13). The NAC domain, which is unique to αS among members of the family [173], presents 12 amino acid residues that are responsible for the aggregation properties of α-synuclein, presumably via inhibition of its degradation and promoting its fibrillation [174].

αS have been shown to exist in various conformations in a dynamic equilibrium and modulated by many factors [175]; indeed, the main accepted hypothesis indicated that the predominant native conformation of α-synuclein might be an unstructured monomer, exhibiting a random coil structure in solution, while the α-helical structure might be only adopted upon membrane binding [176]. However, the normal physiological structure and function of α-synuclein still remain unclear.

Recent studies showed that α-synuclein seems to have an important role in compartmentalization, storage, and recycling of neurotransmitters [176]. In addition, α-synuclein is associated with the physiological regulation of certain enzymes and is thought to increase the number of dopamine transporter molecules [177]. Moreover, neurotransmitter release and interaction with the synaptic SNARE complex (involved in synaptic vesicle biogenesis) are partly mediated by its role as a molecular chaperone [176, 178{Nemani, 2010 #6179].

α-synuclein misfolding and aggregation is associated with a group of diseases collectively known as synucleinopathies, which include Parkinson's disease (PD), Dementia with Lewy bodies (DLB) and Multiple system atrophy (MSA). The majority of them are sporadic, however rare point mutations in the N-terminal domain of α-synuclein result in autosomal dominant familial Parkinson's disease (PD) and PD-like syndromes, presumably caused by misfolding and aggregation of the mutant α-synuclein protein [179]. All known

clinical mutations are present in this N-terminal region, emphasizing the importance of this domain in the pathological dysfunction of α-synuclein [180]. Over 90% of aggregated α-synuclein is phosphorylated at serine 129, while only about 4% of α-synuclein from normal brain is phosphorylated at this site {Fujiwara, 2002 #6380}.
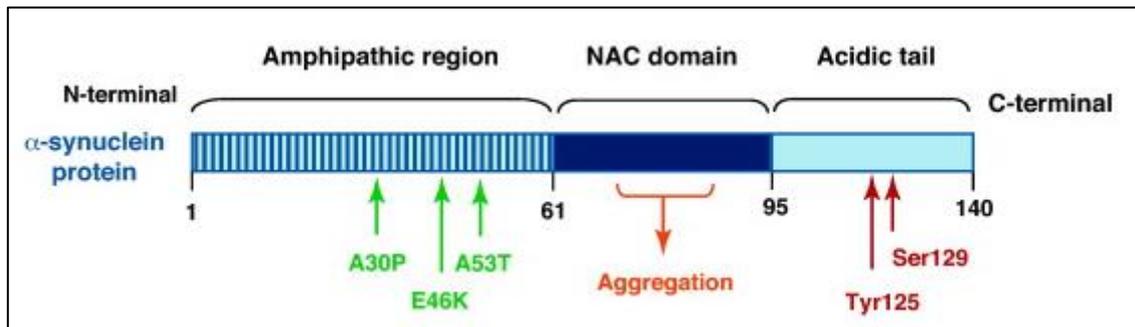
Figure 1.13 Schematic representation of human α-synuclein protein.
Human α-synuclein presents an amphipathic region at the N-terminal, followed by a central NAC (non-amyloid-β component) domain and an acidic tail at the C-terminal of the protein. The three missense mutations known to cause familial PD (A30P, E46K and A53T) lie in the amphipathic region, suggesting an important function for this region of the protein. The central hydrophobic region of α-synuclein is associated with an increased propensity of the protein to form fibrils. The acidic C-terminal tail contains mostly negatively charged residues and is largely unfolded. The most common sites of αS post-translational modifications are depicted in red.

1.3.1. Parkinson's disease (PD)

Parkinson's disease (PD) is the second most common neurodegenerative disorder after Alzheimer's disease (AD), as it affected about 0.3% of the general population (Rizek 2016). Typical onset is between the ages of 55 and 65 years and the prevalence is higher among men than women, for reasons still unknown, with a ratio of 1.5 to 1.0 respectively [181]. The etiology of PD is thought to be multifactorial, resulting from an elaborate interplay of genetic and environmental factors. Genetic PD account only for a limited number of familial (30%) and sporadic cases (3-5%), in which mutations in LRRK2 gene are the most frequent cause of late-onset autosomal-dominant and sporadic PD, known as PARK8 [182].

PD is a progressive neurological disorder characterized by bradykinesia, tremor, rigidity and postural instability. From a neuropathological point of view, it is characterized by two major pathological processes: (i) premature selective loss of dopamine neurons and (ii) accumulation of Lewy bodies [183]. Lewy bodies are intraneuronal cytoplasmatic inclusions (Fig. 1.14) mainly composed of aberrant αS, which display an abnormal conformation promoting its aggregation, but it is also characterized by pathologic post-translational modifications, including phosphorylation, truncation and oxidative damage [184]. In order to compensate for dopamine loss, the dopamine precursor Levodopa (L-Dopa) is an effective and well-tolerated dopamine replacement agent used to improve the quality of life of patients with PD [185].

The presence of αS in cytoplasmic inclusions represents aberrant localization since it is normally enriched in presynaptic terminals [176]. Immunohistochemistry for αS in PD cases reveals the classical Lewy body pathology in vulnerable neurons of the substantia nigra, raphe nuclei, mesopontine tegmentum, locus ceruleus, basal nucleus of Meynert and dorsal motor nucleus of the vagus, but also pale staining inclusions in less vulnerable neuronal populations, such as those in the amygdala and neocortex [186]. These pale staining and poorly circumscribed lesions are referred to as pre-inclusions or cortical type Lewy bodies. Another major location of aberrant α-synuclein in PD is within cell processes (mostly axonal), so-called Lewy neuritis [187].

Based on neuropathologic studies, the progressive degeneration of neurons seems to result in the specific symptomatology of PD: when motor symptoms become evident there is 30–70% cell loss evident in the substantia nigra, whereas cognitive dysfunction, mood disorders, and impulse control disorders are related to deficits of dopamine outside the basal ganglia or in serotonergic and noradrenergic systems [188]. Autonomic dysfunction has been related to pathologies outside the central nervous system, including the spinal cord and peripheral autonomic nervous system. Braak and colleagues developed a PD-related disease staging similar to that of AD [189], showing that neuronal pathology occurs early in the dorsal motor nucleus of the vagus in the medulla and the anterior olfactory nucleus in the olfactory bulb, followed by locus ceruleus neurons in the pons and

then dopaminergic neurons in the substantia nigra. In later stages, pathology extends to the basal forebrain, amygdala and the medial temporal lobe structures, with convexity cortical areas affected at the end of the pathology [189].

1.3.2.   Multiple System Atrophy (MSA)

Multiple system atrophy (MSA) is a neurodegenerative disease characterized by a combination of autonomic, cerebellar, parkinsonian and pyramidal symptoms [190]. Like PD, the onset of MSA is usually in the sixth decade of life, but it progresses faster than other synucleinopathies, with a mean survival time after disease onset of 6–10 years. Depending on the motor phenotype, it is divided into parkinsonian (MSA-P) and cerebellar (MSA-C) variants, with MSA-C being usually less common than MSA-P. MSA-P is characterized by a hypokinetic-rigid parkinsonian syndrome, which tends to be more symmetrical and less responsive to Levodopa than in PD, with an irregular, higher-frequency postural tremor. In MSA-C, the most common symptom is gait ataxia with wide-based movements. Furthermore, ataxia of the limbs, cerebellar oculomotor impairments, scanning dysarthria, and intention tremor are common in MSA-C [191].

Proteinaceous oligodendroglial cytoplasmic inclusions (Papp-Lantos bodies) mainly composed of αS are the major histological hallmark of MSA (Fig. 1.14) [192], often accompanied by Schwann cell cytoplasmic inclusions. Unlike PD and DLB, where α-synuclein filaments are present predominantly in the cytoplasm of nerve cells in the form of Lewy bodies and Lewy neurites, in MSA αS-positive inclusions are found in the cytoplasm and nuclei of prevalently glial cells and some nerve cells [193].

1.3.3.   Dementia with Lewy Bodies (DLB)

Lewy bodies disorders are dementia syndromes associated with Lewy bodies and are subdivided into dementia with Lewy bodies (DLB), one of the most common cause of dementia in the elderly together with AD and PD, and Parkinson's disease with dementia (PDD), usually used to define the cognitive impairment appearing in people diagnosed with Parkinson's disease [194]. The timing of dementia relative to parkinsonism is the

major clinical distinction between DLB and PDD, with dementia arising in the setting of well-established idiopathic Parkinson's disease (after at least 1 year of motor symptoms) denoting PDD, while earlier cognitive impairment relative to parkinsonism denotes DLB [195].

The initial symptoms of DLB consist of a reduction in cognitive performance with fluctuating episodes of poor and better cognitive performance, with deficits involving the naming of objects, verbal fluency, visuospatial abilities, and executive functions. In contrast to AD, memory impairment is not a common or predominant feature in DLB in the early stage of the disease [196]. On the other hand, vivid, recurring or persistent visual hallucinations are frequent, as are delusions, lack of initiative and motivation, depressed moods, and anxiety. Akinetic-rigid movement disorder may already be present at the time of diagnosis but develops over the course of the illness in the majority of cases [197].

Despite the different temporal sequences of motor and cognitive deficits, PDD and DLB show remarkably convergent neuropathological changes, including widespread limbic and cortical Lewy bodies and Lewy neurites composed of aggregates of α-synuclein (Fig. 1.14), loss of midbrain dopamine cells and loss of cholinergic neurons in ventral forebrain nuclei [198]. The overlap of clinical, neuropsychological, and neuropathologic features has led to the hypothesis that PDD and DLB may be different phenotypic expressions of the same underlying process [199].
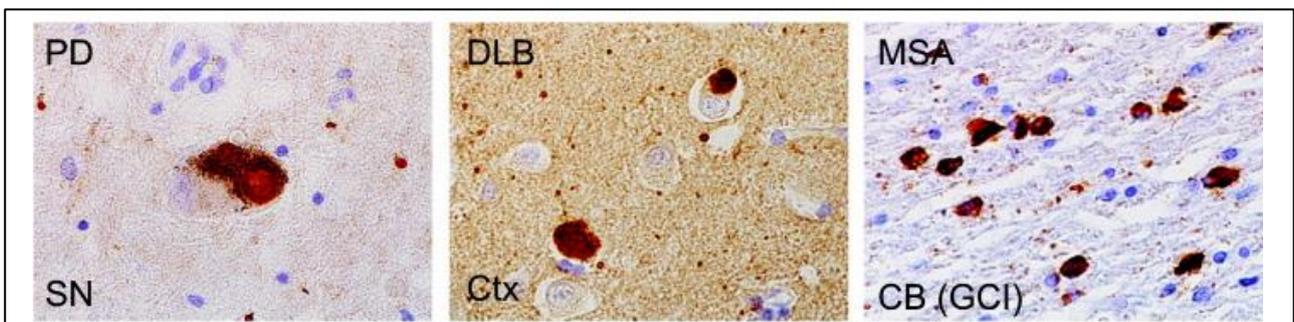

Figure 1.14 Neuropathology of α-synuclein deposits in different synucleinopathies.
α-synuclein aggregates stained by anti-α-synuclein antibody showing different aggregates morphologies and distinct affected areas in PD (SN: substantia nigra), DLB (Ctx: cortex) and MSA (CB: cerebellum; GCI: glial cytoplasmic inclusion).

1.4. Diagnosis of neurodegenerative diseases

Diagnostic approach to neurodegenerative diseases (NDs) aims at recognizing pathological, biochemical and genetic biomarkers so that the diagnosis could be established in the early stages, allowing the stratification between different NDs and the identification of pre-symptomatic individuals at higher risk of developing a certain type of dementia [200].

1.4.1. Biomarkers

Biomarkers are biological molecular indicators of a certain disorder [201]. The principal requirements for a good biomarker is its preciseness and reliability, as it should be also able to distinguish between the healthy and the diseased patients and to differentiate between different diseases [202].

Molecular and biochemical markers are evaluated based upon their sensitivity, specificity, positive predictive value and negative predictive value [203], whose specific meaning is defined in Box. 1.1. Sensitivity and specificity are statistical measures of the performance of a biomarker or a diagnostic method, based on the typical binary classification test that is widely used in medicine [204]. In this field, true or false terminology indicates if the assigned classification is correct or incorrect, while positive or negative denotes the positive or negative output of the medical test [204].

Box 1.1. Statistical evaluations of the performance of a biomarker or a diagnostic method.

Sensitivity (true positive rate)	It refers to the ability of a biomarker to correctly identify diseased patients. It measures the proportion of positives subjects that are correctly identified as having such condition
Specificity (true negative rate)	It refers to the ability of a biomarker to distinguish diseased patients from normal subjects or from other disorders. It measures the proportion of negative subjects that are correctly identified as not having the condition.
Positive predictive value	It is a measure of the percentage of people who have a positive test who can be shown at subsequent *post-mortem* examination to have the disease.
Negative predictive value	It represents the percentage of people resulting as healthy who subsequently at *post-mortem* evaluations prove to not have the disease.

For a clinical usage, biomarkers should have good sensitivity and specificity (e.g. ≥90% each) [205] and a positive predictive value of approximately 80% or more [200].

One of the major problems in the diagnosis of NDs is the lack of a widely accepted sensitive diagnostic test or easily accessible biomarkers able to support neuropsychological evaluation, monitor disease progression and identify affected individuals in the early stages of the disease [206].

Among NDs, certain and valid biomarkers correspond to conformationally altered disease-associated proteins that accumulate within the brain, as previously described in chapters 1.2 and 1.3 [22]. Indeed, morphological and biochemical identification of disease-specific misfolded proteins in *post-mortem* brain collected at autopsy is still the only methodology enabling to formulate a definite diagnosis of NDs [22].

New biomarkers have been recently added in clinical diagnostic criteria for some NDs, such as cerebrospinal fluid (CSF) protein concentrations and imaging biomarkers [207]. However, for many NDs the autoptic confirmatory test is not required, thus the validity of such biomarkers are still under debate. Neuroimaging techniques using structural magnetic resonance imaging (MRI) of gray matter and diffusion tensor imaging (DTI) of white matter within the context of autopsy-confirmed clinical FTD found some regional differences between subtypes of FTLD-Tau and FTLD-TDP [208], nevertheless, only one study have been performed. Several radio-ligands specific for tau pathology have been recently developed to detect and track the progression of tau pathology in living patients [209], however, no specific discrimination between different tauopathies is currently possible [210]. Thus, diagnosis of FTLD syndromes is based only on clinical symptoms and is hampered by the great overlap of the clinical manifestation within the FTLD subtypes and with other types of dementia [211].

CSF analysis has been performed with the aim of finding protein biomarkers, however, the largest body of data exists mainly for AD cases and few studies have been validated for other NDs. The AD CSF signatures are elevated tau and phospho-tau concentrations and decreased $A\beta_{42}$ levels, which have been shown to differentiate AD from

healthy subjects [212] and may help in distinguishing atypical forms of AD pathology associated with clinical FTD from those with underlying FTLD-Tau pathology [213].

Some biomarkers of genetic susceptibility have been also evaluated, such as the presence in a patient with dementia of one or more ε4 alleles of the gene for apolipoprotein E (APOE ε4) which has been significantly associated with Alzheimer's disease (AD) [214]. However, APOE genotyping does not provide sufficient sensitivity or specificity when used alone as a diagnostic test for AD but improves the specificity of diagnosis when used in combination with clinical criteria [215].

1.4.2. Probable or possible diagnosis

Probable or possible diagnosis of NDs might be made on the basis of international consortium guidelines, which reviewed clinical records and compared the sensitivity and specificity of proposed diagnostic criteria with neuropathologically verified cases of NDs [30]. According to the revised criteria, probable diagnosis is usually made in cases that match a significant number of proposed clinically discriminating features, whereas possible diagnosis is made in cases presenting atypical clinical manifestations [30, 216].

Probable or possible diagnosis of different NDs focuses primarily on the evaluation of clinical signs and on the anatomical distribution of neuronal loss. In most NDs cases, clinical symptoms show a high degree of similarity and usually overlap during the course of the disease [19]. However, initial clinical symptomatology may reflect the anatomical distribution of neuronal loss and may be useful for disease discrimination [217]. Based on initial clinical manifestations, neurodegenerative disorders may be divided in two different groups presenting:

1. **cognitive decline, dementia and alterations in high-order brain functions (DEM/FTD phenotype)**: these symptoms are associated with involvement of the entorhinal cortex, hippocampus, limbic system, and neocortical areas. The DEM/FTD phenotype is mainly associated with FTD and its subtypes (PSP, CBD, PiD, FTLD), Alzheimer's disease (AD), Huntington's disease (HD) and Dementia with Lewy bodies (DLB) [20]. Cognitive

impairment is detected and diagnosed through a combination of (1) history-collection from the patient and a knowledgeable informant and (2) an objective cognitive assessment, such as a mental status examination or neuropsychological testing [216].

2. **movement disorders (MD phenotype)**: associated with the involvement of basal ganglia, thalamus, brainstem nuclei, cerebellar cortex and nuclei, motor cortical areas and lower motor neurons of the spinal cord. The MD phenotype is usually observed in motor neuron diseases (MND) such as ALS and SCA, and in Parkinson's disease (PD), however atypical parkinsonisms such as PSP and CBD usually display motor deficits and they also might appear in the late stages of FTD [3].

Although numerous effort has been made in the establishment of consensus criteria, the diagnosis of NDs has been shown some degree of inaccuracy (Table 1.3) [218]. Indeed, twenty-five percent of patients clinically diagnosed with probable AD during their lifetime were not confirmed at autopsy. Thus, diagnostic accuracy is 77% for a clinical diagnosis of AD [219].

Table 1.3 Diagnostic accuracy of current clinical diagnostic criteria for different neurodegenerative diseases.

Neurodegenerative disease	Diagnostic accuracy	References
Alzheimer's disease (AD)	77%	Marwan N. Sabbagh, et al. Neurol Ther (2017) 6 (Suppl 1):S83–S95 ; Guy M. McKhann, et al. Alzheimers Dement. 2011 May; 7(3): 263–269.
Parkinson's disease (PD)	80%	Postuma R.B., et al. Mov Disor (2015) 30, 12:1591 - 601
Dementia with Lewy bodies (DLB)	80%	Rizzo G., et al. J Neurol Neurosurg Psychiatry. 2018 Apr;89(4):358-366.
Frontotemporal dementia (FTD)	90%	Balasa M., et al. Neuropathol Appl Neurobiol. 2015 Dec;41(7):882-92.
Multiple system atrophy (MSA)	62%	Gilman S., Neurology. 2008 Aug 26;71(9):670-6.
Corticobasal degeneration (CBD)	68%	Armstrong M.J., Neurology. 2013 Jan 29;80(5):496-503.
Progressive supranuclear palsy (PSP)	95%	Hoglinger G.U., Mov Disorder. 2017 Jun;32(6):853-864.

Even though the clinical diagnosis of parkinsonism might be relatively simple, the specific diagnosis of PD, especially at the early stages, can be difficult. It has been reported that in patients with possible PD only 26% had autopsy confirmation, while in probable PD the diagnostic accuracy was 82% [220]. In DLB, clinical diagnostic criteria for probable DLB identify αS pathology with a sensitivity of about 80%, however, early diagnosis is less accurate due to the overlapping symptoms with other types of dementia [221]. In addition, 15–20% of patients with confirmed AD at autopsy showed concomitant DLB pathology, with only a minority of patients exhibiting clear diagnostic features of DLB [222].

1.4.3. Definite diagnosis

Definite diagnosis of NDs is based on the evaluation of histological features (e.g., vascular lesions or neuronal loss) and on the presence of intracellular and extracellular protein accumulations, which are analyzed by immunohistochemistry complemented by biochemistry in *post-mortem* tissues [20].

For the definite diagnosis of AD, stages of neurofibrillary degeneration and phases of Aβ deposition are evaluated by immunohistochemistry techniques, as protein pathology in AD usually follows a stereotypical pattern of deposition that was conceptualized by Braak and colleagues [146]. Areas showing tau pathology include the transentorhinal cortex (stage I), entorhinal cortex (stage II), inferior (stage III) and middle temporal gyri (stage IV), while in the end stages the occipital cortex is involved (stage V-VI). Regarding Aβ deposition, five phases were proposed by the progressive involvement of isocortical areas (phase 1), hippocampus and entorhinal cortex (phase 2), basal ganglia and diencephalon (phase 3), brainstem (phase 4) and cerebellum (phase 5). Together with the classical semiquantitative scoring of neuritic plaques, tau and Aβ pathology stages are included in the recent NIA-AA neuropathological criteria for AD [223].

Definite diagnosis of different subtypes of tauopathy is mainly based on the positivity for misfolded hyperphosphorylated tau and on the cellular distribution of tau pathology: PiD, AD, NFT-dementia/PART are disorders showing neuronal tau inclusions, whereas mixed neuronal and glial tau deposits can be found in PSP, CBD and AGD [28].

Some specific morphological features are assessed, such as the presence of round tau-positive "Pick bodies" in neurons that are typical of PiD, CBD-associated ballooned neurons and astrocytic plaques which are different from tufted astrocytes particularly found in PSP cases [224]. Final diagnosis may employ also biochemical evaluation of tau isoforms by Western blot analysis of insoluble tau extracted from *post-mortem* brain tissues, thus differentiating through their banding pattern tau pathology associated with 3R or 4R isoforms and mixed 3R+4R types, as shown in Chapter 2.1 [225].

Regarding the definite diagnosis of synucleinopathies, cellular localization of αS deposits by immunohistochemistry techniques is employed for disease discrimination. Indeed, DLB and PD shows predominance of intraneuronal cytoplasmic and neuritic deposits (cortical and brainstem type Lewy bodies and Lewy neurites), whereas MSA is dominated by glial cytoplasmic inclusions (Papp-Lantos bodies) [195]. In spite of studies suggesting that the biochemical pattern of αS may differ in distinct α-synucleinopathies [226], there are however no biochemical or morphological features that allow unequivocal distinction of potential molecular subtypes of abnormally folded αS [20].

1.4.4. RT-QuIC and PMCA technologies

The recent advances in molecular and structural biology have provided insights into the processes involved in the pathogenesis of neurodegenerative diseases and have made it possible to recapitulate the protein misfolding process *in vitro* in a limited period of time through the development of innovative techniques.

These new methodologies exploit the ability of misfolded proteins to transmit their abnormal conformation to normal monomers, which are used as substrate of reaction [227]. Abnormally folded proteins are able to interact with these substrates and induce monomers to change conformation and subsequently aggregate. Therefore, the addition of misfolded proteins to the substrate is able to trigger an aggregation phenomenon that might be exploited for a diagnostic and therapeutic point of view. The technologies that I will be describing here, are extremely sensitive and the aggregation phenomenon is triggered even by trace-amount of abnormally folded proteins.

These abnormally folded proteins are considered "seeds" and their ability to promote monomers aggregation is known as "seeding effect". These techniques were originally developed in the field of prion diseases to amplify undetectable amount of PrP^{Sc}, however, their applicability for protein misfolding studies in other NDs is very promising.

Protein Misfolding Cyclic Amplification (PMCA) assay is performed in a test-tube and consists of cycles of incubation and sonication (Fig. 1.15) [228]. During the incubation phase, the sample containing minute amounts of PrP^{Sc} is incubated with an excess of PrP^{C} to induce growing of PrP^{Sc} polymers. In the second phase, the sample is subjected to sonication to break down the polymers and to multiply the number of nuclei. After each cycle, the number of seeds increases in an exponential fashion, thus accelerating the seeding-induced conversion of PrP^{C} into PrP^{Sc} [229]. Normal mammalian brain homogenate is typically used as a source of PrP^{C}, whereas any tissue homogenate or biological fluid suspected to contain prions constitutes the seed of the reaction. Final products of the reaction are subjected to mild proteolysis digestion with Proteinase K (PK) in order to completely degrade PrP^{C} and to visualize PK-resistant PrP^{Sc} by immunoblot using anti-PrP antibodies.

PMCA technique has been shown to detect and amplify as little as a single molecule of oligomeric infectious PrP^{Sc} eventually contained in a sample [230]. PMCA amplified products have been shown to exhibit the same biochemical, biological and structural properties as brain-derived PrP^{Sc} and to be infectious when injected into wild-type animals, producing a disease with similar characteristics as the illness produced by brain-isolated prions [231]. PMCA allows the faithful replication of prion strains in many different species of prions, however, it is also possible to use PrP^{C} from one species to replicate prions from a different species thanks to the extremely high flexibility of PrP [232].

Protein Misfolding Cyclic Amplification (PMCA)
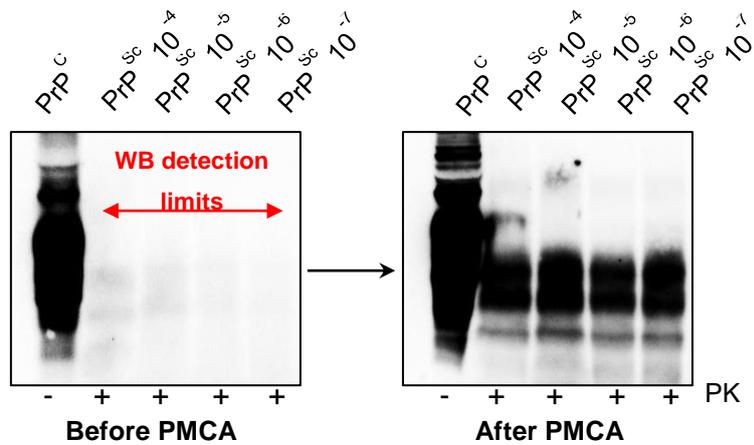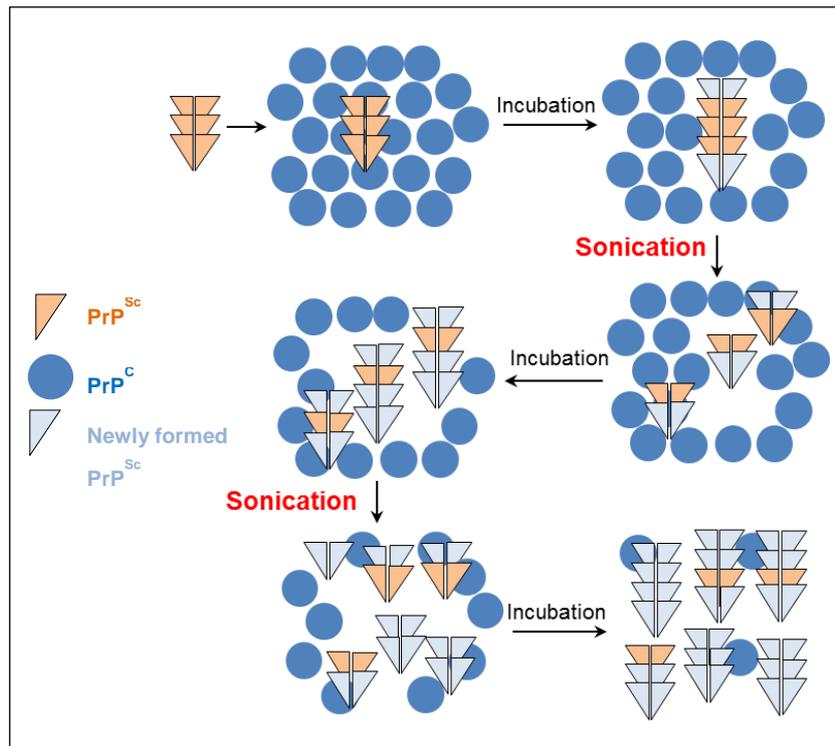
Figure 1.15. Schematic representation of Protein Misfolding Cyclic Amplification (PMCA).
PMCA consist of cycles of incubation and sonication steps that can exponentially amplify minute amounts of PrP^{Sc} through the conversion of PrP^{C} provided as substrate. Western blot (WB) analysis revealed that, after the amplification, it is possible to detect trace-amount of prions undetectable before PMCA (left bottom panel).

Real-Time Quaking Induced Conversion (RT-QuIC) is another extremely sensitive technique based on the same principle, the seeding-nucleation propagation of misfolded proteins (Fig. 1.16). RT-QuIC assay is performed in a multi-well plate, in which the reaction substrate is usually a recombinant or synthetic protein and amyloid formation is monitored by Thioflavin T (ThT), an amyloid-specific fluorescent dye similar to Thioflavin S (ThS). Upon binding to amyloid fibrils, the central C–C bond connecting the benzothiazole and aniline rings of ThT molecule is immobilized and fluorescence signal strongly increases when excited at 450 nm, detected at approximately 482 nm [233]. In RT-QuIC assay, the substrate is usually prone to aggregate, however, the fibrillization reaction is notably accelerated by the presence of pre-formed aggregates in a given sample. Therefore, in seed-containing reactions lag phase is reduced and ThT fluorescence levels exponentially increase [234].

1.4.5.   Contribution of RT-QuIC and PMCA in diagnostics

Recent observations suggested that very low concentrations of disease-specific biomarkers could be present in peripheral tissues of patients with NDs. If this was the case, their identification would be fundamental for formulating a definite diagnosis in the early stages of the diseases thus enabling patient's stratification. Moreover, these tissues can be periodically collected and might allow to monitor disease progression and evaluate the effects of specific drugs in patients under pharmacological treatments. As previously described (chapter 1.3), an important role in biomarkers spreading seems to be played by exosomes.

The advent of these cell-free amplification technologies (RT-QuIC and PMCA) provided the first evidence that trace-amount of such biomarkers are effectively detectable in peripheral tissues and body fluids of patients with different NDs, such as CSF, urine and olfactory mucosa (OM) (Fig. 1.17).

It has been shown that PMCA is capable of detecting as little as a single molecule of oligomeric infectious PrP^{Sc}, thus opening a great promise for the development of a highly sensitive detection method for prions and for understanding the molecular basis of prion replication.

Real Time Quaking Induced Conversion (RT-QuIC)
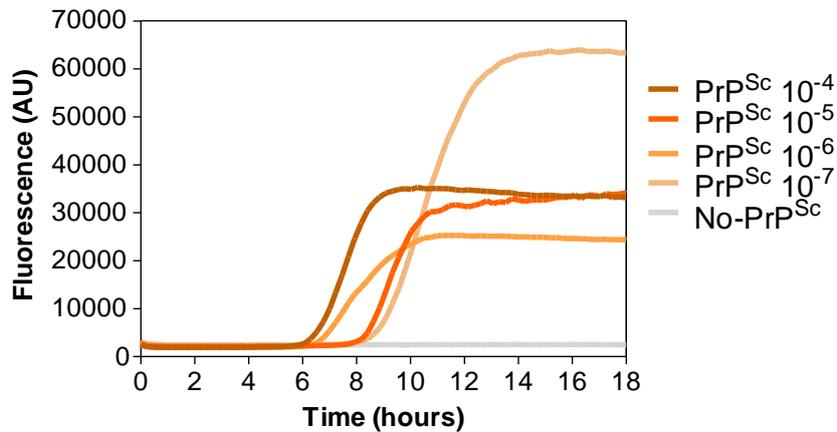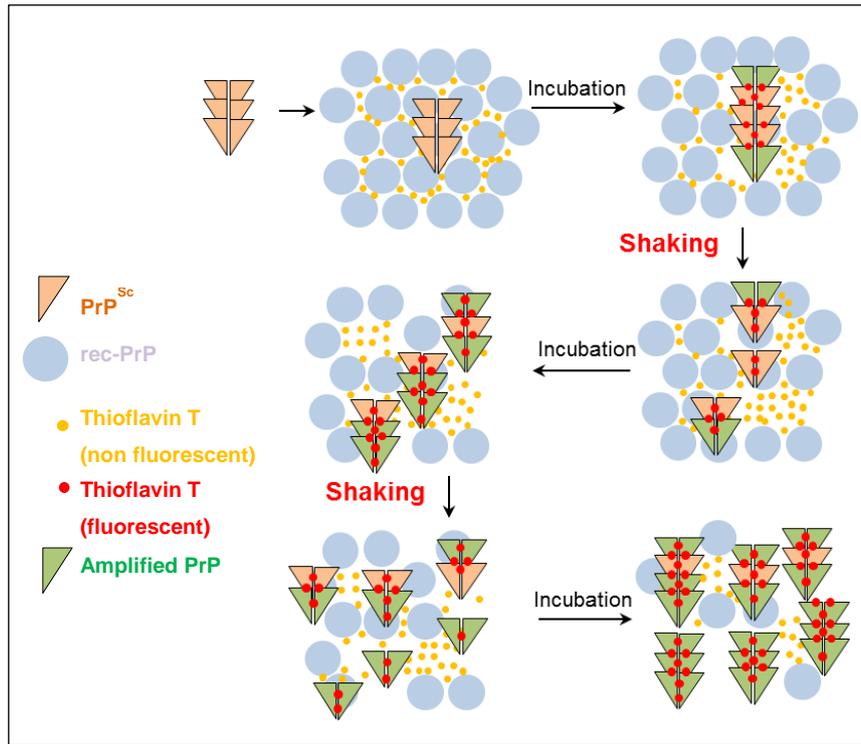
Figure 1.16 Schematic representation of Real-Time Quaking Induced Conversion (RT-QuIC).
In RT-QuIC assay, the formation of aggregates of recombinant PrP (rec-PrP) is induced by the addition of low amount of PrP^{Sc} and is accelerated by cycles of shaking and incubation. Amyloid formation is monitored in real-time using ThT fluorescent dye. Rec-PrP usually do not fibrillate spontaneously (gray line, right bottom panel), however the addition of PrP^{Sc}-containing samples induced its aggregation in a dose-dependent manner (orange lines, right bottom panel).

Indeed, PMCA has been used by various groups to detect PrP^{Sc} in blood of animals experimentally infected with prions during both symptomatic [235] and pre-symptomatic [236] phases of the disease. The technique was then optimized as a non-invasive method for early diagnosis of prion diseases in humans. PMCA assay displayed 100% sensitivity and specificity in the detection of PrP^{Sc} in blood of pre-symptomatic [237] and symptomatic vCJD patients [238]. PMCA was also employed to detect PrP^{Sc} in the urine of patients with vCJD with an estimated sensitivity of 93% and a specificity of 100% [239] and in the CSF of vCJD patients with 100% sensitivity and specificity ([240]. Moreover, PMCA coupled with a new detection method (SOFIA) allows identifying the presence of PrP^{Sc} in CSF of patients with sCJD with 100% sensitivity and 100% specificity [241].
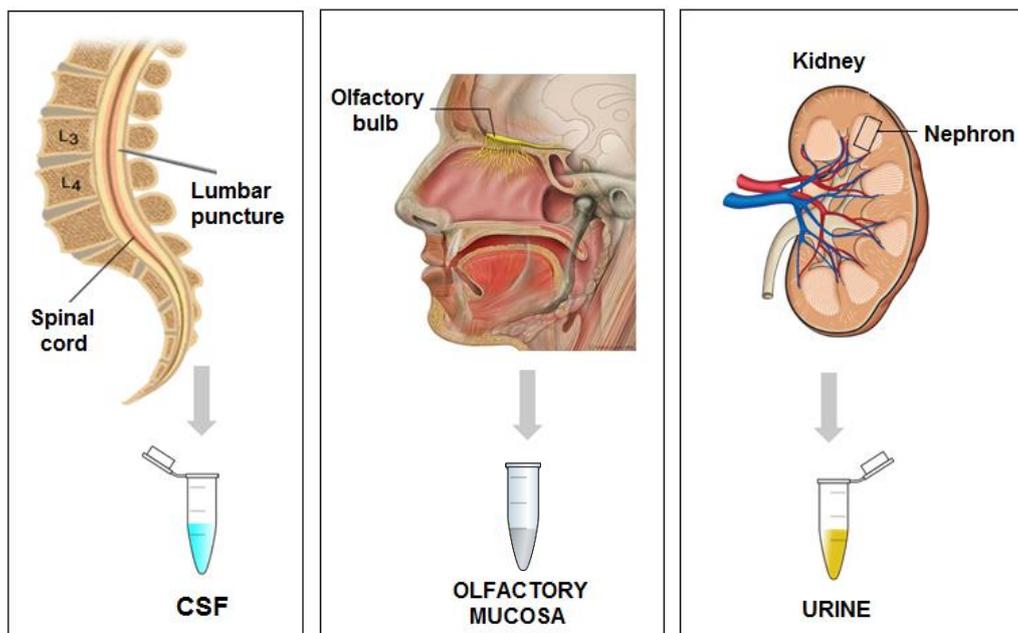
Figure 1.17 Peripheral tissues and body fluids potentially containing abnormally folded proteins. Cerebrospinal fluid (CSF), olfactory mucosa (OM) and urine are accessible specimens that could be tested through PMCA and RT-QuIC assays for the detection of seeding activity exerted by misfolded proteins.

Several research groups have carried out large studies in which CSF samples collected from CJD patients were evaluated using RT-QuIC assays, showing the ability to detect prion seeding activity with sensitivity ranging from 77–97% and specificity of 99–

100% [234, 242]. Some slight variations in RT-QuIC protocol with respect to reaction buffer composition, temperature, shaking motion and speed, and recombinant PrP^C substrate may influence the sensitivity and specificity of the test [243]. Indeed, the first generation of this assay mainly used full-length (23–231) hamster recombinant prion protein (rPrPsen) as RT-QuIC substrate, demonstrating a very high specificity but a suboptimal sensitivity, whereas Orrù and colleagues recently introduced a second-generation RT-QuIC assay for sCJD CSF which uses a truncated form of hamster recombinant PrP (rPrPsen, amino acids 90–231) thus improving diagnostic sensitivity and shortening the testing time [244, 245].

Recently, RT-QuIC assay has been optimized to detect Aβ seeding activity in CSF of patients with AD, with a sensitivity of 90% and specificity of 92%. In this study, Soto and colleagues were able to detect as little as 3 femtograms of Aβ oligomers [246], showing the potential application of RT-QuIC technique in detecting misfolded proteins other than prion. Moreover, Caughey and colleagues developed an RT-QuIC assay able to detect 3R tau seeds in CSF of patients with Pick's Disease (PiD) with 100% sensitivity and 98% specificity [247].

Similar assays have been developed to detect αS seeding activity in body fluids of patients with synucleinopathies. For instance, an RT-QuIC-based assay was able to detect αS aggregation in CSF collected from patients with DLB and PD, characterized by a sensitivity of 92% and 95%, respectively, and with an overall specificity of 100% when compared to AD and healthy controls [248]. Similarly, Soto and colleagues developed an RT-QuIC assay to distinguish CSF samples obtained from patients affected by PD from those collected from individuals affected by other neurologic diseases. Results showed that they were able to correctly identify patients affected by PD with an overall sensitivity of 88.5% and specificity of 96.9%. Moreover, kinetics parameters of the RT-QuIC reaction correlated with disease severity in the PD group [249]. An improved αS RT-QuIC assay has been developed that has similar sensitivity and specificity to the prior assays but can be performed in a shorter period of time. Moreover, it allows the quantitation of relative amounts of αS seeding activity in a very small quantity of CSF samples [250]. Finally, our research group has recently published an article showing that even olfactory mucosa

samples collected from patients with PD and MSA efficiently triggered α-synuclein aggregation by means of RT-QuIC [251], thus suggesting that such tissue can be exploited for diagnostic purposes.

The olfactory mucosa was chosen on the basis of several preliminary results obtained in the prion field. Indeed, prions were found in the olfactory neuroepithelium of CJD patients collected *post-mortem* [252] and it has been shown that olfactory mucosa (OM) was an important tissue for antemortem diagnosis of NDs based on RT-QuIC assay. Indeed, RT-QuIC analysis of OM samples collected from 43 CJD patients showed levels of PrP^{Sc} seeding activity that were orders of magnitude higher (97.5% sensitivity and 100% specificity) than those observed in the CSF collected from the same patients (77% sensitivity and 99% specificity [253].

Our group also investigated the presence of prions in OM from patients with Fatal Familial Insomnia (FFI), revealing that OM specimens collected from two patients with FFI display prion-seeding activity that is detectable by both RT-QuIC and PMCA [254]. Although FFI is a genetic disorder, the evaluation of prion seeding activity through OM analysis might be helpful in assessing the progression of the pathology and in monitoring the efficacy of therapeutical applications.

1.4.6.   Contribution of RT-QuIC and PMCA in therapeutics

PMCA and RT-QuIC methodologies have been also exploited to screen for molecules displaying anti-protein aggregation activities. Both techniques can be used to evaluate the effects and the mechanisms of inhibitors of misfolding proteins formation and propagation *in vitro*.

Indeed, RT-QuIC assay has been used to analyze the impact of specific substances (e.g. doxycycline) on the conversion and aggregation of PrP^{Sc} *in vitro* [255]. Doxycycline was added in different concentrations and at different times to the RT-QuIC reaction mix seeded with brain tissue or CSF from sCJD and control patients. They showed that the addition of doxycycline results in a dose- and time-dependent inhibition of the RT-QuIC seeding activity exerted by brain and CSF samples of patients with sCJD. In contrast, other

tested molecules (e.g. ampicillin and sucrose) did not show any effect on RT-QuIC seeded reactions.

Spillantini and colleagues set up a highly efficient PMCA for α-synuclein and tested the ability of 10 compounds with proven anti-amyloid activity to interfere with αS aggregation. They showed that αS aggregation in PMCA was strongly inhibited by Congo red, curcumin, resveratrol and to a lower extent by epigallocatechin gallate (EGCG), tannic acid and lacmoid [256].

We have also contributed to analyze the effects that 2,4-thiazolidinedione derivatives exerted on tau aggregation by means of RT-QuIC [257]. Thiazolidinediones are sulfur-containing pentacyclic compounds that gained the researcher's attention as they are widely present in nature and exhibited antimicrobial, anticonvulsant, antiviral, anticancer, anti-inflammatory and antioxidant properties, thus being involved in the control of various physiological activities [258]. In this work, one of these compounds was able to reduce tauK18 (4R) and full-length tau (2N4R) aggregation in RT-QuIC, thus demonstrating that this technique can be efficiently used for a preliminary assessment of the efficacy of anti-aggregation compounds.

AIM OF THE STUDY

Aim of my PhD work was to evaluate the ability of Real-Time Quaking Induced Conversion (RT-QuIC) technology to detect seeding activity of misfolded tau protein eventually present in peripheral tissues, such as olfactory mucosa (OM) and body fluids (urine and cerebrospinal fluid) collected from patients with primary (FTDP-17, FTD, PSP, CBD) and secondary (AD) tauopathies. Since the diagnosis of PSP and CBD is often challenging (especially in the early stages) because it might be confused with other parkinsonisms, I have included in my analysis samples belonging to patients with different synucleinopathies (MSA, PD, and DLB). In particular, I have firstly optimized RT-QuIC experimental settings for tau K18 aggregation and I have then exploited the assay for the analysis of biological samples (brain, olfactory mucosa, CSF and urine) collected from inpatients and outpatients with a clinical diagnosis of AD, PSP, CBD, FTDP-17, FTD, MSA, PD and DLB visiting Carlo Besta Institute for diagnostic or therapeutic purposes. Final RT-QuIC products have been subjected to biophysical analysis to verify whether they have acquired "strain" specific features eventually useful for stratifying patients with AD, PSP, and CBD.

MATERIALS AND METHODS

3.1. tauK18 RT-QuIC aggregation protocol optimization

Recombinant tauK18 was diluted in different reaction mixes in order to find the best RT-QuIC aggregation protocol. All reactions were supplemented with 10 µM of Thioflavin-T (ThT) as fluorescent amyloid dye. Heparin (heparin sodium salt from porcine intestinal mucosa, Sigma-Aldrich) was also added in all reaction mixes in a molar ratio heparin:tau=~1:4. tauK18 was initially diluted at a concentration of 8 µM in 1X PBS (pH 7.4, Sigma-Aldrich) or in 10 mM piperazine-N,N'-bis(2-ethanesulfonic acid) (PIPES, pH 6.5, Sigma-Aldrich) buffer and supplemented with 50 µg/ml heparin and 0.1 mM 1,4-Dithiothreitol (DTT, Sigma Aldrich). Subsequently, different biochemical and biophysical conditions were tested: i) 4 µM and 8 µM tauK18, ii) absence or presence of 0.1 mM DTT, (iii) 1' or 14' of incubation time. The resulting reaction mixes were composed as described below and summarized in Table 3.1:

- 8 µM tauK18 + 50 µg/mL heparin + 0.1 mM DTT in PBS buffer (#1 and #5);
- 4 µM tauK18 + 25 µg/mL heparin + 0.1 mM DTT in PBS buffer (#2 and #6);
- 8 µM tauK18 + 50 µg/mL heparin in PBS buffer (#3 and #7);
- 4 µM tauK18 + 25 µg/mL heparin in PBS buffer (#4 and #8).

Reactions were performed in a black 96-well optical flat bottom plate (Thermo Scientific), where each well was supplemented with 100 µL of reaction mix. The plate was sealed with a sealing film (Thermo Scientific), inserted into a FLUOstar OPTIMA microplate reader (BMG Labtech) and subjected to cycles of 1' shaking (600 rpm, double orbital) and 1' incubation at 37 °C (#1, #2, #3, #4) or 1' shaking (600 rpm, double orbital) and 14' of incubation (#5, #6, #7, #8), as described in Table 3.1.

Table 3.1 Biochemical and biophysical conditions tested during the optimization of RT-QuIC tauK18 aggregation protocol.

	1' shaking + 1' incubation		1' shaking + 14' incubation	
	+ DTT	- DTT	+ DTT	- DTT
8 μM tauK18	#1	#3	#5	#7
4 μM tauK18	#2	#4	#6	#8

Fluorescent intensities, expressed as arbitrary units (AU), were taken every 30 minutes using 450 ± 10 nm (excitation) and 480 ± 10 nm (emission) wave-lengths and plotted in a graph against time.

3.2. *In vitro* generation of tauK18, tauK19, αS, Aβ$_{1-40}$ and Aβ$_{1-42}$ PFFs

Condition #1, among the previously described in Paragraph 3.1, was chosen to generate tauK18 aggregates, named tauK18 pre-formed fibrils (tauK18 PFFs). The presence of tauK18 amyloid fibrils was confirmed by negative staining and Transmission Electron Microscopy (TEM) analysis or by classical staining with amyloid-specific dye, such as Congo Red, ThT and Thioflavin-S (ThS). tauK19 (3R-tau fragment), αS, Aβ$_{1-40}$ and Aβ$_{1-42}$ pre-formed fibrils (PFFs) were generated by diluting each recombinant protein (αS, tauK19) or synthetic protein fragment (Aβ$_{1-40}$ and Aβ$_{1-42}$) in its aggregation buffer, previously established in our laboratory. In particular, αS was diluted at 35 μM in 1X PBS buffer and supplemented with 0.1 M NaCl (Sigma) and 10 μM ThT. tauK19 (3R tau fragment) was diluted at 45 μM in 1X PBS buffer and supplemented with 50 μg/mL low molecular weight heparin (Fisher Scientific) and 10 μM ThT. Aβ$_{1-40}$ and Aβ$_{1-42}$ were diluted at 5 μM and 10 μM, respectively, in 100 mM Tris-HCl buffer (pH 7.4, Carlo Erba) and supplemented with 10 μM ThT. Each aggregation reaction was performed in RT-QuIC as previously described in Paragraph 3.1 by subjecting samples to cycles of 1' shaking and 1' incubation. The presence of amyloid fibrils in all RT-QuIC reaction products was confirmed by TEM and they were named αS PFFs, tauK19 PFFs, Aβ$_{1-40}$ PFFs, and Aβ$_{1-42}$ PFFs. Samples were diluted at a final concentration of 5 μM and used for RT-QuIC analysis. The fibril concentrations were considered to be the same as the starting monomer concentration, with the assumption of complete conversion from monomers to fibrils.

3.3. *In vitro* generation of oligomers, early-fibrils, and late-fibrils of αS and tauK18

Recombinant αS was diluted at 20 μM in ultrapure water, supplemented with 10 μM ThT and induced to self-assembly by means of RT-QuIC, as previously described in Paragraph 3.1 (cycles of 1' shaking and 1' incubation). At different time points of the aggregation kinetics, one aliquot of the reaction mix was collected and analyzed by TEM to assess the presence of oligomers and fibrils. Early-fibrils were collected during the exponential phase of αS aggregation kinetics, whereas late-fibrils were collected when the reaction reached the plateau. tauK18 oligomers, early-fibrils, and late-fibrils were also generated by inducing tauK18 self-assembly in RT-QuIC as previously described (condition #1, Paragraph 3.1) and collecting one aliquot at different time points of the aggregation kinetics. The presence of such species in tauK18 aliquots was assessed by TEM.

3.4. *In vitro* generation of different αS PFFs

Distinct αS PFFs (#1, #2, #3 and #4) were generated by diluting recombinant αS at 20 μM in different aggregation buffers, composed as follows:

- Ultrapure water (αS PFFs#1)
- 5 mM Tris-HCl (αS PFFs#2)
- 5 mM Tris-HCl + 150 mM KCl (αS PFFs#3)
- 5 mM Tris-HCl + 100 mM NaCl (αS PFFs#4)

All reactions were supplemented with 10 μM of ThT and were subjected to self-assembly in RT-QuIC, as previously described (Paragraph 3.1, cycles of 1' shaking and 1' incubation). Samples were partially digested with proteinase K (PK) and analyzed by Silver staining or visualized by TEM. αS PFFs (#1, #2, #3 and #4) were then collected and used as seed in RT-QuIC.

3.5. Amyloid-specific stainings of tauK18 PFFs

Two μL of tauK18 PFFs were deposited onto poly-l-lysine coated slides and dried at room temperature (RT). Congo Red staining solution was prepared by dissolving Congo Red (Sigma-Aldrich) at 0.5% (w/v) in 50% ethanol (EtOH). tauK18 PFFs slides were incubated

with Congo Red solution for 20' and washed quickly with 100% EtOH. Slides were dehydrated in 100% xylene two times (2' each) and coverslips were mounted with Eukitt mounting medium (Bio-Optica Milano S.p.A.). Thioflavin-S (ThS) and ThT solutions were prepared by dissolving ThS at 1% (w/v) and ThT at 1 mM in ultrapure water (Sigma). tauK18 PFFs slides were incubated with ThS and ThT solutions for 10' and washed three times with PBS 1X for 1'. Once dried at RT, coverslips were mounted using glycerol mounting medium (Merck Millipore). Bright-field images were acquired with (⊕) or without (⊖) polarizing filters at 40X magnification with a Nikon Eclipse E800 microscope equipped with Nikon digital camera DXM 1200 and Nikon ACT-1 (v2.63) acquisition software. Fluorescence images of tauK18 PFFs fibrils stained with ThT and ThS were imaged using the same microscope equipped with mercury lamp light source.

3.6. Preparation of brain samples for RT-QuIC analyses

Frontal cortices of patients with neuropathologically confirmed diagnoses of Frontotemporal dementia and parkinsonism linked to chromosome 17 associated with P301L tau mutation (FTDP-17, n=1), Progressive supranuclear palsy (PSP, n=1), Alzheimer's disease (AD, n=1), Dementia with Lewy bodies (DLB, n=1) and from a Non-demented patient (NDP, n=1) were homogenized in PBS at 10% (weight/volume) using a glass potter homogenizer. Samples were centrifuged (Eppendorf Centrifuge 5415R) at 800 × g for 1' at 4 °C to remove cellular debris. Collected supernatants were identified as brain homogenates (BH) and stored at −20 °C for RT-QuIC analysis.

3.7. Extraction of insoluble tau from brain samples

Insoluble tau was extracted from the over-mentioned brain tissue samples as previously described [89]. Briefly, approximately 200 mg of frontal cortex were homogenized at 10% (weight/volume) of extraction buffer containing: 10 mM Tris-HCl pH 7.4 (Carlo Erba), 0,8 M NaCl (Carlo Erba), 1 mM EDTA (Sigma-Aldrich), 10% sucrose (Carlo Erba), 0,1% sarkosyl (Sigma-Aldrich). Two aliquots of 900 μL for each sample were processed as follow: each aliquot was centrifuged at 10'000 × g for 10' at 4°C (Eppendorf centrifuge 5415R), pellets were re-extracted twice using 250 μL of the same extraction buffer and supernatants from

all three extractions (S1, S2, and S3) were retained and pooled. Pooled supernatants of both aliquots were collected together and sarkosyl was added to reach a final concentration of 1%. Samples were incubated for 1 hour at 37°C under rotation (TAAB rotator type N). Samples were divided in 2 aliquots of 1 mL and each aliquot was centrifuged for at 300'000 × g for 1 hour at 4°C (Beckman TLA 120.2). Each pellet was re-suspended in 100 µL of PBS 1X and briefly sonicated (sonicator Q700, Qsonica). Pellets were pooled (200 µL) and further centrifuged at 10'000 × g for 30' at 4°C to remove large debris. Supernatants containing PHF-tau were analyzed by bicinchoninic acid (BCA) assay (ThermoFisher Scientific) for total protein concentration and stored at −20 °C.

3.8. Conformational stability assay

Two hundred and fifty ng of PHF-tau extracts were denatured with the following concentrations of Guanidine hydrochloride (GdnHCl) for 30 min at 37°C: 0 M, 1 M, 2 M, and 3 M. Samples were diluted 1:3 and digested with 1 µg/µl of PK for 30' at 37°C, followed by centrifugation at 45'000 rpm for 30'. Pellets were re-suspended in 20 µL of LDS loading buffer for Western blot analysis. Densitometric analysis of PHF-tau PK resistance after denaturation with different concentrations of GdnHCl was performed using ImageJ software (1.48v).

3.9. Proteinase K digestion

Twenty microliters of final tauK18 RT-QuIC products were treated with 20 µg/mL of Proteinase K (PK, Invitrogen) for 30' at 37 °C under shaking (550 rpm). αS PFFs#1, #2, #3 and #4 were digested with 1 µg/mL of PK for 1 hour at 37 °C under shaking (550 rpm). Digestion was stopped directly by the addition of LDS-PAGE loading buffer and analyzed by Western blot or Silver staining.

3.10. Silver staining

Samples were supplemented with LDS loading buffer (Invitrogen), heated at 100 °C for 10 minutes and loaded into 12% Bolt Bis-Tris Plus gels (Invitrogen). Proteins were separated

by means of SDS-PAGE and visualized directly on polyacrylamide gels by Pierce Silver Stain Kit (ThermoFisher Scientific).

3.11. Western blotting

Samples were supplemented with LDS loading buffer (Invitrogen), heated at 100 °C for 10 minutes and loaded into 12% Bolt Bis-Tris Plus gels (Invitrogen). Proteins were separated by means of SDS-PAGE, transferred onto Polyvinylidene difluoride (PVDF) membranes (Immobilon-P, Millipore) and incubated with 5% (weight/volume) non-fat dry milk (prepared in Tris-HCl with 0.05% Tween-20) for 1 hour at room temperature under shaking. PVDF membranes were incubated overnight at 4°C under shaking with PHF-6 antibody (phosphorylated tau at Thr231 mouse monoclonal antibody, Thermo Fischer Scientific) or with RD4 antibody (4-repeat isoform tau mouse monoclonal antibody, clone 1E1/A6, Thermo Fischer Scientific) to visualize PHF-tau extracts or final RT-QuIC products, respectively. Membranes were also incubated with mouse monoclonal antibody against exosomal marker CD63 (Thermo Fischer Scientific). Finally, membranes were incubated with anti-mouse secondary antibody conjugated with horseradish peroxidase (GE) and developed with a chemiluminescent system (ECL Prime). Reactions were visualized using a G:BOX Chemi Syngene system.

3.12. Collection and preparation of olfactory mucosa samples

A total number of 24 samples of olfactory mucosa (OM) were collected from patients with clinical diagnosis of Frontotemporal dementia and parkinsonism linked to chromosome 17 associated with P301L tau mutation (FTDP-17), Progressive supranuclear palsy (PSP), Corticobasal degeneration (CBD), Alzheimer's disease (AD), genetic AD (gAD, PSEN1 mutation), Dementia with Lewy bodies (DLB), Parkinson's disease (PD), genetic PD (gPD, PARK8 subtype), Multiple system atrophy (MSA) and Multiple sclerosis (MS). The number of OM samples collected for each condition and the acronym used in this study is summarized in Table 3.2.

Before collection, the nasal cavity was treated with a topical anesthetic (Ecocain, Molteni Dental) for 10 minutes. OM were collected from the medial turbinate of each nasal cavity

using a cotton swab (FLOQSwabs^{TM} Copan Italia, Brescia, Italy) through a procedure called nasal brushing, as previously described [253, 254]. After collection, both cotton swabs were immersed in saline solution and vortexed 3 times for 1' to separate olfactory cells from the cotton swab. Suspended cells were pelleted at 800 × g for 20' at 4 °C, the supernatant was removed and OM was stored at −80 °C. For RT-QuIC analysis, approximately 2 μg of pellets were collected with the use of inoculating loops. Such material was then transferred into a tube containing 25 μL of PBS and used for RT-QuIC analyses.

Table 3.2. List of OM samples analyzed in this study, showing patient clinical diagnosis and acronym used.

Number of OM samples	Clinical diagnosis	Acronym
Primary Tauopathies		
2	Frontotemporal dementia and parkinsonisms linked to chromosome 17 (P301L mutation)	FTDP-17
4	Progressive supranuclear palsy	PSP
2	Corticobasal degeneration	CBD
Secondary Tauopathies		
2	Alzheimer's disease	AD
1	Genetic Alzheimer's disease (PSEN1 mutation)	gAD (PSEN)
Synucleinopathies		
2	Genetic Parkinson's disease (PARK8 subtype)	gPD (PARK8)
2	Parkinson's disease	PD
2	Multiple system atrophy	MSA
2	Dementia with Lewy bodies	DLB
Other conditions		
2	Multiple sclerosis	MS
Total number		
21		

3.13. Immunocytochemistry of olfactory mucosa samples

Cotton swabs immersed in saline solution were vortexed for 1' and 400 μL of suspended solution was transferred into special tubes. Sample was centrifuged (Cytospin™ 4 Cytocentrifuge Gain, Thermo Scientific) at 500 × g for 8 minutes at RT to allow the deposition of suspended cells onto slides for immunocytochemical analysis. The final

preparation was dried and fixed with 4% paraformaldehyde (4°C overnight). In order to block the action of endogenous peroxidases, slides were incubated for 15' at RT with H_2O_2 (6 %) and subsequently washed in ultrapure water (Sigma) 3 times for 5'. To permeabilize the cells, slides were coated with PBS + 0.05% Triton X-100 (Sigma-Aldrich) for 10' and then washed with PBS (3 times for 5 minutes). Sections were incubated with 10% goat serum (Normal Goat Serum, Dako) diluted in PBS for 30'. Serum was removed and sections were incubated with rabbit polyclonal antibody directed against receptors expressed by olfactory mucosa neurons (Olfactory marker protein, Abcam) overnight at RT. Samples were incubated with a biotinylated anti-rabbit secondary antibody (Vector BA- 2000) for 1 hour at RT. To increase signal detection, the ABC procedure was performed using the Vector commercial kit (VECTASTAIN® Elite® ABC-HRP Kit): slides were incubated for 45' with a solution composed of avidin and biotinylated horseradish peroxidase (HRP) and then washed one time in PBS for 5' and 2 times in distilled water for 5'. Reaction was developed with a solution of 0.05% 3-3'-diaminobenzidine (DAB - Vector Labs) containing 0.02% H_2O_2 for 2' and quickly blocked by immersing slides in distilled water. Finally, a counterstaining with Carazzi's hematoxylin was performed for about 30''. The samples were then dehydrated with serial passages in EtOH (from 70% to 100%) of 30-60'' each and immersed in 100% Xylene for 5' (2 steps). Cover slides were mounted with Eukitt (Bio Optica) and observed under an optical microscope (Nikon).

3.14. Extraction of exosomes from urine

Urine was collected from patients with a clinical diagnosis of Alzheimer's disease (AD), Frontotemporal dementia (FTD), Progressive supranuclear palsy (PSP), Corticobasal degeneration (CBD), as described in Table 3.3. Urine from four healthy subjects (HC) were also collected and used as controls. Five mL of urine was divided into ten aliquots of 0.5 mL. Each aliquot was centrifuged at 3'500 × g for 10' at 4°C to remove cellular debris and supernatants were centrifuged twice at 4'500 × g for 10' at 4°C. Supernatants of all aliquots were pooled together and PBS 1X was added to reach a final volume of 10 mL. The sample was subjected to ultra-centrifugation at 110'000 × g for 1 hour at 4°C (Beckman TLA

120.2). Fifty μL of PBS was used to re-suspend pellet. Samples were analyzed by means of Western blot as previously described using monoclonal primary antibody against the exosomal marker CD63 (ThermoFisher Scientific) or stored at -80°C for RT-QuIC analysis.

Table 3.3 List of subjects from which urinary exosomes were collected and analyzed in this study, reporting the number of samples and the acronym used.

Number of urine samples	Clinical diagnosis	Acronym
Primary Tauopathies		
3	Frontotemporal dementia	FTD
1	Progressive supranuclear palsy	PSP
1	Corticobasal degeneration	CBD
Secondary Tauopathies		
8	Alzheimer's disease	AD
Other conditions		
4	Healthy control	HC
Total number		
17		

3.15. Collection of cerebrospinal fluid samples

Cerebrospinal fluid (CSF) samples were collected from patients with a clinical diagnosis of Alzheimer's disease (AD) and from Non-demented patients (NDP) by lumbar puncture following a standard procedure. After collection, CSF was centrifuged at 1'000 × g for 10' and stored in polypropylene tubes at −80 °C until RT-QuIC analysis. The number of CSF samples for each condition and the acronym used in this study were summarized in Table 3.4.

Table 3.4 List of patients from which CSF was collected and analyzed in this study, reporting the number of samples for each condition and the acronym used.

Number of CSF samples	Clinical diagnosis	Acronym
Secondary Tauopathy		
8	Alzheimer's disease	AD
Other conditions		
8	Non-demented patient	NDP
Total number		
16		

3.16. RT-QuIC analysis of tauK18, αS, tauK19, Aβ$_{1-4o}$ and Aβ$_{1-42}$ PFFs and brain homogenates

The solution containing tauK18 PFFs was sonicated 3 times for 1' at 200 W and serially diluted (from 10^{-1} to 10^{-14} volume/volume) in its own reaction buffer. Five µL of pure or diluted tauK18 PFFs (10^{-2}, 10^{-4}, 10^{-6}, 10^{-8}, 10^{-10}, 10^{-12}, 10^{-14}) was added to 95 µL of reaction mix. In the cross-seeding experiment, five µL of each solution containing tauK18, αS, tauK19, Aβ$_{1-40}$ or Aβ$_{1-42}$ PFFs was added to 95 µL of reaction mix. Brain homogenates (BHs) from neuropathologically confirmed cases of FTDP-17, PSP, AD, DLB, and NDP were prepared as previously described (Paragraph 3.6) and diluted from 10^{-1} to 10^{-6} in 1X PBS. Two µL of pure or diluted BH (10^{-2}, 10^{-4} and 10^{-6}) was added to 98 µL of reaction mix. Condition #5, among the previously described in Paragraph 3.1, was chosen for evaluating tauK18 RT-QuIC seeding abilities of (i) tauK18 PFFs, (ii) FTDP-17, PSP, AD, DLB, and NDP BHs and (iii) αS, tauK19, Aβ$_{1-40}$ or Aβ$_{1-42}$ PFFs, with some modifications. In particular, all reagents used for the preparation of the reaction mix were filtered through a 0.22 µm filter and all RT-QuIC reactions were performed in triplicate. The average fluorescence intensity of the three replicates was calculated and resulting values were plotted in a graph against time together with standard error from the mean (±SEM).

3.17. RT-QuIC analysis of OM, urinary exosomes and CSF samples

Different amount of OM (2, 5 or 10 µL of pure or diluted 1:10 and 1:50 volume/volume samples), CSF (5 or 10 µL) and urinary exosomes (5 µL) samples was added to RT-QuIC reaction mix reaching a final volume of 100 µL in each well. RT-QuIC reaction mix was prepared as previously described (condition #5, Paragraph 3.1), with some modifications: tauK18 concentration was initially used as in condition #5 and then increased to 20 µM. Reactions with OM samples were incubated at 37°C, whereas CSF and urine exosomes were incubated at 35°C. A sample was considered "capable of seeding tauK18 aggregation" if at least 2 out 3 replicates induced the aggregation of tauK18 in RT-QuIC. The average fluorescence intensity of the two or three replicates capable of seeding activity was calculated and plotted against time together with the standard error of the

mean (±SEM). If only one (or none) of the replicates triggered tauK18 aggregation, we considered the sample as "incapable of seeding tauK18 aggregation" and the average fluorescence intensity of replicates that do not display fluorescence increasing was calculated (±SEM). Additionally, a threshold settled at 10'000 AU of fluorescence intensity and at 10 hours from the beginning of reaction was applied in the analysis of urinary exosomes and CSF samples to distinguish samples characterized by a higher seeding activity from those who triggered tauK18 aggregation with less efficiency. Samples who induced tauK18 aggregation before this threshold were considered as "positive", whereas the other samples were considered as "negative".

3.18. Transmission electron microscopy analyses

Ten μL of samples was dropped onto 200-mesh Formvar-carbon coated nickel grids for 30 minutes and dried using filter papers. The grids were subsequently stained with 25% Uranyl Acetate Replacement (UAR, negative staining, Electron Microscopy Sciences) for 10'. After this step, the remaining solution was removed using filter papers and the grids were air-dried for 15' before Transmission Electron Microscopy (TEM) analyses. Images were recorded at 120 kV with FEI Tecnai Spirit transmission electron microscope, equipped with an Olympus Megaview G2 camera.

3.19. Fourier transform infrared spectroscopy

Fourier-transform infrared (FTIR) spectroscopy was performed in attenuated total reflection (ATR) as previously reported [259]. In particular, 100 μL of final tauK18 RT-QuIC products from self-assembly and reactions seeded with tauK18 PFFs or AD, CBD, PSP and PD OM were centrifuged at 100'000 × g and the resulting pellet was re-suspended in 20 μL of 1X PBS. Two μL of sample aliquots were deposited on the single reflection (ATR-1R) or nine reflections (ATR-9R) diamond crystal of the ATR device and the FTIR spectra were collected after solvent evaporation. A 670-IR spectrometer (Varian Australia, Mulgrave, Australia) equipped with a nitrogen-cooled mercury cadmium telluride detector was used for FTIR analysis. The second derivatives of the measured spectra were obtained after Savitsky-Golay smoothing using the Resolutions-Pro software (Varian Australia).

3.20. Atomic force microscopy analysis

Final tauK18 RT-QuIC reaction products were diluted 1:1 with 10 mM HCL and analyzed by Atomic force microscopy (AFM). Briefly, twenty µL was spotted onto freshly cleaved mica (Bruker AFM probes) at RT for 5'. Samples were washed with 8 mL of ultrapure water and finally dried under gentle nitrogen flow. AFM measurements were carried out on a Multimode AFM with a Nanoscope V system operating in tapping mode, using standard antimony-doped silicon probes (Bruker AFM probes).

3.21. Statistical analyses

Graphpad Prism (v5.0) was used for all statistics and graphic representation of RT-QuIC kinetics (GraphPad Software, San Diego, California, USA). TEM images were analyzed with Gwyddion software (free software, GNU General Public License) for measuring fibrils length and cross-over periodicity. Final values were compared with a double-tailed unpaired t-test (Mann-Whitney U test).

RESULTS

4.1. Optimization of tauK18 aggregation protocol in RT-QuIC

Two different experimental conditions for tauK18 aggregation in RT-QuIC have been initially tested, in order to find the best aggregation buffer for tauK18 among the acidic PIPES (pH 6.5) and the neutral PBS buffer (pH 7.4).

An increase in fluorescence values was observed in both conditions within few hours (Fig 4.1), indicating that we have efficiently set up a protocol for tauK18 aggregation. Notably, by the use of acidic PIPES buffer (Fig 4.1, blue line) the aggregation of the protein was extremely rapid, starting within 1 hour from the beginning of the reaction and reaching the plateau almost immediately. In contrast, tauK18 self-assembly in PBS buffer (Fig 4.1, rede line) displayed the typical sigmoidal kinetics of amyloid formation, showing a lag phase of 5 hours and reaching the plateau after 20-25 hours, thus indicating that PBS might be a suitable buffer for our aggregation studies.
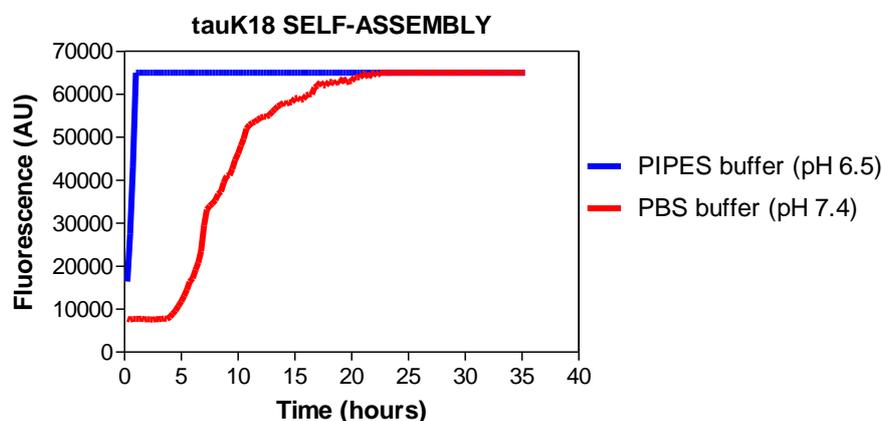
Figure 4.1 Comparison of tauK18 self-assembly in RT-QuIC using PIPES or PBS buffer.
tauK18 self-assembly in RT-QuIC using the acidic PIPES buffer (blue line) was extremely rapid, as measured by the increase in fluorescence values (AU), and its aggregation kinetics reached the plateau within 1 hour from the beginning of the reaction. Fibrillization of tauK18 using the neutral PBS buffer (red line) displayed the typical sigmoidal curve with a lag phase of 5 hours and a plateau phase reached at 20-25 hours.

The presence of amyloid fibrils in final RT-QuIC products of tauK18 self-assembly in PBS buffer (Fig. 4.1, red line) was then assessed by collecting samples at the end of the reaction and performing TEM analysis and staining with amyloid-specific dyes, such as Congo Red, ThT and ThS.
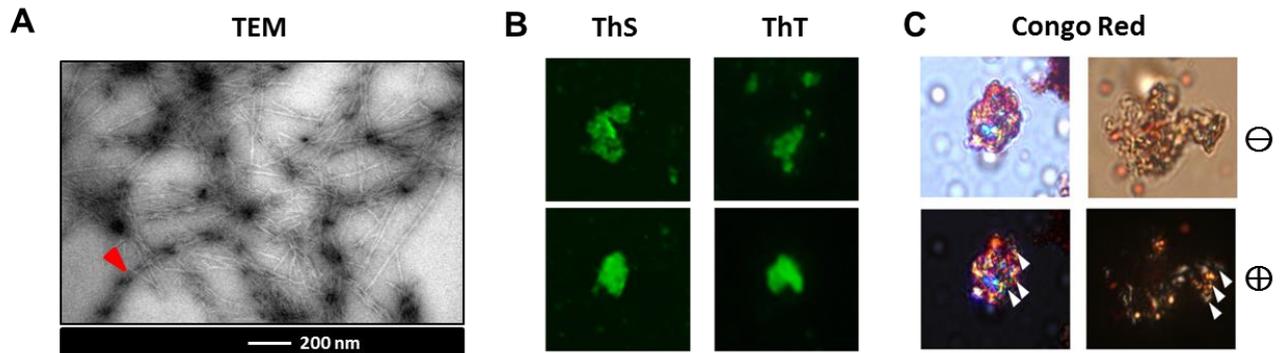
Figure 4.2 Characterization of final RT-QuIC products of tauK18 self-assembly in PBS buffer.
A) TEM analysis of final RT-QuIC products of tauK18 self-assembly in PBS buffer showed the presence of an intricate tangle of amyloid fibrils. Some pair twisted protofilaments were also observed (red arrow); B) ThS and ThT staining of final aggregates displayed the presence of β-sheet structures as a strong fluorescence signal was detected at approximately 482 nm when samples were excited at 450 nm; C) Congo Red staining showed the presence of amyloid-like aggregates characterized by an orange-red appearance under light microscopy (⊖) and apple-green birefringence under polarized light (⊕, white arrow); B) and C) images were acquired at 40X of magnification .

As showed in Fig. 4.2A, TEM analysis displayed the presence of well-structured fibrils forming an intricate tangle. Some fibrils were found to be composed of two twisted protofilaments (Fig. 4.2A, red arrow) and resembled the disposition acquired by tau fibrils in Paired Helical Filaments (PHFs) observed in AD brains.

Similarly, ThS and ThT dyes positively stained aggregates characterized by a strong green fluorescence signal (Fig. 4.2B), indicating the presence of β-sheet structures. Congo Red staining confirmed the presence of amyloid aggregates with typical apple-green birefringence under polarized light (Fig.4.2C, ⊕) that disappears with un-polarized light (Fig.4.2C, ⊖). Therefore, we decide to perform our tauK18 aggregation studies by using PBS buffer and we collected final RT-QuIC products of the reaction, named tauK18 preformed fibrils (tauK18 PFFs), for seeding studies.

In order to slow down tauK18 self-assembly to eventually observe an acceleration of its aggregation kinetics in seeding assays, a set of experimental conditions were tested. In particular, (i) we decreased the concentration of the protein (from 8 μM to 4 μM), (ii) we excluded DTT from the reaction mix and (iii) we prolonged the incubation time, thus reducing the total number of shakings. Combination of these modifications resulted in four reaction mixes (see Materials and methods for details, paragraph 3.1) that were subjected to cycles of 1' shaking and 1' incubation (Fig 4.3A, named #1, #2, #3, #4) or to cycles of 1' shaking and 14' incubation (Fig 4.3B, named #5, #6, #7, #8) in RT-QuIC.
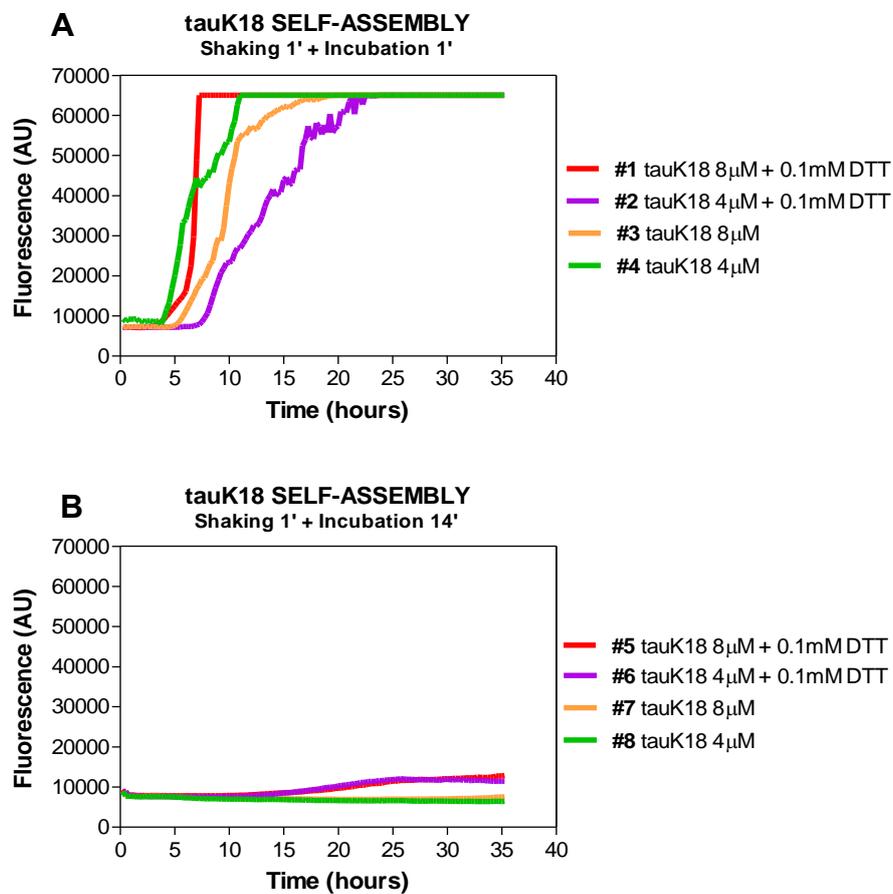
Figure 4.3 Evaluation of tauK18 self-assembly in RT-QuIC under different experimental settings.
Four tauK18 reaction mixes were subjected to A) cycles of 1' shaking and 1' incubation, showing in all conditions a rapid aggregation of the protein as indicated by increase in fluorescence at 4 (#1 and #4), 5 (#3) and 7 hours (#2) from the beginning of the reaction; B) 1' shaking and 14' incubation, displaying a slower aggregation kinetics in all conditions characterized by no (#7 and #8) or very little (#5 and #6) increase in fluorescence values after 20 hours.

We observed that, despite the biochemical condition used, the extension of incubation time from 1' to 14' (Fig. 4.3B) almost abolished tauK18 self-assembly as indicated by no (#7 and #8, orange and green lines) or very little increase in fluorescence values after approximately 20 hours (#5 and #6, red and purple lines). In contrast, cycles of 1' shaking and 1' incubation (Fig. 4.3A) induced a very rapid aggregation of the protein as indicated by increase in fluorescence at 4 (#1 and #4, red and green lines), 5 (#3, orange line) and 7 hours (#2, purple line) from the beginning of the reaction.

Given that we need a slow self-assembly kinetics to perform seeding experiments, cycles of 1' shaking and 14' incubations (Fig. 4.3B) were chosen as experimental setting for our tauK18 seeding assays in RT-QuIC.

4.2. Evaluation of PFFs seeding activity for tauK18 in RT-QuIC

We evaluated the ability of tauK18 PFFs to promote or accelerate tauK18 aggregation kinetics in RT-QuIC when added at the beginning of the reaction in conditions #5, #6, #7 and #8. To this aim, 10 μL or 5 μL of tauK18 PFFs (which were estimated to contain aggregates in the range of micrograms and nanograms, respectively) were added to four new reaction mixes and their aggregation kinetics were compared to the self-assembly of tauK18 (Fig. 4.4).

Results showed a strong increase in fluorescence within few hours after the addition of tauK18 PFFs (both nanograms and micrograms) in all experimental conditions indicating a strong seeding ability of PFFs in our RT-QuIC assay (Fig. 4.4).

In particular, in condition #5, tauK18 PFFs showed the highest seeding efficiency, reaching the plateau within 1 and 3 hours from the beginning of the assay (Fig. 4.4, red and light red lines). In conditions #6, #7 and #8, the plateau was reached between 5 and 10 hours (Fig. 4.4, orange, purple and green lines). Notably, in condition #8 kinetics of seeded samples reached fluorescence values between 30'000 and 40'000 AU (Fig. 4.4, green and light green lines), which were lower if compared to the other conditions, characterized by fluorescence values above 60'000 AU (Fig. 4.4, red, orange and purple lines).
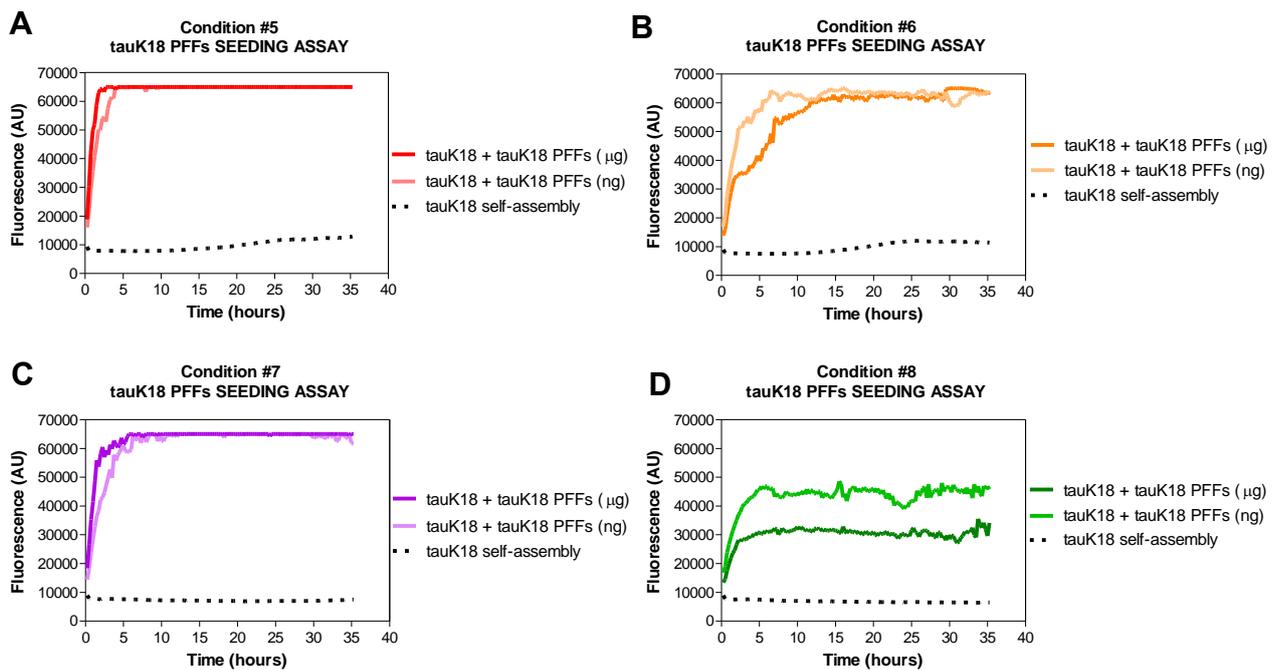
Figure 4.4 Evaluation of tauK18 PFFs seeding assay in RT-QuIC under different experimental conditions
A-D) tauK18 aggregation was induced almost instantly by the addition of micrograms or nanograms of tauK18 PFFs (colored lines) in all conditions, whereas no aggregation or very little increase in fluorescence values was observed in self-assembly reactions (black dotted line). However, the aggregation kinetics in seeded reactions displayed some differences among the condition tested: A) in condition #5, seeded reactions (red an light red lines) reached the plateau within 1 and 3 hours; B, C, and D) in condition #6, #7 and #8, tauK18 aggregation kinetics (orange, purple and green lines) reached the plateau phase between 5 and 10 hours; D) in condition #8, tauK18 aggregation kinetics reached lower fluorescence levels at the plateau (between 30'000 and 40'000 AU) if compared to the other conditions (above 60'000 AU).

Given that in condition #5 tauK18 PFFs showed the highest seeding efficiency, this experimental setting was chosen for our tauK18 seeding assays in RT-QuIC.

In particular, we evaluated whether the addition of lower amounts of PFFs was still able to promote tauK18 aggregation and whether this acceleration might show a dose-dependent response. To this aim, tauK18 PFFs were serially diluted, ranging from nanograms to attograms, and each dilution was added in triplicate to a new reaction mix in RT-QuIC.

tauK18 PFFs SEEDING ASSAY

Legend:
- tauK18 + tauK18 PFFs (500 ng)
- tauK18 + tauK18 PFFs (5 ng)
- tauK18 + tauK18 PFFs (500 pg)
- tauK18 + tauK18 PFFs (5 pg)
- tauK18 + tauK18 PFFs (500 fg)
- tauK18 + tauK18 PFFs (5 fg)
- tauK18 + tauK18 PFFs (500 ag)
- tauK18 + tauK18 PFFs (5 ag)
- tauK18 self-assembly
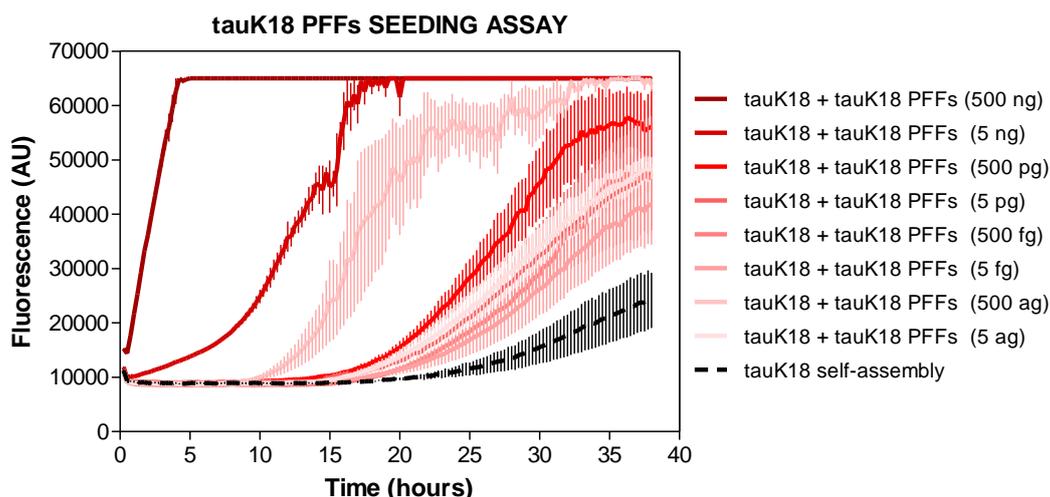
Figure 4.5 Evaluation of the seeding activity of different amounts of tauK18 PFFs in RT-QuIC.
tauK18 aggregation kinetics in RT-QuIC was accelerated by the addition of all the amounts of PFFs tested (colored lines), whose mass was estimated to be in the range of nanograms (brown and dark red lines) to attograms (pink and light pink lines). tauK18 PFFs seeding activity was almost proportional to the amount of seeds added, as indicated by the proportional decrease in lag phases if compared to the self-assembly of the protein (black dotted line). Reactions were performed in triplicate and the average fluorescence intensities were plotted against time (±SEM).

As shown in Fig. 4.5, all PFFs dilutions (colored lines) efficiently accelerated tauK18 aggregation in RT-QuIC if compared to the self-assembly of the protein (black dotted line), indicating that attograms of tauK18 PFFs were still capable of seeding activity in our assay (pink and light pink lines).

Interestingly, the seeding effect was almost proportional to the amount of seeds added. Indeed, the addition of 500 ng of PFFs instantly induced the aggregation of tauK18 (brown line), whereas tauK18 fibrillization in the presence of 50 ng and 500 pg of PFFs displayed a lag phase of 5 hours (dark red line) and 15 hours (red line), respectively. Similarly, the addition of 5 pg, 500 fg and 5 fg of PFFs induced the aggregation of tauK18 at 17, 18 and 19 hours from the beginning of the reaction, respectively (light red lines). Conversely, samples seeded by 500 ag and 5 ag of PFFs (pink and light pink lines) were characterized by a shorter lag phase (10 and 16 hours) if compared to the seeding activity of higher amounts of seeds.

Therefore, with our experimental setting, we were able to observe an acceleration of tauK18 aggregation kinetics after the addition of attograms of tauK18 PFFs in RT-QuIC.

77

4.3. RT-QuIC analysis of brain homogenates collected from patients with primary and secondary tauopathies

Considering the high level of RT-QuIC sensitivity, we decided to verify its ability to detect pathological tau aggregates present in neuropathologically confirmed brain samples of patients with AD, FTDP-17, and PSP. Brains from a Non-demented patient (NDP) and from a neuropathologically confirmed case of DLB were used as controls.

Firstly, we evaluated the presence of insoluble tau associated with the presence of PHFs in those brains, named PHF-tau. Brain samples were homogenized and subjected to serial steps of high-speed centrifugation in order to isolate insoluble PHF-tau aggregates.

Western blot analyses confirmed the presence of insoluble PHF-tau only in brain homogenates of patients with AD, PSP, and FTDP-17 (Fig. 4.6A). Indeed, as previously described in Paragraph 1.2, Western blot of PHF-tau showed the presence of the typical AD-triplet at 60, 64 and 69 kDa (tau60, 64 and 69) in AD brain and the typical PSP-doublet at 60 and 64 kDa (tau60, 64) in the PSP case. Moreover, the same tau doublet (tau60, 64) was detected in the FTDP-17 brain, which is in line with insoluble tau usually found in cases associated with P301L tau mutation. No insoluble PHF-tau was detected in DLB and NDP brains (Fig. 4.6A).

Preliminary TEM analysis also showed the presence of fibrils in PHF-tau extracted from AD, PSP and FTDP-17 brains, which seemed to be characterized by different sizes and morphologies (Fig.4.6B). Additionally, conformational stability assay showed that PHF-tau extracts from AD and FTDP-17 cases possessed an overall higher resistant to GdnHCl denaturation if compared to PSP samples, thus suggesting the presence of different conformations of insoluble PHF-tau in our brain extracts (Fig. 4.6C).
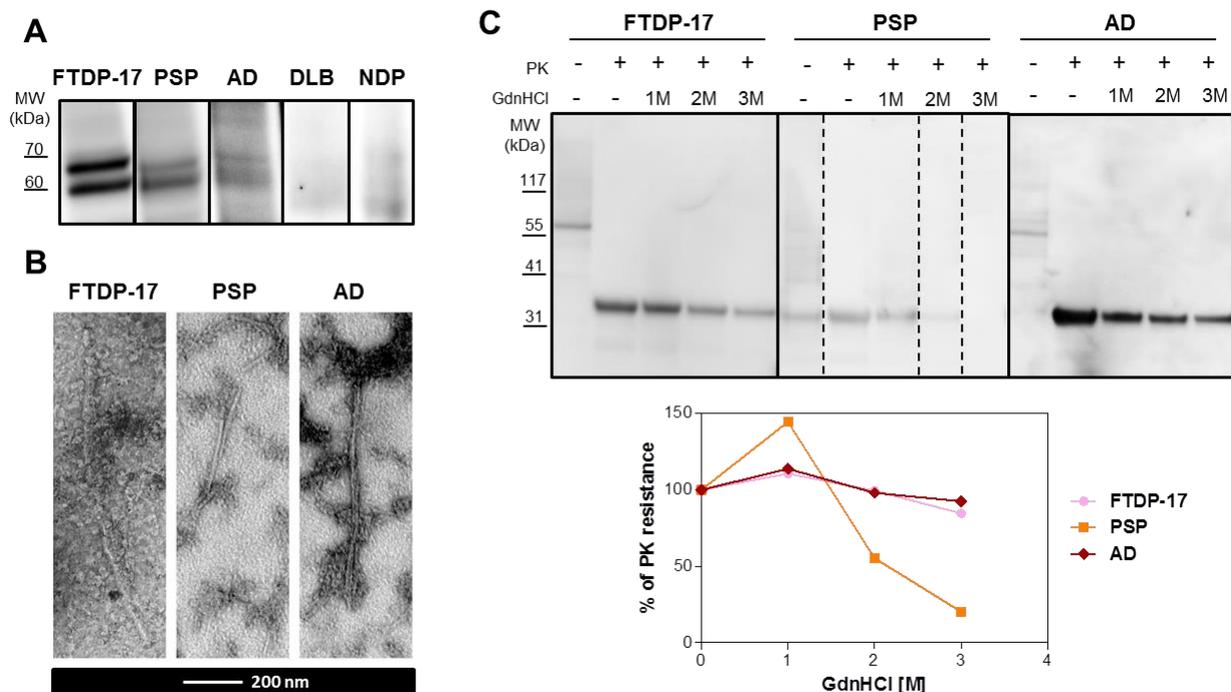
Figure 4.6 Characterization of PHF-tau extracts from FTDP-17, PSP and AD brains.
A) The presence of insoluble PHF-tau in brains of patients with tauopathies were confirmed by Western blot analysis using PHF-6 antibody, showing the typical tau doublet in FTDP-17 and PSP (migrating at 60 and 64 kDa) and the typical tau triplet (at 60, 64 and 69 kDa) in the AD sample. B) TEM analysis of PHF-tau extracts revealed the presence of fibrils in PHF-tau extracted from FTDP-17, PSP and AD samples. C) Western blot and densitometric analysis of the conformational stability assay of insoluble PHF-tau showed that FTDP-17 and AD extracts possess an overall higher resistance to denaturation if compared to PSP. Dashed lines indicate cropped images from distant samples in the same gel.

Therefore, the same brain homogenates (BH) were analyzed by means of RT-QuIC to evaluate their ability to induce tauK18 aggregation. As shown in Fig. 4.7A, brain samples from AD (brown line), PSP (orange line) and FTDP-17 (pink line) cases efficiently accelerated tauK18 aggregation kinetics in RT-QuIC. NDP BH (green line) also induced a slight increase in tauK18 aggregation, however, its seeding activity was less efficient if compared to tauopathies samples. Interestingly, DLB sample seemed to delay tauK18 aggregation (blue line).

A   **BH SEEDING ASSAY**

Legend:
- tauK18 + FTDP-17 BH
- tauK18 + PSP BH
- tauK18 + AD BH
- tauK18 + NDP BH
- tauK18 + DLB BH

B   **Comparison between tauopathies and non-tauopathies**

Legend:
- tauopathies
- non-tauopathies
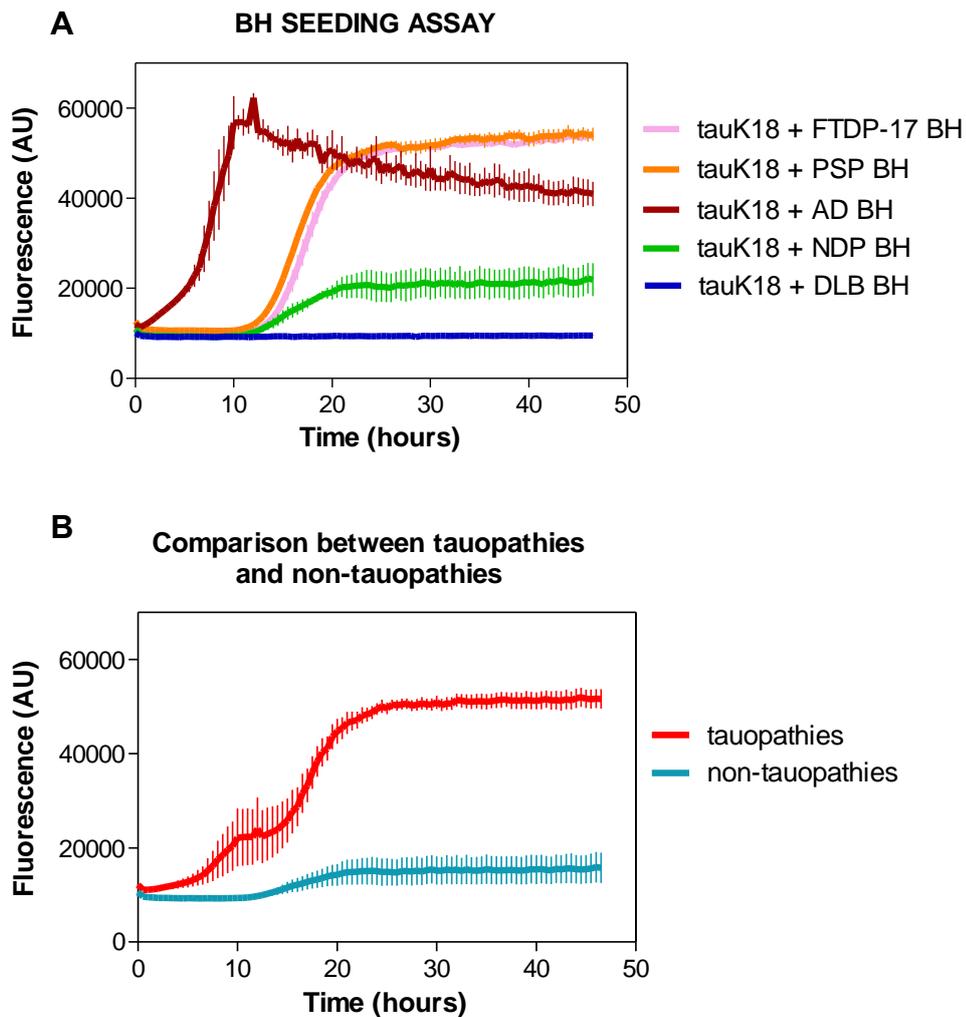
Figure 4.7 RT-QuIC analysis of brain homogenates from patients with definite diagnosis of primary and secondary tauopathies, compared to non-tauopathies cases.

A) tauK18 aggregation was efficiently induced in RT-QuIC by the addition of BH from neuropathologically confirmed cases of AD, PSP and FTDP-17: AD BH sample (brown line) triggered the aggregation almost immediately, whereas PSP (orange line) and FTDP-17 (pink line) BH samples were characterized by a lag phase of 12 and 14 hours, respectively. A slight aggregation of the protein was observed after the addition of NPD BH (green line), whereas no increase in fluorescence was detected in the DLB BH sample (blue line). B) Comparison between aggregation kinetics of tauopathies (red line) and non-tauopathies (navy blue line) BH samples, showing that tauopathies were the most efficient in triggering tauK18 aggregation in RT-QuIC. Reactions were performed in triplicate and the average fluorescence intensities were plotted against time (±SEM).

By analyzing aggregation kinetics of tauopathies and comparing them with non-tauopathies samples (Fig. 4.7B), it is clearly visible that tauopathies (red line) triggered the aggregation of tauK18 with higher efficiency if compared to the others BH (Fig. 4.7B, navy blue line).

Thus, our tauK18 RT-QuIC assay was able to detect tau seeding activity in brain homogenates collected from patients with primary and secondary tauopathies.

Additionally, we evaluated the ability of our assay in detecting pathological tau aggregates present in serial dilutions of brain samples to assess its sensitivity.

Similar results were obtained by adding BHs diluted at 10^{-2} (volume/volume), even if the efficiency of tauopathies in triggering tauK18 aggregation was less evident. Indeed, all samples induced tauK18 aggregation (Fig. 4.8A), with FTDP-17 and PSP samples reaching significantly higher fluorescence values. However, AD BH even delayed tauK18 aggregation. When fluorescence intensities of tauopathies samples were pooled together (Fig. 4.8B), we still observed differences in tauK18 aggregation kinetics between tauopathies and non-tauopathy samples (NDP and DLB), thus allowing us to distinguish between these conditions.

Conversely, when we tested higher dilutions of BH samples, these differences were no more visible. Indeed, all BH samples diluted at 10^{-4} and 10^{-6} displayed the same seeding activity on tauK18 aggregation and all kinetics were comparable in time and in fluorescence values reached (Fig. 4.8C and E). The lack of differences was clearly visible also by pooling together all tauopathies and comparing them to non-tauopathy samples (Fig. 4.8D and F).

4.4. RT-QuIC analysis of OM collected from patients with tauopathies

Given that our tauK18 RT-QuIC assay was able to detect tau seeding activity in brain homogenates collected from patients with definite diagnosis of primary and secondary tauopathies, we decide to evaluate seeding activity of olfactory mucosa (OM) samples from patients with a clinical diagnosis of AD, PSP, CBD and FTDP-17 and to compare them to OM samples from patients with clinical diagnosis of synucleinopathies (PD, DLB and MSA) and Multiple sclerosis (MS).
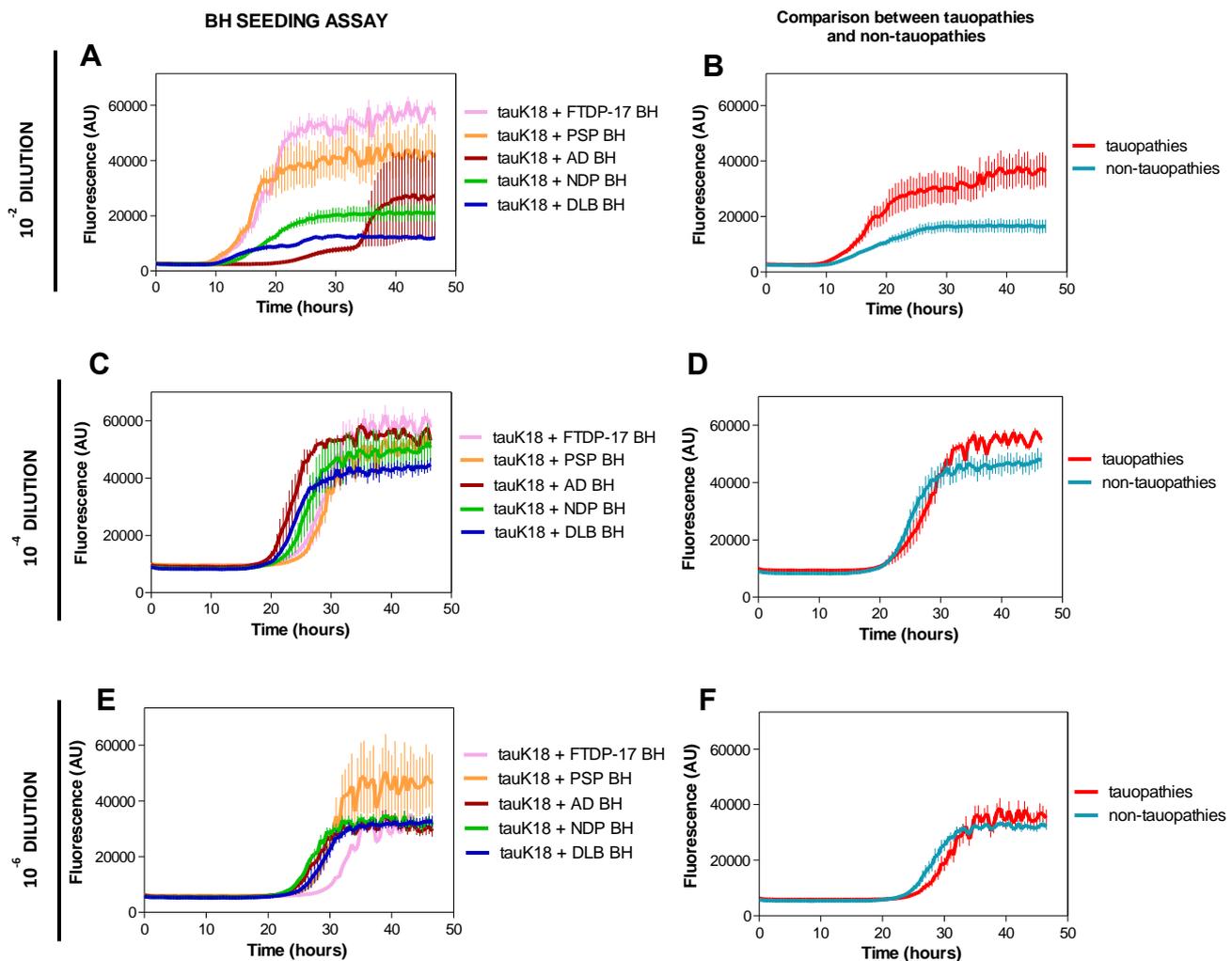
Figure 4.8 RT-QuIC analysis of serial dilutions of brain homogenates from patients with definite diagnosis of primary and secondary tauopathies, compared to non-tauopathies cases.
A) BH collected from patients with tauopathies and diluted at 10^{-2} (volume/volume) were less efficient than pure BH in seeding tauK18 aggregation, however B) they reached higher fluoresce levels if compared to non-tauopathy cases. C) and E) all BH samples diluted at 10^{-4} and 10^{-6} displayed the same seeding activity on tauK18 aggregation in RT-QuIC, as indicated by pooling aggregation kinetics of tauopathies samples and comparing them to non-tauopathy cases (D and F). Reactions were performed in triplicate and the average fluorescence intensities were plotted against time (±SEM).

OM were collected with a non-invasive procedure, called nasal brushing, depicted in Fig. 4.9A. First of all, we assessed the presence of olfactory neurons in OM samples by depositing collected cells (Fig. 4.9B) on microscope glass slides. Immunocytochemistry revealed the presence of olfactory neurons (red arrow, Fig. 4.9C), which were immunoreactive to olfactory marker protein antibody and were characterized by the

presence of spheroidal soma and long axons. Supporting cells (Fig. 4.9C) were also visible as they were characterized by an ellipsoidal nucleus, elongated soma, and numerous thin microvilli.
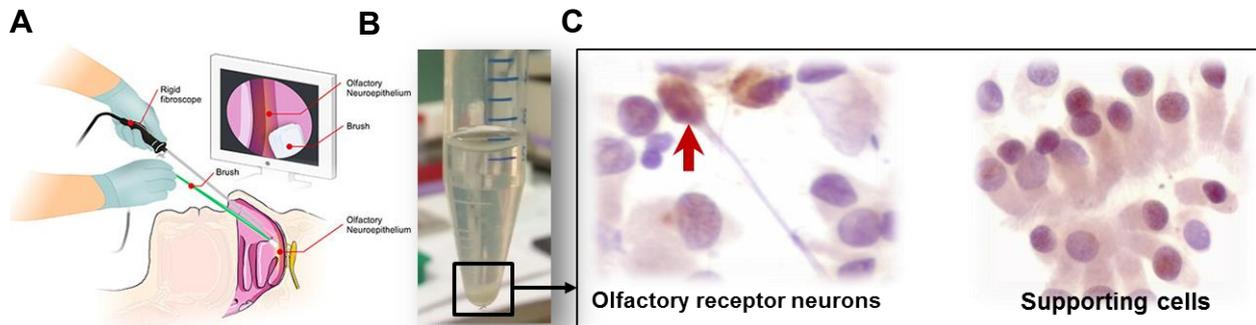

Figure 4.9 Collection and immunocytochemistry of olfactory mucosa (OM) samples.
A) OM can be obtained by a non-invasive procedure, known as nasal brushing, in which a cotton swab was rubbed against the medial turbinate of the nasal cavity. B) OM cells were released from the cotton swab by vortexing and were precipitated by centrifugation. C) The presence of olfactory receptor neurons (red arrow) and supporting cells was confirmed by hematoxylin staining and immunocytochemistry using the olfactory marker protein antibody.

In a preliminary experiment, different volumes of OM samples collected from patients with a clinical diagnosis of FTDP-17 (n=2), PSP (n=1), CBD (n=1) and AD (n=3) were tested in order to find the best experimental setting for our OM RT-QuIC assay. As shown in Fig. 4.10, few OM displayed seeding activity on tauK18 aggregation. In particular, by adding 2 µL of OM, tauK18 aggregation was slightly induced only by AD OM#3 sample (brown line) after 80 hours from the beginning of the reaction.

The addition of 5 µL of OM efficiently triggered tauK18 aggregation in one CBD sample (OM#1, purple line), reaching fluorescence values above 7'000 AU. No seeding activity has been observed in any of the reaction mixes supplemented with 10 µL of OM. Thus, we considered 5 µL of OM as a suitable volume for our tauK18 RT-QuIC assay.

OM SEEDING ASSAY

A   2 μL

- tauK18 + CBD OM#1
- tauK18 + PSP OM#1
- tauK18 + FTDP-17 OM#1
- tauK18 + FTDP-17 OM#2
- tauK18 + AD OM#1
- tauK18 + AD OM#2
- tauK18 + AD OM#3

B   5 μL

- tauK18 + CBD OM#1
- tauK18 + PSP OM#1
- tauK18 + FTDP-17 OM#1
- tauK18 + FTDP-17 OM#2
- tauK18 + AD OM#1
- tauK18 + AD OM#2
- tauK18 + AD OM#3

C   10 μL

- tauK18 + CBD OM#1
- tauK18 + PSP OM#1
- tauK18 + FTDP-17 OM#1
- tauK18 + FTDP-17 OM#2
- tauK18 + AD OM#1
- tauK18 + AD OM#2
- tauK18 + AD OM#3
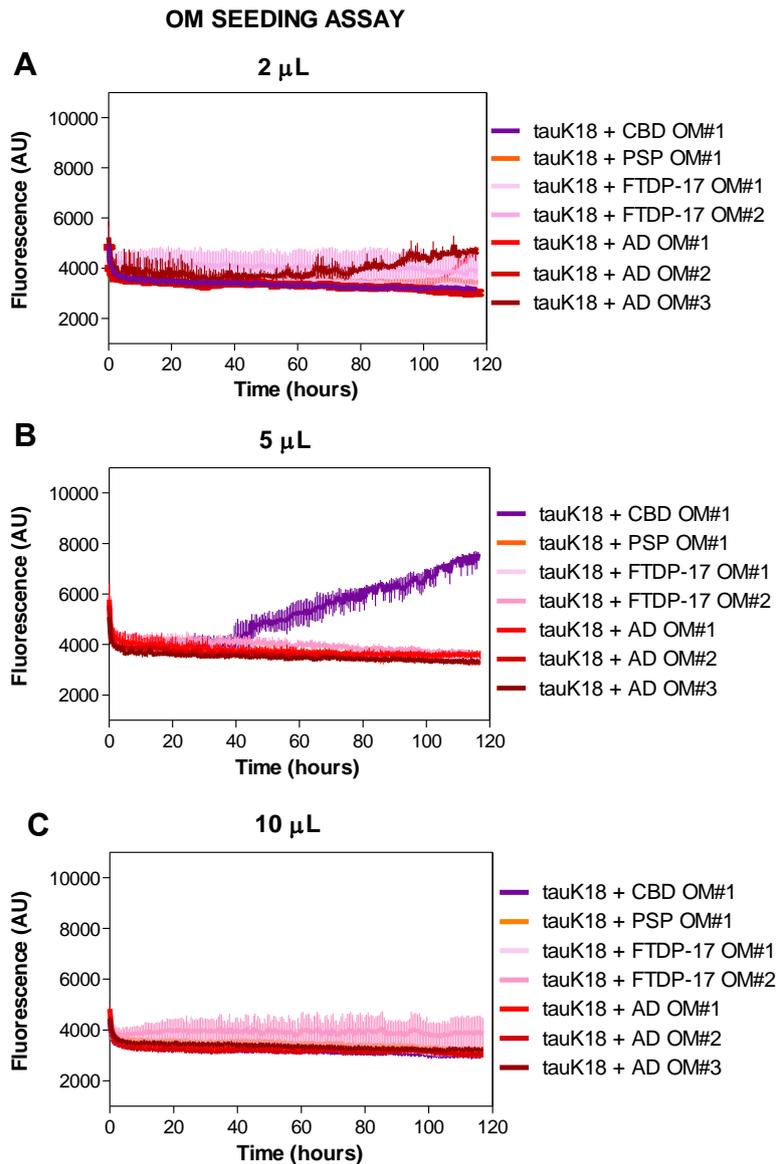
Figure 4.10 Optimization of RT-QuIC analysis of OM samples, evaluating the effect exerted by the addition of different volumes of OM collected from patients with clinical diagnosis of primary and secondary tauopathies.
A) The addition of 2 μL of OM samples from patients with CBD (OM#1, purple line), PSP (OM#1 dark orange line), FTDP-17 (OM#1 and OM#2, pink and light pink lines) and AD (OM#1, OM#2 and OM#3, red, dark red and brown lines) did not efficiently induce tauK18 aggregation, as only a slight increase in fluorescence was observed in the AD OM#3 sample (brown line) after 80 hours from the beginning of the reaction. B) tauK18 aggregation was significantly induced by the addition of 5 μL of OM collected from one CBD case (OM#1, purple line), whereas no seeding activity has been observed in the other samples. C) No increase in fluorescence was detected after the addition of 10 μL of OM collected from CBD, PSP, FTDP-17, and AD cases. Reactions were performed in triplicate and the average fluorescence intensities were plotted against time (±SEM).

Given the overall low level of tauK18 aggregation in this preliminary experiment, presumably due to the presence of OM components able to interfere with tauK18 aggregation, we decide to modify the experimental setting in order to increase sensitivity and specificity of our RT-QuIC assay: (i) we increased tauK18 concentration to 20 μM to provide an higher amount of substrate available for the conversion in RT-QuIC and (ii) we diluted OM samples 1:10 to decrease the concentration of OM constituents that might interfere with tauK18 aggregation in RT-QuIC.

With this new experimental setting, we evaluated tauK18 seeding ability of OM samples collected from patients with a clinical diagnosis of FTDP-17 (n=2), CBD (n=2), PSP (n=4), gAD (PSEN, n=1), AD (n=1), gPD (PARK8, n=2), PD (n=1) and MS (n=2).

OM SEEDING ASSAY

Legend:
- tauK18 + CBD OM#1
- tauK18 + CBD OM#2
- tauK18 + PSP OM#1
- tauK18 + PSP OM#2
- tauK18 + PSP OM#3
- tauK18 + PSP OM#4
- tauK18 + gAD OM#1
- tauK18 + AD OM#1
- tauK18 + FTDP-17 OM#1
- tauK18 + FTDP-17 OM#2
- tauK18 + gPD OM#1
- tauK18 + gPD OM#2
- tauK18 + PD OM#1
- tauK18 + MS OM#1
- tauK18 + MS OM#2
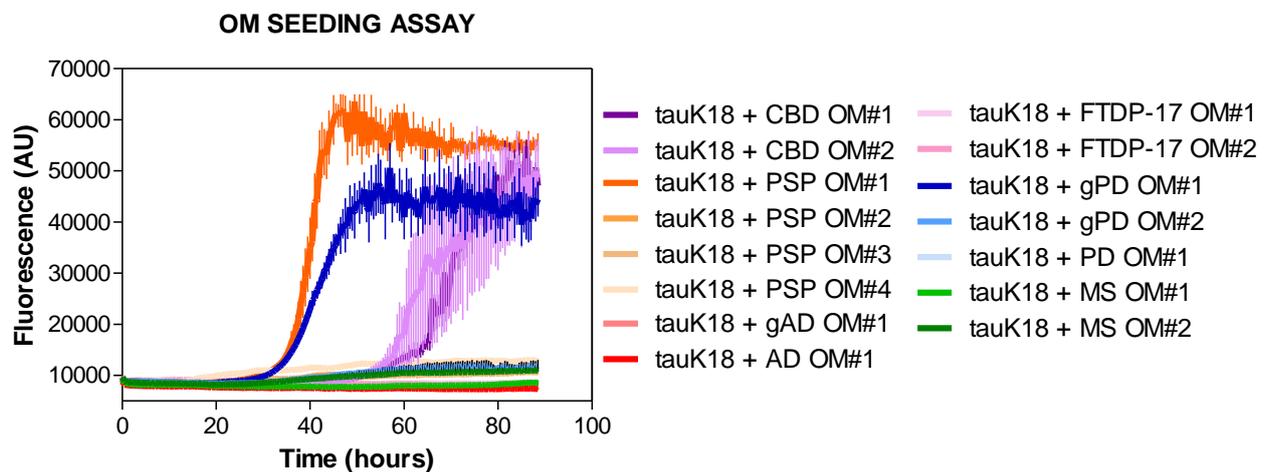
Figure 4.11 RT-QuIC analysis of OM collected from patients with clinical diagnosis of primary and secondary tauopathies, compared to synucleinopathies and Multiple sclerosis OM samples.
The addition of OM collected from 2 CBD (OM#1 and OM#2, purple and light purple lines), PSP OM#1 (dark orange line) and 1 gPD (OM#1, dark blue line) efficiently triggered tauK18 aggregation in RT-QuIC, reaching fluorescence values above 40'000 AU and displaying a lag phase of 30 hours (PSP and gPD) and 50 hours (CBD). 3 PSP (OM#2, OM#3 and OM#4, orange, light orange, and dark yellow lines), 1 gPD (OM#2, blue line) and 1 MS (OM#2, dark green line) samples induced a slight increase in fluorescence values (between 10'000 and 15'000 AU). All FTDP-17 (OM#1 and OM#2, pink and light pink lines) and AD (gAD and AD, red and light red lines) samples, together with 1 PD (light blue line) and 1 MS (OM#1, light green line), were not able to trigger tauK18 aggregation. Reactions were performed in triplicate and the average fluorescence intensities were plotted against time (±SEM).

Thanks to this new experimental setting, some OM triggered the aggregation of tauK18 with high efficiency (Fig. 4.11). In particular, 1 PSP (OM#1, dark orange line), 2 CBD (OM#1 and OM#2, purple and light purple lines) and 1 gPD (OM#1, dark blue line) OM induced tauK18 aggregation reaching fluorescence intensities above 40'000 AU. Some OM samples, such as 3 PSP (OM#2, OM#3 and OM#4, orange, light orange and dark yellow lines), 1 gPD (OM#1, blue line) and 1 MS (OM#2, dark green line), were less efficient in triggering tauK18 aggregation and induced a slight increase in fluorescence values (between 10'000 and 15'000 AU). Among OM samples that triggered the aggregation, one group (3 PSP, 2 gPD, 1 PD and 1 MS) displayed seeding activity between 20 and 30 hours from the beginning of the reaction, whereas a second group composed by 2 CBD samples seeded the aggregation after 50 hours. Conversely, all FTDP-17 (OM#1 and OM#2, pink and light pink lines) and AD (AD OM#1 and gAD OM#1, red and light red lines) OM, together with 1 PD (OM#1, light blue line) and 1 MS (OM#1, light green line), were not able to trigger tauK18 aggregation as no increase in fluorescence values was detected in those samples.

Given the low specificity of our tauK18 RT-QuIC assay, we decide to further dilute OM samples from 1:10 to 1:50 (volume/volume) to decrease the amount of OM molecules potentially able to influence tauK18 aggregation in RT-QuIC.

Additionally, we noticed that OM samples from atypical parkinsonisms (PSP, CBD, and PD) have shown a greater seeding activity in our experimental conditions if compared to AD and FTDP-17 samples. Therefore, we have decided to focus our attention on this group of diseases with the aim of recognizing parkinsonian syndromes associated with tau pathology and to distinguish them from those associated with α-synuclein (αS) accumulation. Thus, we tested OM samples from PSP (n=4), CBD (n=2) and PD (n=2) and we included other parkinsonian syndromes, such as MSA (n=2) and DLB (n=2).

Results are reported in Fig. 4.12 and showed that several OM samples triggered in tauK18 aggregation in RT-QuIC.

OM SEEDING ASSAY

Legend:
- tauK18 + PSP OM#1
- tauK18 + PSP OM#2
- tauK18 + PSP OM#3
- tauK18 + PSP OM#4
- tauK18 + CBD OM#1
- tauK18 + CBD OM#2
- tauK18 + PD OM#1
- tauK18 + PD OM#2
- tauK18 + MSA OM#1
- tauK18 + MSA OM#2
- tauK18 + DLB OM#1
- tauK18 + DLB OM#2
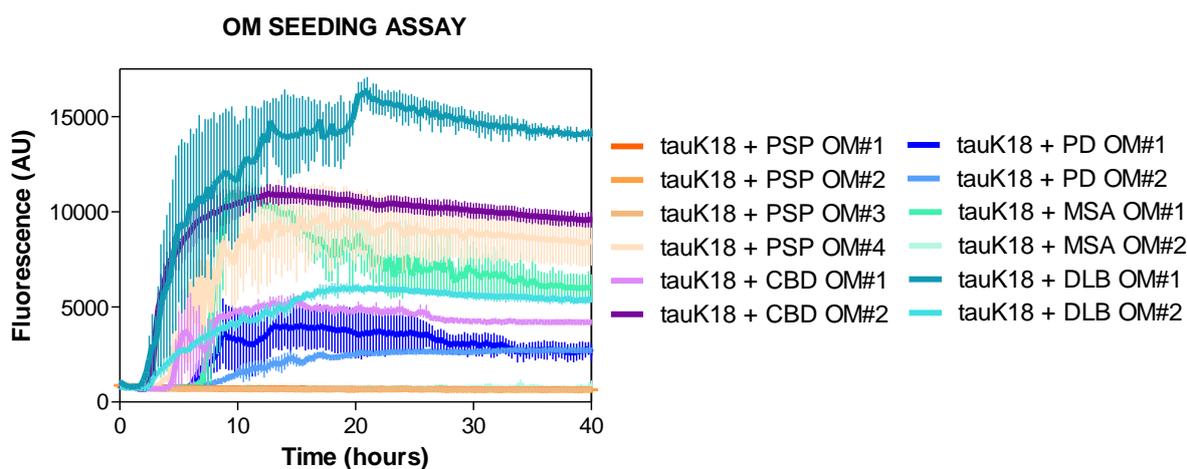
Figure 4.12 RT-QuIC analysis of OM collected from patients with clinical diagnosis of atypical parkinsonisms and Parkinson's disease.
tauK18 aggregation was efficiently induced by 2 CBD (OM#1 and OM#2, purple and light purple lines), 1 PSP (OM#4, dark yellow line), 1 MSA (OM#1, turquoise line), 2 PD (OM#1 and OM#2, blue and light blue lines) and 2 DLB (OM#1 and OM#2, navy blue and light navy blue lines) samples. No seeding activity was detected after the addition of 3 PSP (OM#1, OM#2 and OM#3, dark orange, orange, and light orange lines) and 1 MSA (OM#2, light turquoise line) samples. Reactions were performed in triplicate and the average fluorescence intensities were plotted against time (±SEM).

Indeed, tauK18 aggregation was efficiently induced by OM samples from 2 CBD (OM#1 and OM#2, purple and light purple lines), 1 PSP (OM#4, dark yellow line), 1 MSA (OM#1, turquoise line) 2 PD (OM#1 and OM#2, blue and light blue lines) and 2 DLB (OM#1 and OM#2, navy blue and light navy blue lines). An increase in fluorescence values was observed almost instantly in samples seeded with DLB and CBD OM. Conversely, no seeding activity was detected after the addition of 3 PSP (OM#1, OM#2 and OM#3, dark orange, orange, and light orange lines) and 1 MSA (OM#2, light turquoise line) OM, as no increase in fluorescence values was observed in those samples.

In order to improve the sensitivity and specificity of our tauK18 RT-QuIC assay, we decide to further decrease the volume of OM seed to reduce cross-seeding activity eventually exerted by other protein aggregates (e.g. α-synuclein) or by other molecules present in OM samples.

Thus, we added 2 μL of OM to a new reaction mix to test the effect of the same OM samples on tauK18 aggregation. Results (Fig. 4.13A) showed that tauK18 aggregation was triggered unspecifically by OM samples of both synucleinopathies and tauopathies. Indeed, tauK18 aggregation was accelerated by 1 CBD (OM#1, purple line), 2 PSP (OM#1 and OM#3, dark orange and light orange lines), 2 MSA (OM#1 and OM#2, turquoise and light turquoise lines) and 2 DLB samples (OM#1 and OM#2, navy blue and light navy blue lines). PD OM samples (OM#1 and OM#2, blue and light blue lines) in this case did not display tauK18 seeding activity. Conversely, 1 MSA (OM#2, light turquoise) and 2 DLB OM were the most efficient in seeding the reaction (within 10 hours) and fluorescence intensities reached the highest values if compared to other samples.
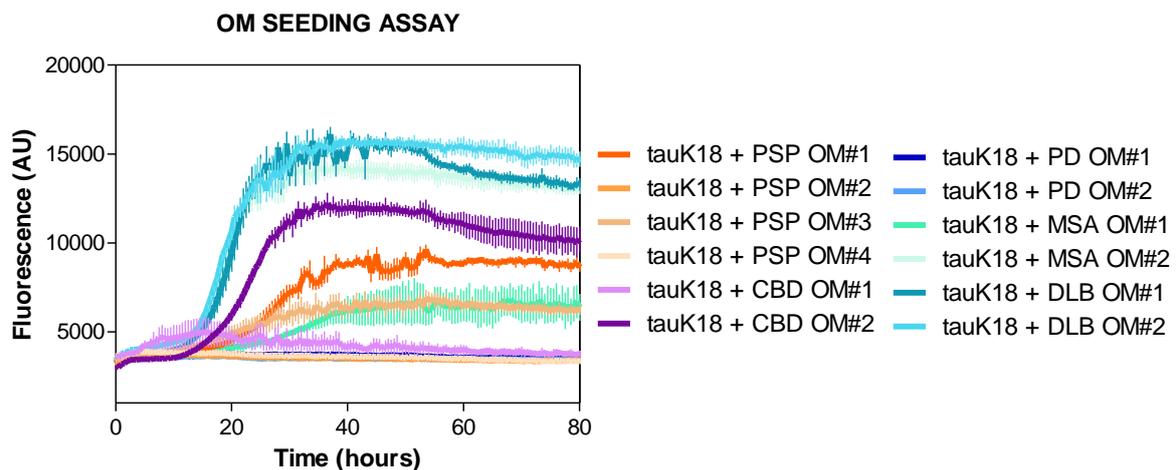

Figure 4.13 RT-QuIC analysis of OM collected from patients with clinical diagnosis of atypical parkinsonisms and Parkinson's disease.
tauK18 aggregation was efficiently triggered by 1 CBD (OM#2, purple line), 2 PSP (OM#1 and OM#3, dark orange and light orange lines), 2 MSA (OM#1 and OM#2, turquoise and light turquoise lines) and 2 DLB samples (OM#1 and OM#2, navy blue and light navy blue lines). Both PD OM#1 and OM#2 (dark blue and blue lines) did not display tauK18 seeding activity.

Indeed, when fluorescence intensities of OM samples collected from tauopathies were compared to those of synucleinopathies and PD cases (Fig. 4.14), tauK18 seeding ability showed to be higher in atypical parkinonisms associated with αS pathology (navy blue line) rather than in those associated with tau (magenta red line).

OM SEEDING ASSAY
Comparison between different parkinsonian syndromes

Legend:
- atypical parkinsonisms_tau
- atypical parkinsonisms_αS
- Parkinson's disease
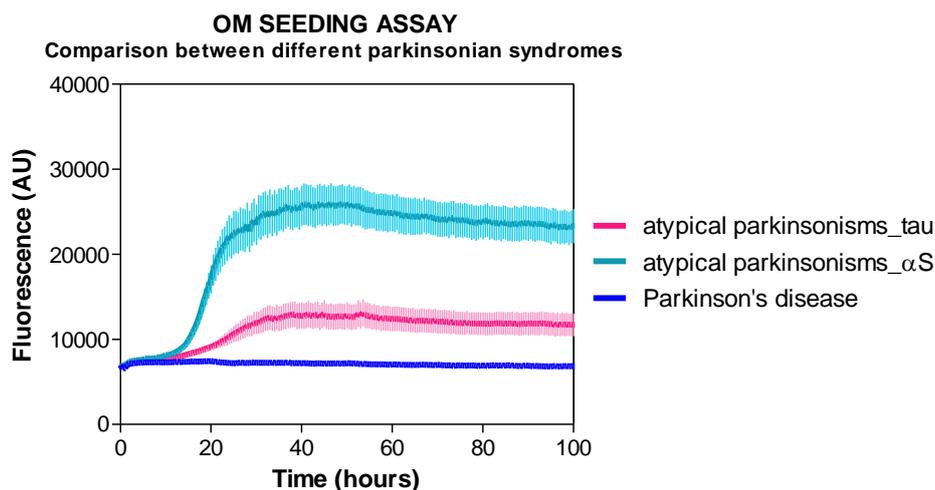
Figure 4.14 Comparison of tauK18 seeding activity in RT-QuIC exerted by OM collected from patients with atypical parkinsonisms and Parkinson's disease.

tauK18 seeding activity of OM collected from different parkinsonian syndromes showed that samples from atypical parkinsonism associated with αS pathology (navy blue line) reached higher fluorescence intensities if compared to parkinsonism associated with tau pathology (magenta red line) and Parkinson's disease (PD) (blue line).

4.5. Biochemical and structural characterization of final tauK18 RT-QuIC aggregates seeded by OM in RT-QuIC

Since different OM samples (either from patients with synucleinopathies or tauopathies) efficiently induced tauK18 aggregation, we decided to analyze final aggregates with biochemical and biophysical techniques with the aim of verifying whether tauK18 might have acquired different conformations (presumably driven by different pathological seeds), thus allowing us to discriminate between pathologies and to stratify patients with different tauopathies.

Therefore, we collected final tauK18 products seeded by different OM samples from RT-QuIC assay reported in Fig. 4.11 and we performed preliminary structural investigations by Transmission electron microscopy (TEM), Fourier-transform infrared (FTIR) spectroscopy and Atomic force microscopy (AFM).

First, tauK18 final RT-QuIC aggregates were analyzed by TEM in order to morphologically evaluate the size and cross-over periodicity of tauK18 fibrils seeded by different OM samples. We analyzed tauK18 aggregates seeded with 1 PSP (Fig. 4.11, OM#1, dark orange line), 1 CBD (Fig. 4.11, OM#1, purple line) and 1 gPD (Fig. 4.11, OM#1, dark blue line) OM, and 1 AD (Fig. 4.11, OM#1, red line) sample that did not displayed tauK18 seeding activity. Images of OM-seeded tauK18 aggregates are reported in Fig. 4.15A and showed the presence of an intricate tangle of tauK18 fibrils in CBD and PSP samples, whereas dispersed fibrils were observed in the PD sample.
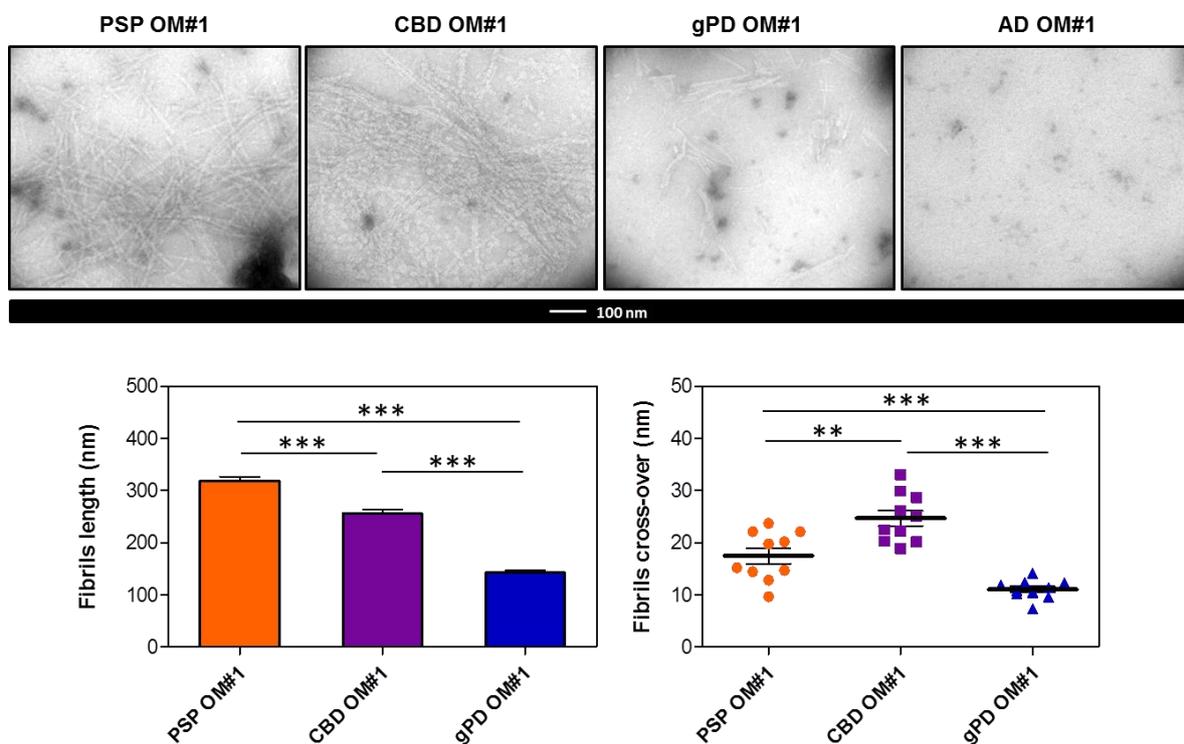

Figure 4.15 TEM analysis of tauK18 aggregates seeded by different OM samples.
A) RT-QuIC products of tauK18 seeded by different OM samples were analyzed by TEM, showing the presence of an intricate tangle of fibrils in CBD and PSP OM#1 samples and some dispersed fibrils in gPD OM#1 sample. No fibrils were detected in the AD OM#1 sample. B) tauK18 average fibrils length were found to be significantly different among each samples (p-value < 0.0001, ***) and was measured as 319.0±7.21 nm (mean±SEM, n=193), 255.5±8.26 nm (mean±SEM, n=161) and 142.2±4.02 nm (mean±SEM, n=219) in PSP, CBD and gPD OM samples, respectively. C) tauK18 fibrils cross-over periodicity was also found to be significantly different among each condition: PSP OM#1 fibrils showed an average cross-over periodicity of 17.46±1.48 nm (mean±SEM, n=10), CBD OM#1 fibrils of 24.67±1.49 nm (mean±SEM, n=10) and gPD OM#1 fibrils of 11.05±0.58 nm (mean±SEM, n=10). P-value of CBD vs PSP was 0.0031 (**), whereas PD vs PSP displayed a p-value of 0.0008 and PD vs CBD a p-value < 0.0001. B) and C) Statistical analysis was performed with a double-tailed unpaired t-test (Mann-Whitney U test).

No fibrils were observed in the AD OM sample confirming that it did not induce tauK18 aggregation.

Fibrils length and cross-over periodicity were also evaluated (Fig. 4.15B), showing that gPD-seeded tauK18 fibrils possess the lowest average fibril length, estimated to be around 142.2±4.02 nm (mean±SEM, n=219), and the smallest cross-over periodicity, around 11.05±0.58 nm (mean±SEM, n=10). PSP-seeded tauK18 fibrils are characterized by an average length of 319.0±7.21 nm (mean±SEM, n=193) and a cross-over periodicity of 17.46±1.48 nm (mean±SEM, n=10), whereas CBD sample displayed fibrils with 255.5±8.26 nm (mean±SEM, n=161) of average length and 24.67±1,49 nm (mean±SEM, n=10) of cross-over periodicity. These differences were statistically significant, possibly indicating that tauK18 conformation might be differently driven by distinct OM seeds.

The same samples were also analyzed by FTIR to gain structural information regarding the secondary structure of tauK18 seeded by different OM samples in RT-QuIC. Fibrils generated by tauK18 self-assembly or seeded by tauK18 PFFs were included in the analysis. tauK18 aggregates were precipitated by ultra-centrifugation, to exclude the monomeric native protein from the analysis and to avoid the presence of salts able to interfere with FTIR measurements, and subjected to Attenuated Total Reflection (ATR) analysis in FTIR characterized by a single or multiple reflections (1R or 9R, respectively).

The results of measurements in ATR-1R are shown in Fig. 4.16A, where the absorption spectra are listed in the region of the Amide I (1700-1600 cm^{-1}) and Amide II bands (1600-1500 cm^{-1}) associated with the absorption of the peptide bond. Amid I, in particular, is the most sensitive to protein secondary structures. The absorption spectra of PSP (red line) and CBD (yellow line) OM-seeded tauK18 showed a very evident band in the spectral region of β-sheet structures (1620-1640 cm^{-1}) , whereas the spectra of the other samples was more centered in the region around 1652 cm^{-1}, assignable to random coil structures with a possible contribution of α-helices. This could indicate that a part of the protein has remained disordered.
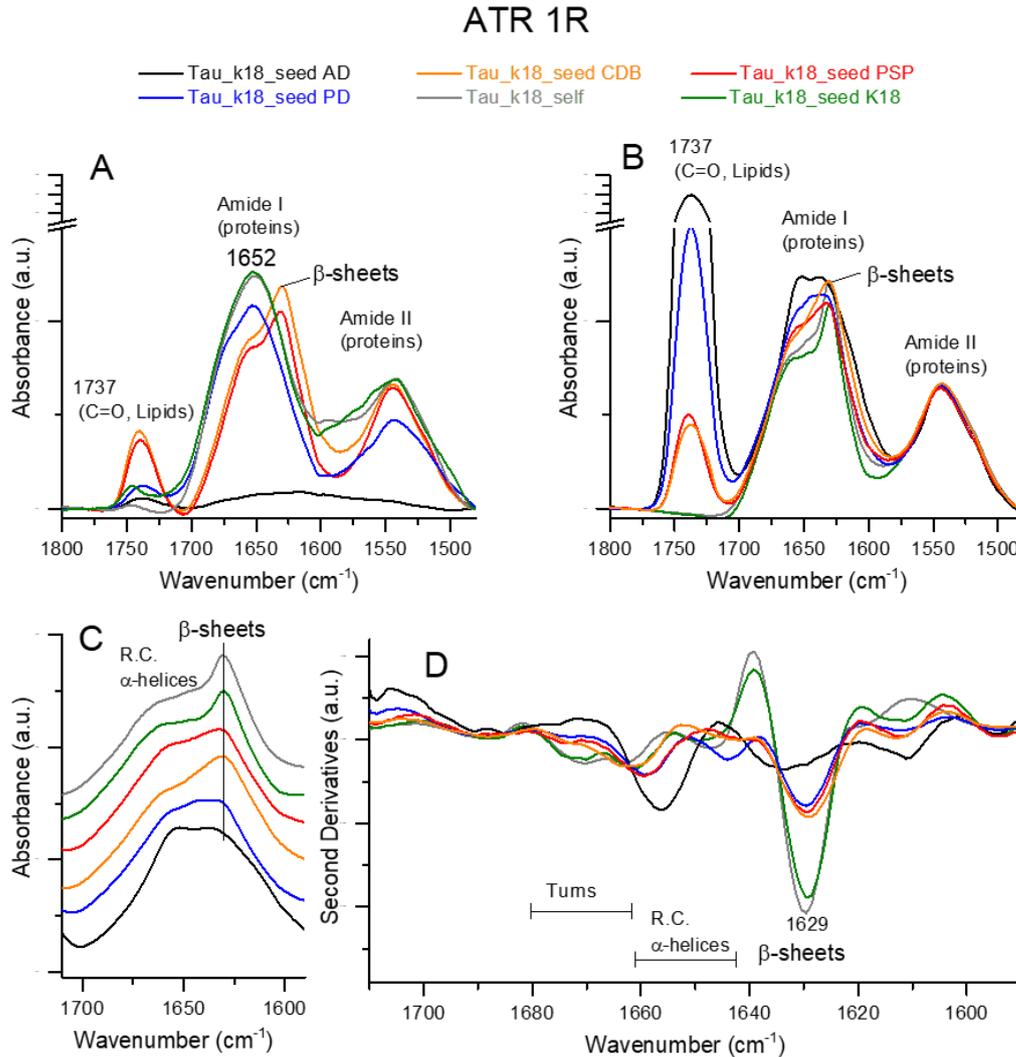
Figure 4.16 FTIR-ATR 1R analysis of tauK18 aggregates seeded by different OM samples.
A) Absorption spectra in the region 1800-1480 cm^{-1} of tauK18 final aggregates seeded by OM samples in RT-QuIC showed that PSP (red line) and CBD (yellow line) samples possessed a very evident band in the spectral region of β-sheet structures, whereas the spectra of the other samples showed a peak in the region of random coil structures. B) Samples were re-precipitated to further purify aggregates and re-analyzed, thus allowing the identification of peaks corresponding to β-sheet structures in tauK18 self-assembly (gray line) and PFFs-seeded (green line) samples. No β-sheet structures were identified in AD (black line) and gPD (blue line) OM samples. C) Zoom in the Amide I region of absorbance spectra obtained in B) was used to better visualize the spectral region of β-sheet structures and confirmed results showed in B). D) The second derivative of the absorption spectra reported in C) showed that tauK18 self-assembly and PFFs-seeded samples may possess a higher content of β-sheets if compared to the other samples analyzed.

The signal of tauK18 sample seeded by AD OM (black line) was not analyzable in these conditions, thus samples were re-precipitated to further purify aggregates and re-analyzed.

The results are reported in Fig. 4.16B and 4.16C, where this additional purification step allowed us to identify peaks corresponding to β-sheet structures also in tauK18 self-assembly (gray line) and PFFs-seeded samples (green line). No β-sheet structures were still identified in AD and gPD (blue line) OM samples. Second derivative of the absorption spectra obtained in Fig. 4.16B allowed us to identify high peaks at 1629 cm^{-1} in tauK18 self-assembly (gray line) and PFFs-seeded samples (Fig. 4.16D), thus suggesting that these samples might possess a higher content of β-sheets if compared to the other samples.

Given that the signal obtained with ATR-1R FTIR analysis was not satisfactory, probably due to the low amount of tauK18 used as substrate in our experiments, samples were re-analyzed with a 9-reflective ATR accessory (ATR-9R) and results are shown in Fig. 4.17. The first analysis (Fig.17A) showed that PSP (red line) and CBD (yellow line) OM-seeded tauK18 possessed a very evident band in the spectral region of β-sheet structures, similar to what observed with ATR-1R FTIR. However, after the purification step, the highest sensitivity of the ATR-9R allowed to better identify β-sheet structures in all tauK18 samples except for the sample seeded by AD OM (Fig. 4.17B).

This evidence was confirmed by the second derivative analysis shown in Figure 4.17C: tauK18 self-assembly and PFFs-seeded samples displayed the highest content in β-sheets, whereas tauK18 seeded by PSP, CBD, and gPD OM also possess β-sheets structures but in lower amount. tauK18 seeded by AD OM showed a predominant random coil structure, with the possible contribution of α-helices.

Incidentally, the analysis of the region around 1740 cm^{-1} indicates that samples with OM seeds might contain lipids, as they present peaks in the region corresponding to C=O binding of lipid esters. Interestingly, AD OM sample displayed a very high peak in this region, thus suggesting a potential higher content of lipids if compared to other OM samples.
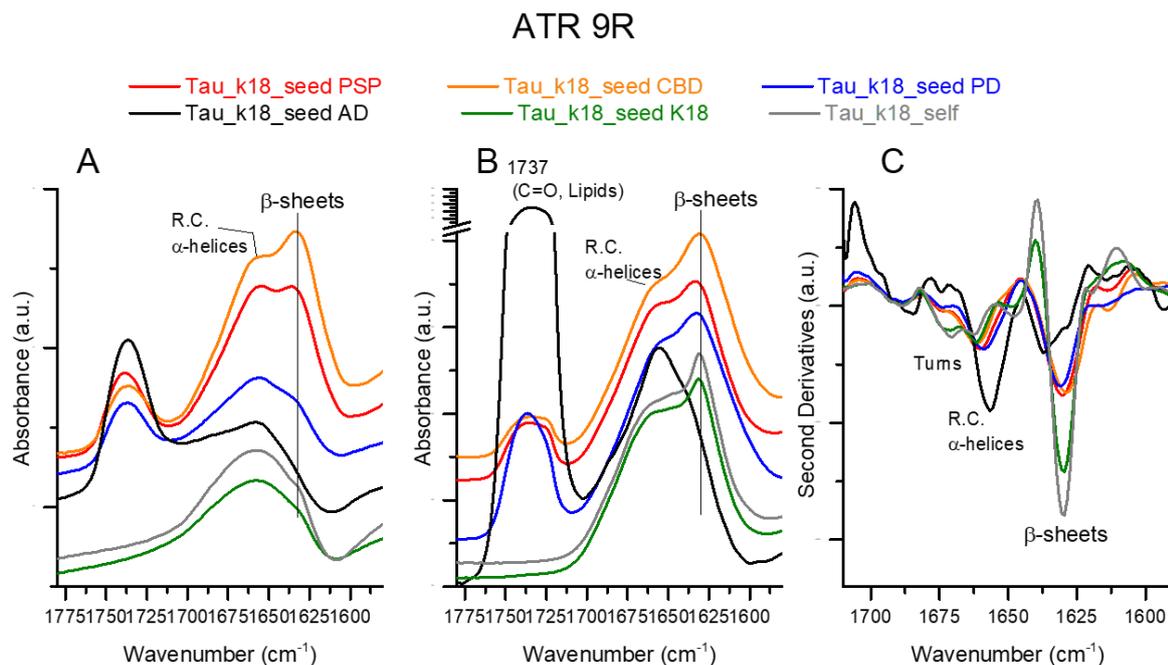
ATR 9R

Figure 4.17 FTIR-ATR 9R analysis of tauK18 aggregates seeded with different OM samples.
A) Absorption spectra in the region 1800-1480 cm^{-1} of tauK18 final aggregates seeded by OM samples in RT-QuIC were obtained with FTIR-ATR 9R and showed similar results of ATR1R analyses, as also in this case PSP (red line) and CBD (yellow line) samples possessed a very evident band in the spectral region of β-sheet structures, whereas other samples were characterized by random coil structures. B) The second analysis of purified samples showed the presence of β-sheet structures in all samples with the exception of AD (black line). By contrast, AD sample was characterized by a high peak in the region of lipid esters. C) The second derivative of the absorption spectra reported in B) showed that tauK18 self-assembly and PFFs-seeded samples may possess a higher content of β-sheets if compared to the other samples analyzed.

Another preliminary structural study was conducted by analyzing OM-seeded tauK18 aggregates with AFM with the aim of discriminating between different tauopathies. Indeed, final tauK18 RT-QuIC products seeded by PSP OM#1, CBD OM#1, and AD OM#1 were adsorbed onto the mica surface and subjected to AFM analysis. The results are reported in Fig. 4.18, in which PSP OM-seeded tauK18 aggregates showed the presence of around 1 µm long fibrils dispersed among thin and presumably fragmented fibrils, whereas thin CBD-OM seeded sample present only few long fibrils and less fragmented filaments. No fibrils were detected in tauK18 sample seeded by AD, indicating that no protein aggregation occurred.
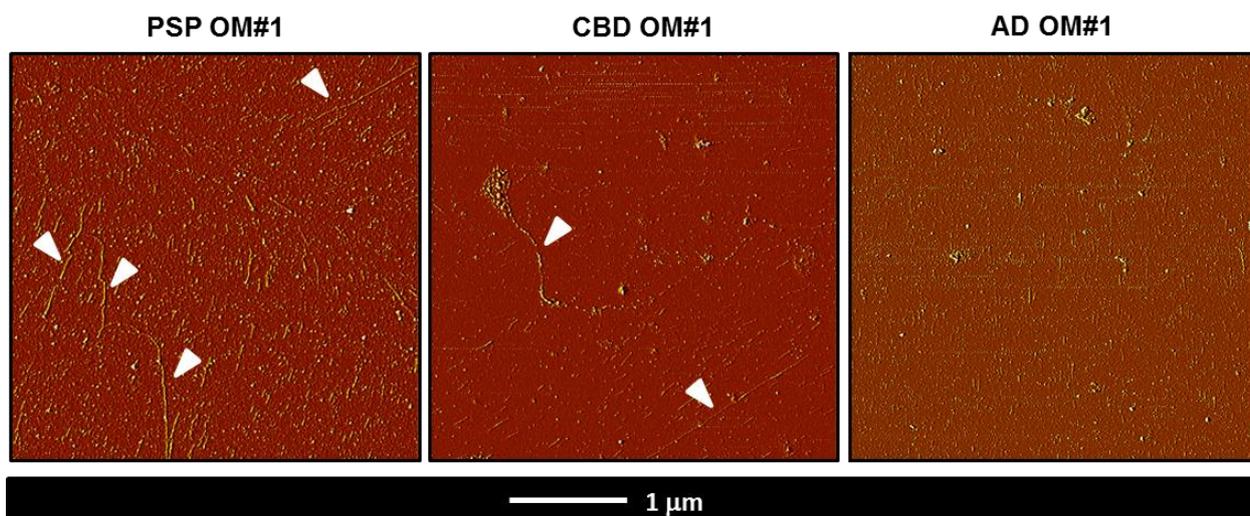
Figure 4.18 AFM analysis of final tauK18 aggregates seeded with different OM samples.
AFM analysis of final tauK18 RT-QuIC products seeded by PSP OM#1, CBD OM#1, and AD OM#1 showed the presence of long fibrils (around 1 µm, white arrowS) and a large amount of thin, presumably fragmented, filaments in the PSP sample, whereas CBD sample present only few long fibrils (white arrowS) and less fragmented filaments. No fibrils were detected in tauK18 sample seeded by AD, indicating that no protein aggregation occurred.

Given that tauK18 fibrils seeded by different OM samples displayed some morphological differences in our preliminary structural studies, we also collected final tauK18 RT-QuIC reaction products from the experiment reported in Fig. 4.13 and we performed a proteolytic digestion with Proteinase K (PK) to evaluate if tauK18 might have acquired different conformations when seeded by distinct OM samples, thus displaying different levels of PK-resistance.

First, monomeric tauK18, RT-QuIC products of tauK18 self-assembly and PFFs-seeded reactions were collected and evaluated by Western blot analysis (Fig. 4.19A). Monomeric tauK18 sample showed the presence of a single band at 13.8 kDa corresponding to tauK18 monomers. tauK18 self-assembly and PFFs-seeded samples were characterized by an analogous band corresponding to monomeric tauK18 which have been not assembled into fibrils and by bands with higher MW presumably corresponding to dimers, trimers,

oligomers, and larger tauK18 aggregates. Secondly, we treated samples with different concentrations of PK.

We observed that, by treating samples with 20 µg/mL of PK for 30', monomeric tauK18 and aggregates generated by the self-assembly of the protein were completely digested, whereas PFFs seeded sample displayed a higher degree of PK-resistance which led to the formation of bands with a MW ranging from 6 to 62 KDa (Fig. 4.19B). According to these results, we decided to subject tauK18 final RT-QuIC products seeded by different OM samples to the same PK treatment. Conversely, all samples were completely digested (Fig. 4.19C), thus indicating that OM seeding has produced tauK18 fibrils less resistant to proteolysis digestion if compared to tauK18 PFFs and, more important, no differences in PK-resistance were observed among OM samples subjected to this proteolytic treatment.
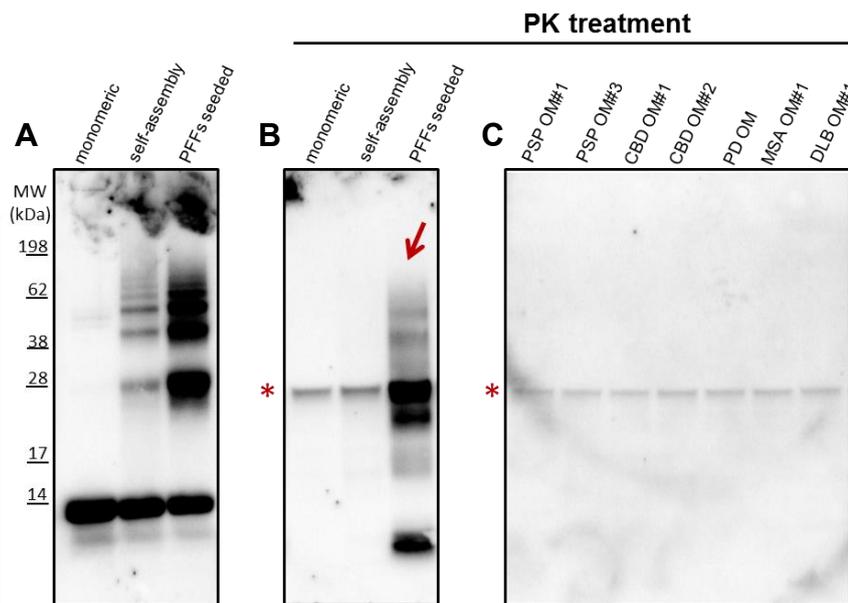
Figure 4.19 Biochemical analysis of tauK18 aggregates seeded by different OM samples.
A) Western blot of monomeric, self-assembled and PFFs-seeded tauK18 RT-QuIC products, showing the presence of a single band at 13.8 kDa corresponding to tauK18 monomers and bands with higher MW corresponding to dimers, trimers, and oligomers in RT-QuIC products of both self-assembly and PFFs-seeded reactions. B) PK treatment completely digested both monomeric and self-assembled tauK18, whereas RT-QuIC products of PFFs-seeded reaction were partially resistant to this treatment (red arrow). C) Absence of PK resistant bands in PK-treated tauK18 aggregates seeded by different OM samples. Blots were immunostained with the RD4 antibody. Asterisk indicates antibody cross-reaction with PK.

4.6. RT-QuIC analysis of urinary exosomes collected from patients with primary and secondary tauopathies

Given the overall low level of sensitivity and specificity of our tauK18 RT-QuIC assay in detecting tau seeding activity in OM of patients with tauopathies, we decided to analyze other peripheral body fluids, such as urine. Urine is a sample very easy to collect, however, it contains several metabolic products that might alter tauK18 RT-QuIC assay. Thus, we decide to purify urinary exosomes and to assess their effect on tauK18 aggregation.

First, we established a protocol to efficiently isolate exosomes from 5 mL of urine by steps of centrifugation at high speed. As shown in Fig. 4.20, the presence of exosomes was confirmed by means of Western Blot using an antibody directed against the exosomal marker CD63 (Fig. 4.20A). Moreover, TEM analysis of urine extracts showed the presence of vesicles characterized by a diameter comprised between 40 and 100 nm, in line with the putative size of exosomes (Fig. 4.20B).
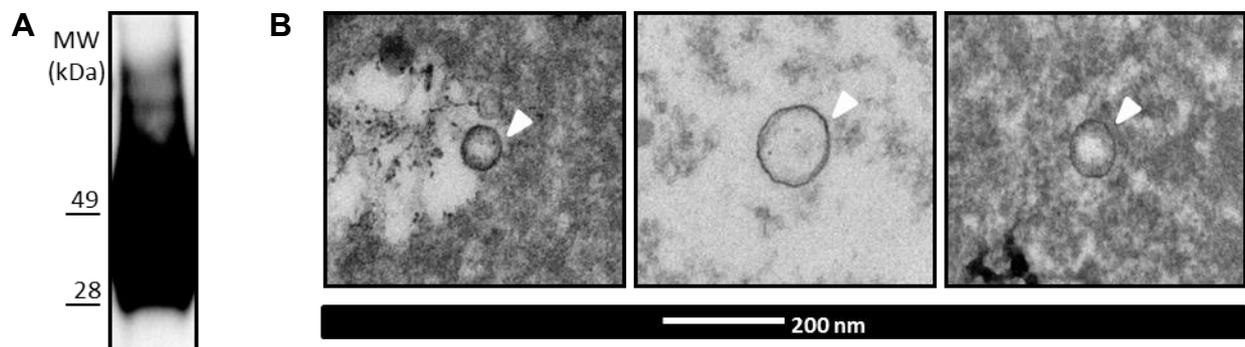
Figure. 4.19 Biochemical and TEM analysis of urinary exosomes extracts.
A) Western blot analysis of urine extracts showed the presence of a large band between 30 and 60 kDa corresponding to the exosomal marker CD63. B) TEM images of urine extracts showed the presence of vesicles with a diameter ranging from 40 to 100 nm, in line with the putative size of exosomes.

Exosomes were isolated from patients with a clinical diagnosis of FTD (n=3), PSP (n=1), CBD (n=1), AD (n=8) and from healthy controls (HC, n=4) and analyzed by means of RT-QuIC. The results are reported in Fig. 4.20A, indicating that exosome isolations from all tauopathies triggered tauK18 aggregation. The majority of these samples displayed an efficient seeding activity, characterized by a lag phase of 5-10 hours. Conversely, one HC

sample (EXO#2, dark olive green line) induced the aggregation of tauK18 within 10 hours from the beginning of the reaction, similarly to tauopathies samples. One PSP (EXO#1, orange line) and two HC (EXO#1 and EXO#4, olive green and dark green lines) sample seeded tauK18 aggregation with less efficiency (after 10 hours). One HC exosome preparation (EXO#3, light green line) did not display tauK18 seeding activity. These observations suggested us to apply a threshold settled at 10'000 AU of fluorescence intensity and at 10 hours from the beginning of reaction, to distinguish samples characterized by a higher seeding activity from those who triggered tauK18 aggregation with less efficiency (Fig. 4.20A, black dotted lines). Samples who induced tauK18 aggregation before this threshold were considered as "positive", whereas the other samples were considered as "negative". By applying this threshold, we were able to identify as positive 4/5 primary tauopathies (3/3 FTD and 1/1 CBD) and 8/8 AD samples. Only one out of four HC samples (EXO#2, dark olive green line) was considered positive. Conversely, PSP sample was considered negative.
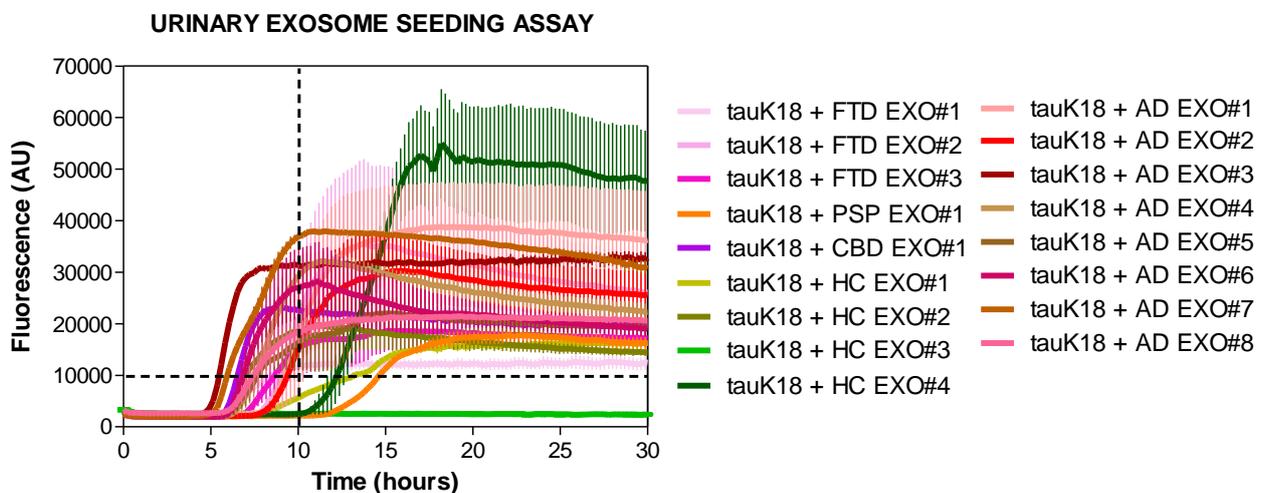
Figure 4.20. RT-QuIC analysis of urinary exosomes collected from patients with tauopathies and healthy controls.

A) tauK18 aggregation was efficiently triggered by exosomes isolated from patients with tauopathies and by some HC samples. A threshold was settled at 10'000 AU and 10 hours from the beginning of the reaction to distinguish samples characterized by higher (considered as "positive") and lower tauK18 seeding activity (considered as "negative"). By applying this threshold (black dotted line), 4/5 primary tauopathies (3/3 FTD and 1/1 CBD) and 8/8 AD samples were considered positive, together with 1/4 HC sample (EXO#2, dark olive green line). PSP (orange line) and 3/4 HC samples (EXO#1, EXO#4 and EXO#3, olive green, dark green and light green lines) were considered negative.

When tauK18 aggregation kinetics triggered by exosomes isolated from primary and secondary tauopathies were analyzed together and were compared to HC samples, it was possible to confirm that secondary tauopathy (AD, dark red line) samples seeded tauK18 aggregation with higher efficiency and reached an average higher fluorescence values if compared to primary tauopathies (FTD, CBD and PSP, light red line) and healthy controls (green line) (Fig. 4.21), thus allowing us to potentially discriminate between these conditions. Additional studies with a higher number of samples are required to validate the specificity and sensitivity of our tauK18 RT-QuIC assay, however, this preliminary experiment showed that urinary exosomes collected from patients with tauopathies might possess tau seeding activity *in vitro*.
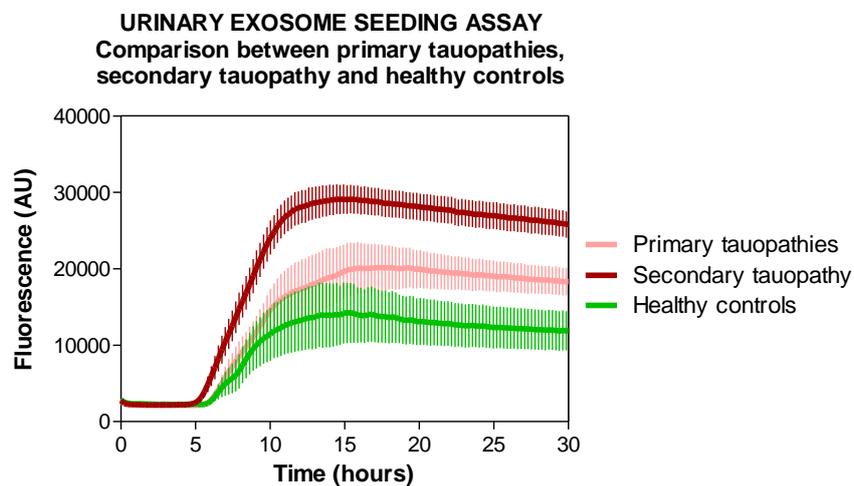

Figure 4.21 RT-QuIC analysis of urinary exosomes collected from patients with tauopathies and healthy controls.
Comparison between tauK18 aggregation kinetics seeded by primary (FTD, CBD, and PSP, light red line) and secondary (AD, dark red line) tauopathies and healthy controls (green line), showing that AD urine exosomes possessed the highest tauK18 seeding activity in RT-QuIC.

4.7. RT-QuIC analysis of CSF collected from patients with Alzheimer's disease

To further evaluate the potential applicability of our tauK18 RT-QuIC assay, we decide to analyze CSF samples collected from AD patients and to compare their seeding activity with CSF collected from Non-demented patients (NDP).

In a preliminary experiment, we compared tauK18 seeding ability of 3 AD CSF to 3 NDP CSF samples in RT-QuIC. Results (Fig. 4.22) revealed the ability of 2 out of 3 AD CSF (CSF#1 and CSF#2, light red and red lines) to efficiently accelerate tauK18 aggregation. No increase in fluorescence was observed after the addition of CSF collected from non-demented patients.

CSF SEEDING ASSAY
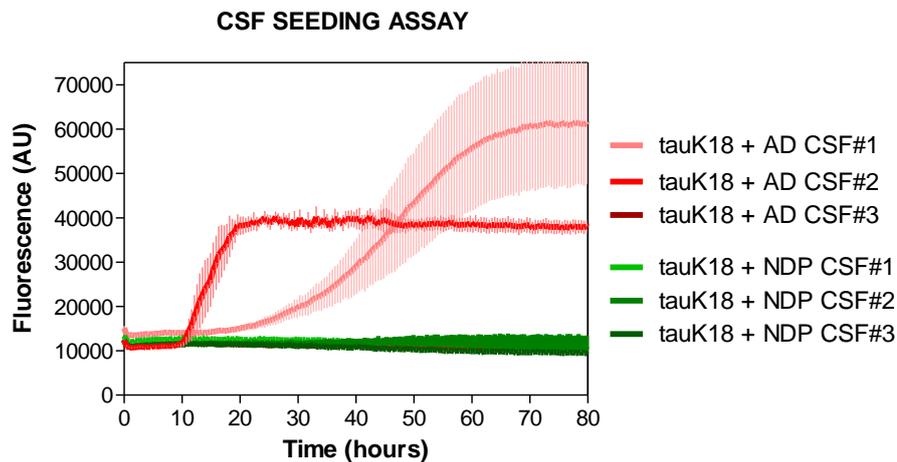
Figure 4.22 RT-QuIC analysis of CSF collected from patients with AD and non-demented patients.
RT-QuIC preliminary analysis of CSF samples showed that tauK18 aggregation was triggered by 2 out of 3 CSF samples from patients with AD (CSF#1 and CSF#2, light red and red lines). No increase in fluorescence was observed after the addition of CSF collected from non-demented patients.

Given that CSF seemed to have an inhibitory effect on tauK18 aggregation, we performed another experiment by adding a lower volume of CSF and we analyzed 8 AD and 8 NDP CSF samples.

Results showed that, with this new experimental setting, a greater number of CSF samples triggered tauK18 aggregation (Fig. 4.23). In particular, all AD CSF samples displayed tauK18 seeding activity, together with 7 out of 8 NDP CSF samples. Similarly to what we have done in the analysis of urinary exosomes, we apply a threshold settled at 10'000 AU of fluorescence intensity and at 10 hours from the beginning of reaction, to distinguish samples characterized by a higher seeding activity from those who triggered tauK18 aggregation with less efficiency (Fig. 4.23, black dotted lines). Samples who induced tauK18 aggregation before this threshold were considered as "positive", whereas the other samples were considered as "negative". Thus, we identified as positive 7/8 AD CSF samples

and 5/8 NDP CSF samples. One AD CSF sample (CSF#6, pink line) was considered negative as it induced tauK18 aggregation after 20 hours from the beginning of the reaction. Similarly, 2 NDP CSF samples (CSF#3 and CSF#8, dark green and emerald green lines) displayed tauK18 seeding activity between 15 and 20 hours, thus they are considered as negative. One NDP sample (CSF#1, green line) did not induce tauK18 aggregation, showing to possess the same activity to that observed in the previous experiment (Fig. 4.22).
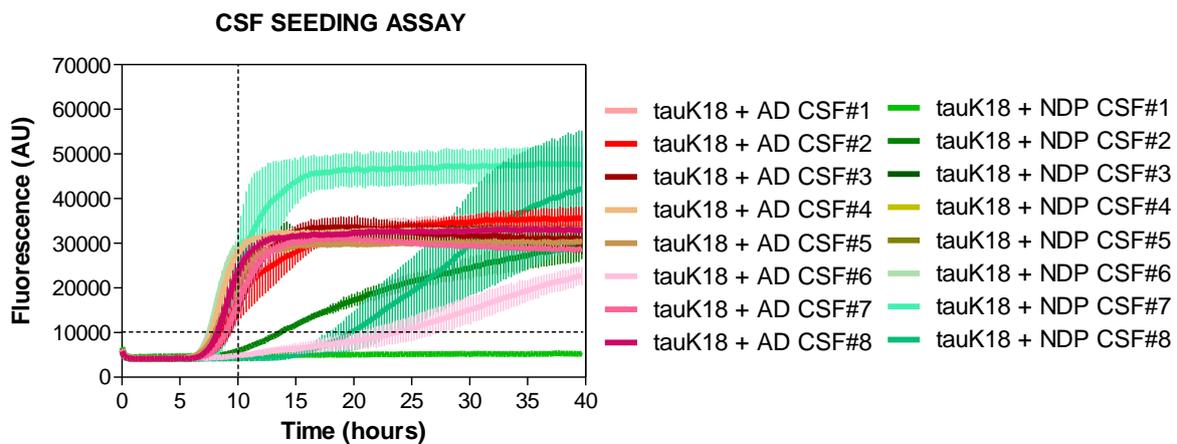
Figure 4.23 RT-QuIC analysis of CSF collected from patients with AD and non-demented patients.
RT-QuIC analysis of CSF samples with this new experimental setting showed that all AD CSF samples and 7 out of 8 NDP CSF samples displayed tauK18 seeding activity. Samples characterized by higher (considered as "positive") and lower tauK18 seeding activity (considered as "negative") were discriminated by applying a threshold settled at 10'000 AU of fluorescence intensity and at 10 hours from the beginning of reaction (black dotted line). 7/8 AD CSF samples were considered as positive and 5/8 CSF samples were considered as negative. No increase in fluorescence was observed after the addition of one NDP CSF sample (CSF#1, green line).

Similar results were also obtained when we analyzed aggregation kinetics of all AD CSF samples and we compared it to NDP samples (Fig. 4.24).

Indeed, no differences in the average lag phases and fluorescence intensities have been observed among the two groups, thus indicating that with this experimental setting AD and NDP CSF samples displayed the same tauK18 seeding activity in RT-QuIC.
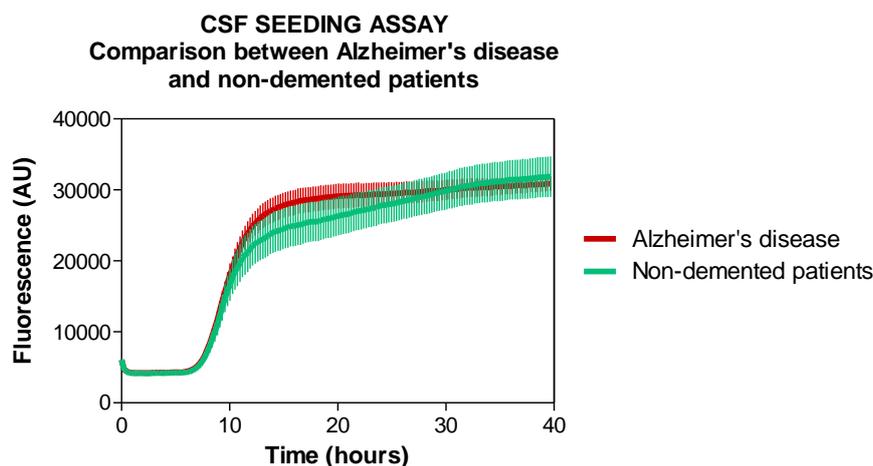
CSF SEEDING ASSAY
**Comparison between Alzheimer's disease and non-demented patients**

Figure 4.21 RT-QuIC analysis of CSF collected from patients with Alzheimer's disease and non-demented patients.

Comparison between tauK18 aggregation kinetics seeded by AD (dark red line) and non-demented patients (green line), showing that both groups displayed the same tauK18 seeding activity in RT-QuIC.

4.8. Evaluation of cross-seeding activity of different amyloidogenic proteins on tauK18 aggregation in RT-QuIC

When performing the analysis of peripheral tissues collected from patients with different forms of dementia, the discrete level of inaccuracy in the aforementioned clinical diagnosis might present an issue for the correct interpretation of RT-QuIC results. Thus, we tried to recapitulate *in vitro* the effect that other misfolded proteins commonly found in NDs might exert on tauK18 aggregation in RT-QuIC to evaluate if they are capable of cross-seeding activity in our assay.

To this aim, we firstly generated aggregates of tauK19 (3R tau fragment), αS, Aβ_{1-40}, Aβ_{1-42} by inducing their self-assembly into PFFs in RT-QuIC, following specific experimental conditions for each protein previously settled in our laboratory. tauK18 PFFs were generated as previously described (Paragraph 4.1) and were used as control. The presence of fibrils was confirmed by TEM, as shown in Fig 4.22. Given that tauK18, tauK19, αS, A$\beta_{1-40,}$ and Aβ_{1-42} PFFs were generated starting from different protein concentrations, we diluted all PFFs sample in order to add the same amount of fibrils (estimated to be in the order of nanograms) in each reaction mix.
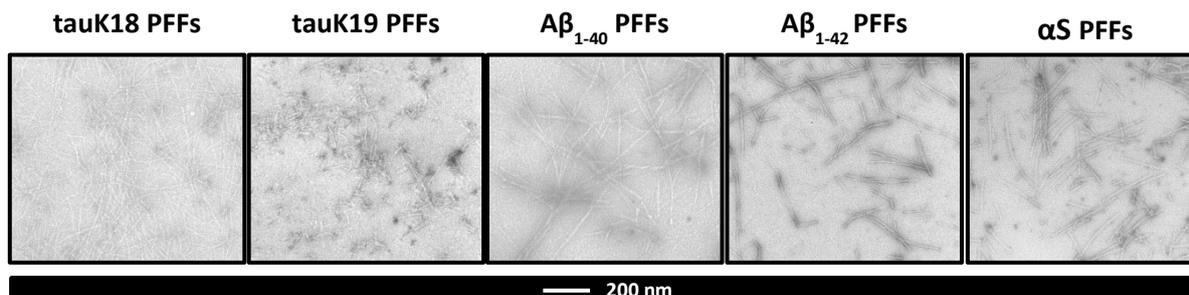
Figure 4.22 TEM images of tauK18, tauK19, tauK19, αS, Aβ$_{1-40}$, and Aβ$_{1-42}$ PFFs

TEM analysis of final RT-QuIC products of self-assembly reactions showed the presence of fibrils in tauK18, tauK19, αS, Aβ$_{1-40,}$ and Aβ$_{1-42}$ PFFs samples.

As reported in Fig. 4.23, tauK18 aggregation was specifically accelerated only by tauK18 PFFs homologous seeding (red line). The addition of Aβ$_{1-40}$ and Aβ$_{1-42}$ PFFs did not modify tauK18 aggregation, as its fibrillization kinetics in both samples (green and purple lines) was comparable to that of tauK18 self-assembly (black dotted line). Conversely, tauK19 and αS PFFs delayed tauK18 aggregation, as no increase in fluorescence intensities was observed even after 40 hours from the beginning of the reaction (orange and blue lines). These results suggested that homologous seeding should be more efficient than heterologous one in our RT-QuIC assay under these experimental settings.
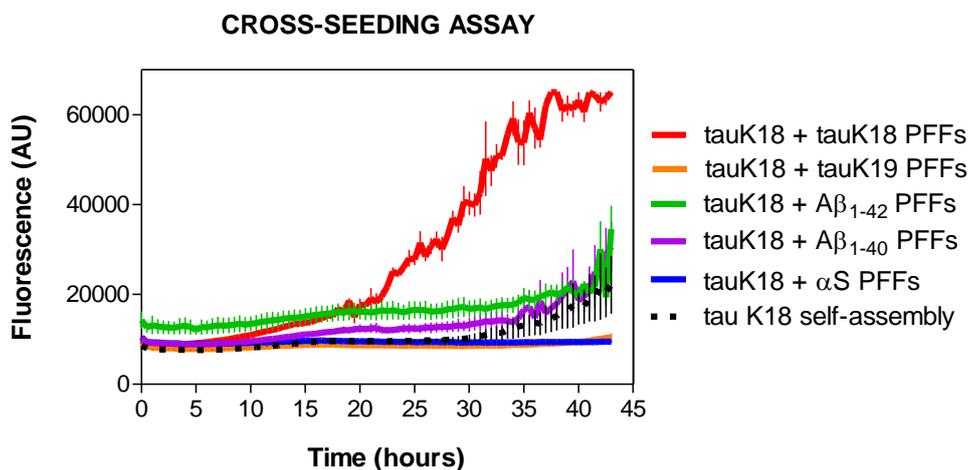
Figure 4.22 RT-QuIC analysis of tauK18, tauK19, αS, Aβ$_{1-40}$, and Aβ$_{1-42}$ PFFs

RT-QuIC analysis of the effect exerted by tauK19, αS, Aβ$_{1-40}$ and Aβ$_{1-42}$ PPFs on tauK18 aggregation showed the absence of cross-seeding activity from heterologous PFFs in our experimental setting. tauK18 PFFs were used as comparison and efficiently induced tauK18 aggregation, thus confirming that homologous seeding was more efficient than heterologous one.

To investigate whether the presence of other amyloidogenic proteins might have induced the formation of tauK18 fibrils with different morphologies, final tauK18 RT-QuIC reaction products were collected and analyzed by means of TEM and AFM. TEM and AFM images are shown in Fig. 4.23 and revealed morphologically different tauK18 fibrils in each sample. Interestingly, such differences were comparable between TEM and AFM analysis. Indeed, tauK18 self-assembly generated thin and unstructured fibrils, whereas tauK18 homologous seeding induced the formation of well-structured fibrils arranged in intricate tangles. Few disperse tauK18 fibrils were observed in samples containing tauK19, αS and $A\beta_{1-42}$ PFFs. The addition of $A\beta_{1-40}$ PFFs induced the formation of long tauK18 fibrils characterized by a circular morphology. These preliminary results suggested that the addition of different seeds, although not accelerating the aggregation of the substrate, might influence the morphology of tauK18 final RT-QuIC fibrils.
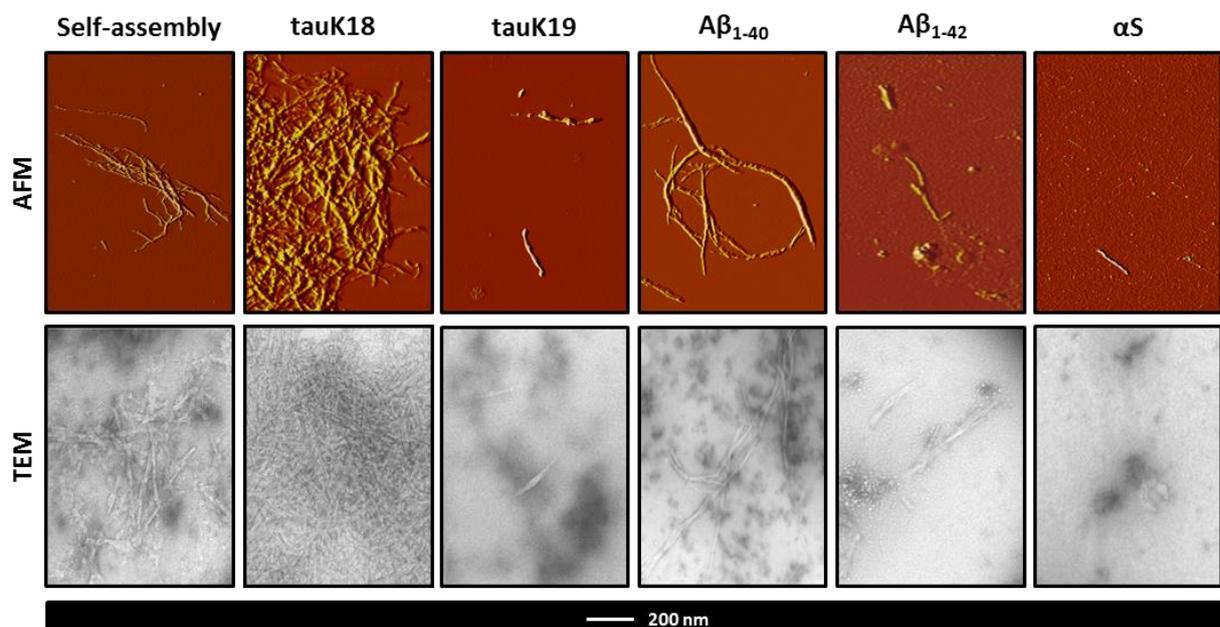
Figure 4.23. TEM and AFM analysis of tauK18 final RT-QuIC products after the addition of tauK18, tauK19, tauK19, αS, $A\beta_{1-40}$, and $A\beta_{1-42}$ PFFs

TEM and AFM analysis of final products of tauK18 self-assembly and reactions supplemented with different PFFs, showing that self-assembly reaction generated thin and unstructured fibrils, whereas tauK18 homologous seeding induced the formation of well-structured fibrils arranged in intricate tangles. Few disperse tauK18 fibrils were observed in samples containing tauK19, αS and $A\beta_{1-42}$ PFFs. The addition of $A\beta_{1-40}$ PFFs induced the formation of long tauK18 fibrils characterized by a circular morphology.

Given that we observed tauK18 seeding activity in RT-QuIC after the addition of OM samples collected from patients with a clinical diagnosis of synucleinopathies, we further investigated the effect exerted by different species of αS aggregates (oligomers, early-fibrils, and late-fibrils) on tauK18 aggregation.

Thus, we induced αS to self-assembly by means of RT-QuIC and we collected oligomers, early-fibrils, and late-fibrils at different time points of the aggregation kinetics, as depicted in Fig. 4.24A. The same species of tauK18 aggregates were also generated and used as controls (Fig. 4.23B). The presence of such species was confirmed by TEM (Fig. 4.23C and D) in both αS and tauK18 samples. Indeed, oligomers were observed as protein aggregates with different diameters and arranged in a linear fashion (Fig. 4.23C and D, light blue and orange arrows). Early-fibrils samples displayed the presence of short filaments (Fig. 4.23C and D, blue and red arrows), whereas late-fibrils were composed by clusters of long filaments (Fig. 4.23C and D, dark blue and dark red arrows).
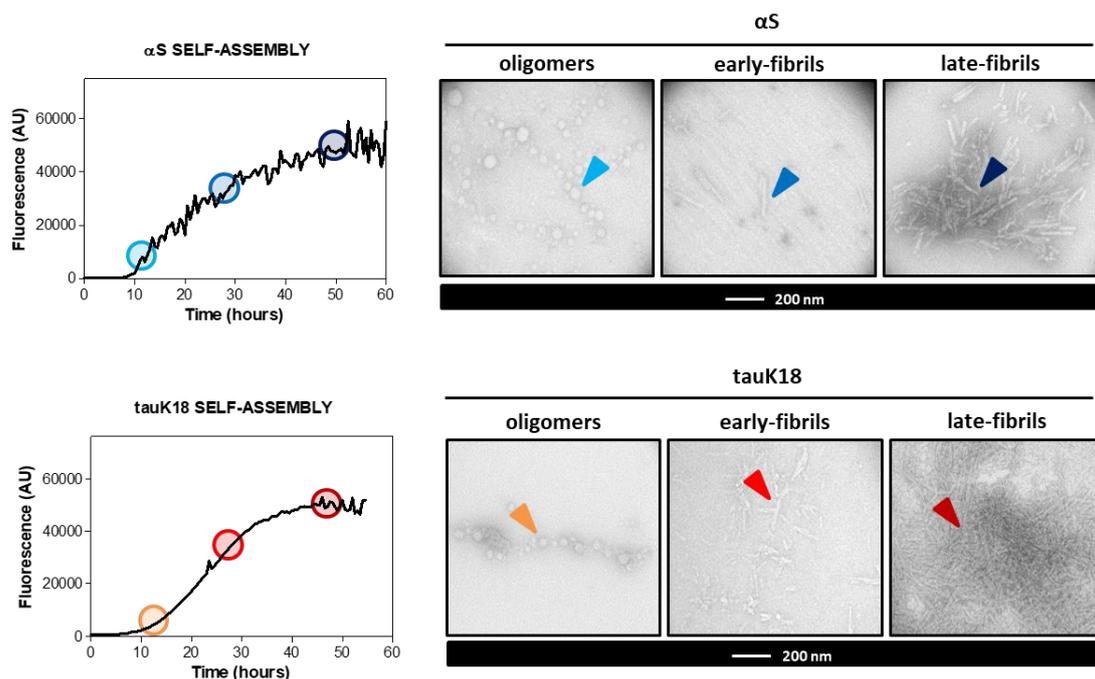
Figure 4.24. Generation of oligomers, early-fibrils, and late-fibrils of αS and tauK18
A) αS self-assembly in RT-QuIC, showing the collection of oligomers (light blue circle), early-fibrils (blue circle) and late-fibrils (dark blue circle). B) tauK18 self-assembly in RT-QuIC, showing the collection of oligomers (orange circle), early-fibrils (red circle) and late-fibrils (dark red circle). C) TEM analysis of the species collected confirmed the presence of αS oligomers (light blue arrow), early-fibrils (blue arrow) and late-fibrils (dark blue arrow). D) TEM analysis of the species collected showed the presence of tauK18 oligomers (orange arrow), early-fibrils (red arrow) and late-fibrils (dark red arrow).

Oligomers, early-fibrils, and late-fibrils were subsequently added to new tauK18 reaction mixes and their seeding ability was assessed in RT-QuIC. Conversely, all the misfolded αS species generated were able to interfere with tauK18 aggregation (Fig. 4.25), thus confirming results obtained with the previous experiment.
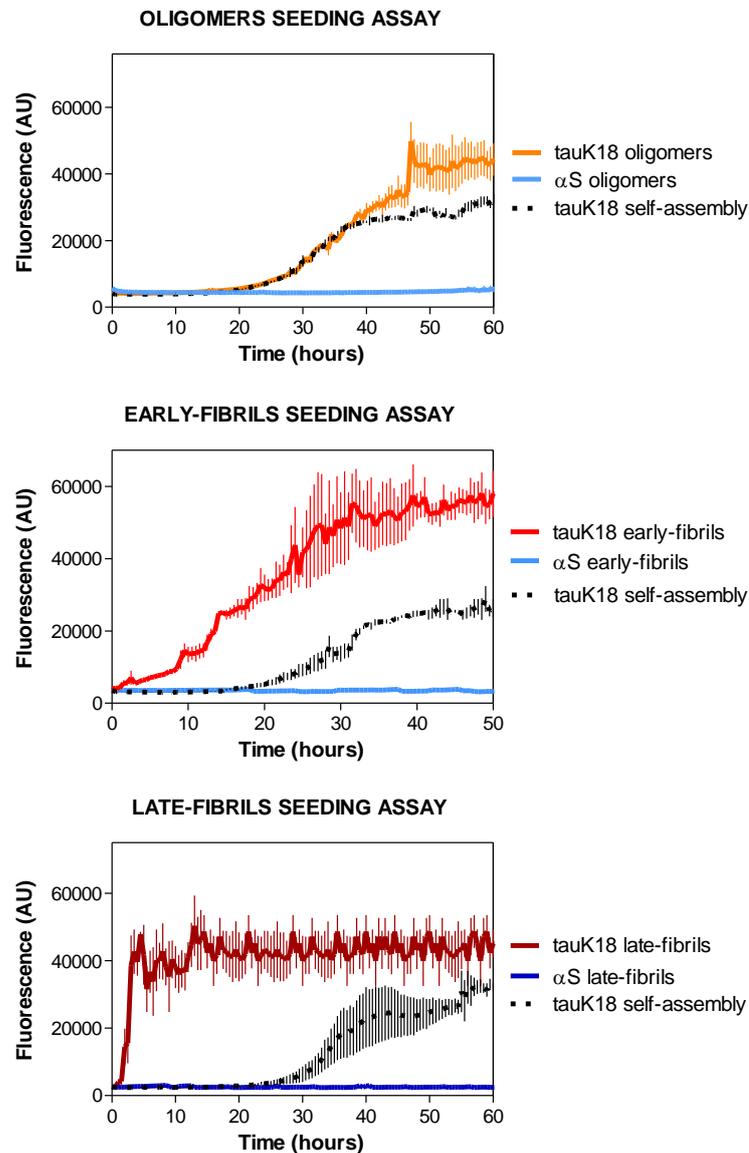
OLIGOMERS SEEDING ASSAY

EARLY-FIBRILS SEEDING ASSAY

LATE-FIBRILS SEEDING ASSAY

Figure 4.23 RT-QuIC analysis of the effect exerted by αS oligomers, early-fibrils, and late-fibrils on tauK18 aggregation.

RT-QuIC seeding assay showed that all αS species tested were able to interfere with tauK18 aggregation, as no increase in fluorescence intensities was observed after the addition of αS oligomers (light blue line), early-fibrils (blue line) and late-fibrils (dark blue line), even after 60 hours from the beginning of the reaction. tauK18 late-fibrils (dark red line) triggered tauK18 aggregation almost instantly. tauK18 oligomers (orange line) did not accelerate tauK18 aggregation, however, its kinetics reached higher fluorescence values if compared to self-assembly reaction (black dotted line).

106

Indeed, no increase in fluorescence intensities was observed after the addition of αS oligomers (light blue line), early-fibrils (blue line) and late-fibrils (dark blue line), even after 50 hours from the beginning of the reaction.

Interestingly, tauK18 late-fibrils (dark red line) showed to possess the highest seeding activity if compared to early-fibrils (red line), as they triggered tauK18 aggregation almost instantly. Oligomers (orange line) did not seem to accelerate tauK18 aggregation, although its kinetics reached higher fluorescence values at the plateau if compared to self-assembly reaction (black dotted line).

To explore the possibility that different conformational variant of the same misfolded protein might display different seeding activities on tauK18 aggregation, we generated four different conformational variants of αS aggregates (αS PFFs#1, PFFs#2, PFFs#3 and PFFs#4) by inducing its self-assembly in RT-QuIC using different aggregation buffers characterized by specific salts composition. The presence of misfolded αS characterized by different conformations was assessed by structural (Fig. 4.24A) and biochemical studies (Fig. 4.24B).
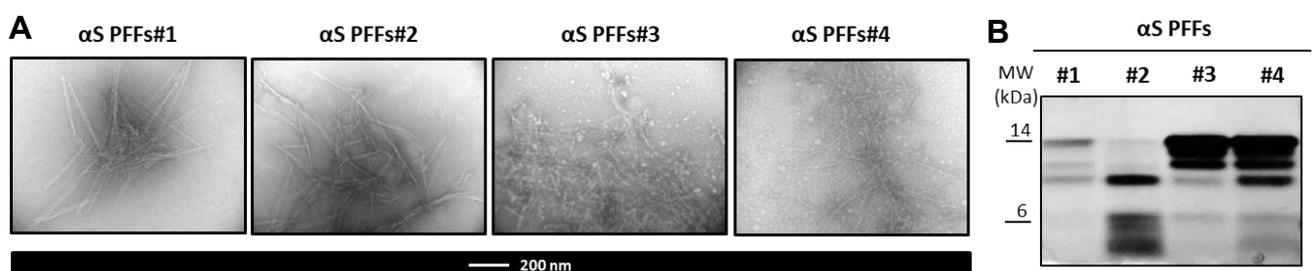
Figure 4.24 Structural and biochemical analysis of αS PFFs#1, PFFs#2, PFFs#3 and PFFs#4
A) TEM analysis αS PFFs generated by the use of different aggregation buffers showed the presence of straight fibrils with no (PFFs#1) or a very little amount of cross-overs (PFFs#2). PFFs#3 and PFFs#4 samples displayed the presence of short and long twisted fibrils, respectively. Some oligomers were also observed in PFFs#3 and PFFs#4 samples, but not in PFFs#1 and PFFs#2. B) Silver staining of PK-treated PFFs revealed different profiles of PK-resistance: misfolded αS in PFFs#1 was partially resistant to proteolytic digestion (band at 14 kDa), whereas digested monomers led to the formation of 2 fragments with a MW in the range comprised between 12 and 10 kDa; in PFFs#2, misfolded αS was almost completely digested and were cleaved producing a main fragment of approximately 10 kDa and other small fragments of 6-3 kDa; misfolded αS in PFFs#3 and #4 showed to possess the higher PK-resistance as intense bands were present at 14 kDa, however, their partial digestion produced fragments with a MW ranging from 12 and 3 kDa, and characterized by bands with different intensities.

TEM analysis of αS PFFs#1 and #2 showed that they were composed of straight fibrils with no (PFFs#1) or some cross-overs (PFFs#2). PFFs#3 and PFFs#4 samples displayed the presence of short and long twisted fibrils, respectively, together with some oligomers.

Proteolytic digestion of αS PFFs samples showed that misfolded αS was characterized by different levels of resistance to PK-digestion in each PFFs (Fig. 4.24B). In particular, misfolded αS in PFFs#1 was partially resistant to such treatment, thus a band corresponding to αS monomers was still visible at 14 kDa. However, some monomers were digested and led to the formation of 2 fragments with a MW of 12 and 10 kDa. In PFFs#2, misfolded αS was almost completely digested by PK (a very faint band was visible at 14 kDa) and its cleavage produced a main fragment of approximately 10 kDa, together with other small fragments of 6-3 kDa, which might represent the portion of the protein cleaved by PK. Misfolded αS in PFFs#3 and #4 showed to possess the higher PK-resistance as intense bands were present at 14 kDa. However, a partial digestion occurred and produced fragments with a MW ranging from 12 and 3 kDa. Interestingly, in PFFs#4 the band at 10 kDa was more intense than in PFFs#3, thus suggesting that in this sample the conformation acquired by misfolded αS have influenced the proteolytic cleavage which was more efficient in generating this fragment in respect to the others.
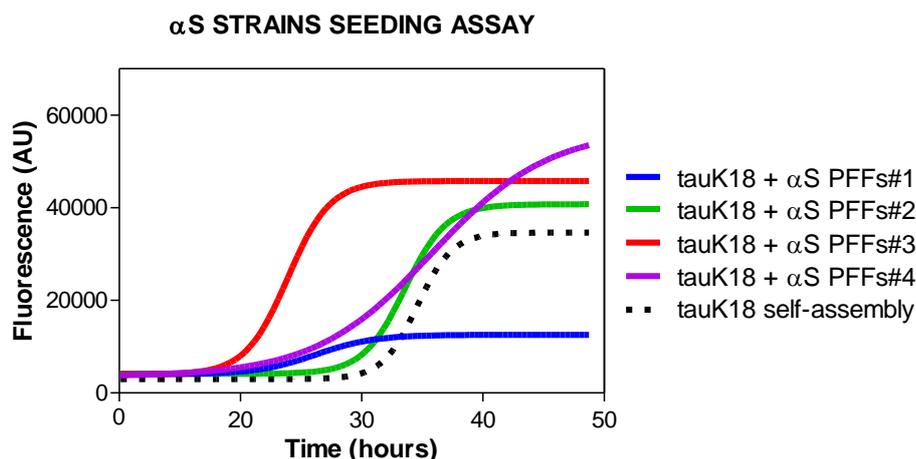
Figure 4.25 RT-QuIC analysis of αS PFFs#1, PFFs#2, PFFs#3 and PFFs#4.
RT-QuIC analysis of different αS PFFs displayed distinct seeding abilities on tauK18 aggregation. PFFs#3 (red line) and #4 (purple line) were able to trigger tauK18 aggregation, whereas PFFs#1 (blue line) seemed to interfere with the aggregation of the substrate. tauK18 aggregation was not influenced by the presence of PFFs#2 (green line), as its kinetics was comparable to tauK18 self-assembly (black dotted line).

When αS PFFs#1, #2, #3 and #4 were added to new reaction mixes, they displayed different seeding abilities on tauK18 aggregation. Indeed, tauK18 aggregation kinetics was accelerated by αS PFFs#3 and PFFs#4, whereas PFFs#1 delayed the aggregation of the substrate. Interestingly, tauK18 aggregation in the presence of PFFs#2 was comparable to that of tauK18 self-assembly, thus suggesting that such strain was not able to influence tauK18 aggregation. Taken together, these studies suggested that different conformational variants of αS may differentially influence the aggregation of tauK18 in RT-QuIC, thus representing an issue for our RT-QuIC assay.

DISCUSSION

NDs are conditions associated with the intracerebral accumulation of abnormally folded proteins, which are considered disease-specific biomarkers (DSB). Definitive diagnosis of NDs relies on neuropathological examination of brain collected at autopsy with the aim of detecting and identifying DSB. However, recent findings suggest that DSB might circulate in peripheral tissues at concentrations that are under the detection limits of the classical diagnostic techniques (e.g. ELISA, Western blot). Therefore, clinical diagnosis of NDs is very challenging, especially in the early stages of the disease. This is mainly due to the fact that some clinical manifestations might overlap between different conditions. Moreover, the lack of tools useful for detecting peripheral DSB limits the diagnostic accuracy of such diseases.

The advent of cell-free amplification systems such as the PMCA and RT-QuIC stimulated unprecedented advancement in terms of developing robust diagnostic tests for many NDs, identifying novel therapeutic strategies and disinfection procedures. Originally developed and successfully applied in the field of prion disease diagnosis, both techniques are currently being optimized for the analysis of the aggregation process of other proteins, including Aβ, tau and α-synuclein (αS). In particular, several RT-QuIC studies have been carried on CSF samples that are often collected from patients with a clinical diagnosis of NDs. However, our research group was aimed at optimizing this technique for the analysis of olfactory mucosa (OM) and urine samples which are less invasive to be collected than CSF. In this regard, since 2013, our research group has been collecting olfactory mucosa samples from patients with NDs and now owns more than 300 samples of OM ready to be subjected to RT-QuIC and PMCA analyses aimed at detecting DSB.

We have recently demonstrated a successful application of the RT-QuIC technology in detecting αS seeding activity in OM samples collected from patients Parkinson's disease

(PD) and Multiple system atrophy (MSA) [251]. Interestingly, final RT-QuIC products acquired biochemical and structural features that were disease-dependent. PD and MSA are parkinsonian syndromes whose diagnosis is challenged due to their overlapping symptoms with other atypical parkinsonisms, such as Progressive supranuclear palsy (PSP) and Corticobasal degeneration (CBD), which are instead characterized by the deposition of tau.

For this reason, my PhD thesis aimed at optimizing an RT-QuIC assay where human recombinant tau (the 4R fragment, named tauK18) was used as reaction substrate. We decided to use this fragment for different reasons. First of all, preliminary experiments showed that the aggregation properties and kinetics of tauK18 were much more reproducible if compared to that obtained with the use of the full-length 4R tau. Secondly, we decided to focus our study on the analysis of primary tauopathies mainly characterized by the accumulation of 4R tau (CBD and PSP). We also included the analysis of secondary tauopathies, such as Alzheimer's disease (AD) patients, because of the presence of both 4R and 3R tau. Given that misfolded 4R tau in patients with tauopathies showed to be conformationally different, the tauK18 fragment could represent an ideal RT-QuIC reaction substrate for the amplification of different conformational variants of 4R tau as it contains the aggregation-prone domain of the protein identified as the core of 4R tau fibrils.

Therefore, we have hypothesized that our RT-QuIC technology could have been useful for detecting seeding activity of 4R tau present in peripheral tissues (OM and urine) of patients with PSP and CBD with high efficiency. Data from the literature have shown that 3R full-length tau is able to hamper the aggregation of 4R tau [260], thus we were expecting a lower seeding activity in samples collected from Alzheimer's disease patients.

First, we performed several experiments to find the optimal conditions for tauK18 aggregation in RT-QuIC. Subsequently, we focused on seeding studies. Our results have demonstrated that the technique is very sensitive in detecting seeding activity of extremely low levels (attograms) of tauK18 preformed fibrils (PFFs) artificially produced *in vitro*.

Given the high sensitivity of the assay, we decide to assess if tauK18 aggregation might be similarly accelerated by pathological misfolded tau present in brains of patients

with primary and secondary tauopathies. Interestingly, our RT-QuIC assay was able to detect tau seeding activity in BH of patients with primary and secondary tauopathies, whereas HC BH sample also slightly induced tauK18 aggregation. Its fluorescence values, however, reached significantly lower levels if compared to other BH samples. Its mild seeding ability might be due to the presence of BH components able to unspecifically trigger tauK18 aggregation. In our second hypothesis, it might be due to the presence of misfolded proteins, as they are increasingly found in cognitively normal subjects [261-263], potentially capable of cross-seeding activity.

The finding that DLB BH delayed tauK18 aggregation was quite surprising, as several *in vitro* and *in vivo* observations reported that misfolded αS might act as a strong inductor of tau aggregation [264]. Even if αS did not cross-seed tauK18 in our assay, we were not expecting such an inhibitory effect. It is possible that also in this case BH components influenced tauK18 RT-QuIC assay. Indeed, it is important to mention that endogenous polar brain lipids were shown to inhibit prion amplification in RT-QuIC, therefore representing a potential issue for our assay [265]. Or, the presence of aggregated αS in the brain of a patient with DLB may have interfered with tauK18 self-aggregation.

Interestingly, the use of AD brain homogenate efficiently promoted tauK18 aggregation. This effect might be associated with a higher seeding efficiency of 4R if compared to 3R aggregates, which have been shown to inhibit 4R tau aggregation. It is also possible that other factors concurred in inducing tauK18 aggregation. For instance, in the amyloid cascade hypothesis, Aβ can trigger tau aggregation [266]. In this regard, it may be possible that, although the presence of 3R tau might have exerted an inhibitory effect on tauK18 aggregation, the presence of 4R tau and Aβ might have significantly promoted the aggregation propensities of tauK18.

When we tested dilutions of brain samples, our assay demonstrated a lower sensitivity and specificity in detecting pathological tau from brain samples if compared to tauK18 PFFs seeding assay. However, although we estimated that our tauK18 RT-QuIC assay is able to detect tau seeding activity exerted by attograms of tauK18 PFFs, it is conceivable that this ability is strictly related to the fact that these aggregates were

generated *in vitro* starting from the same protein fragment (tauK18) and without any other material that can interfere with the assay.

Therefore, even if the sensitivity of tauK18 RT-QuIC assay in detecting BH pathological tau was lower than tauK18 PFFs, we decided to analyze tau seeding activity in peripheral tissues and body fluids of patients with a clinical diagnosis of CBD, PSP, FTDP-17, and AD, as these samples might contain less amount of molecules able to alter tauK18 aggregation in RT-QuIC. We initially focused our attention on olfactory mucosa (OM) samples as they are easy to collect with a non-invasive procedure and they have been shown to contain olfactory neurons likely containing misfolded proteins in patients with NDs. Indeed, neuropathological evaluation of olfactory epithelium collected at autopsy from patients with AD showed the presence of Aβ plaques and PHF-tau pathology [267].

To this aim, we analyzed OM samples collected from several primary and secondary tauopathies and we compared their seeding abilities with OM collected from synucleinopathies and Multiple sclerosis (MS). We were able to observe tau seeding activity in some OM samples collected from patients with PSP and CBD, while those collected from FTDP-17 and AD patients did not. The lack of seeding abilities of FTDP-17 and AD OM samples might be explained by the presence of molecules (e.g. lipids) able to inhibit tau18 aggregation. Indeed, OM is composed of a mucous layer rich in lipids that cover the surface of receptors at the epithelium surface and assist in transporting odorant molecules to the olfactory receptors [268]. In support of this hypothesis, FTIR analysis of final tauK18 RT-QuIC products of OM seeding incidentally showed the presence of absorbance peaks in the region around 1740 cm^{-1} which indicated the presence of lipids in those samples. Interestingly, AD OM sample displayed a very high peak in this region, thus suggesting a potential higher content of lipids if compared to other OM samples. Numerous efforts have been made to exclude such factors from our assay, however, by diluting OM samples it is possible that also seeding-competent tau was diluted, altering the sensitivity of our tauK18 RT-QuIC assay.

Given that OM samples from atypical parkinsonisms (PSP, CBD, and PD) have shown a greater seeding activity in our experimental conditions if compared to AD and FTDP-17

samples, we have decided to focus our attention on this group of diseases with the aim at recognizing parkinsonian syndromes associated with tau pathology and to distinguish them from those associated to αS accumulation. Surprisingly, some OM samples from patients with PD, DLB, and MSA triggered tauK18 aggregation in RT-QuIC. Given that DLB BH sample displayed an inhibitory effect, we hypothesized that different strains of αS might differentially influence tau aggregation in our assay.

We tried to recapitulate such condition by generating different conformational variants of αS PFFs and by evaluating their effect of tauK18 aggregation. We noticed that some PFFs triggered tauK18 aggregation, whereas one PFFs delayed its aggregation, thus indicating that the conformation acquired by αS aggregates might play a role in influencing their cross-seeding abilities in our assay. On the other hand, we also hypothesized the presence of misfolded tau in patients with PD, DLB, and MSA. Indeed, an increasing number of studies are reporting the presence of concomitants αS and tau pathologies in several NDs, often associated with a faster disease progression and the worst prognosis [85, 269]. Moreover, PARK8 subtype of genetic PD has been shown at neuropathological examination to contain also tau deposits with or without forming neurofibrillary tangles [270]. This finding might explain seeding activity of gPD (PARK8) OM in our tauK18 RT-QuIC assay.

Finally, the discrete level of inaccuracy in the aforementioned clinical diagnosis might present an issue for the correct interpretation of RT-QuIC results. For this reason, we assessed the cross-seeding abilities of other amyloidogenic proteins commonly found in other NDs. Thus, we tested the effect that αS, tauK19 (3R-tau), Aβ$_{1-40}$ and Aβ$_{1-42}$ PFFs might exert on tauK18 aggregation. Initially, the substrate showed to be specifically accelerated only by tauK18 PFFs. However, this observation is strictly related to the specific experimental conditions used in our assay and to the fact that such PFFs were generated *in vitro*, thus not resembling pathological misfolded proteins found *in vivo*. Indeed, when we generated different conformational variants of αS, some of them showed to accelerate tauK18 aggregation, whereas one PFFs seemed to interfere with tauK18 aggregation. Thus, we hypothesized that DLB brain might contain one strain of αS not capable of tauK18

seeding activity, whereas DLB OM can contain αS aggregates able to induce tauK18 aggregation in RT-QuIC. In the field of prion diseases, it has been shown that two or more prion strains can co-exist in sporadic cases of CJD [271{Puoti, 1999 #7503, 272]. Moreover, in PDD cases Lewy bodies in the substantia nigra showed biochemical dissimilarities from LBs in neocortical areas of the same patients, thus suggesting that different misfolded αS conformations might accumulate in different cerebral areas [35].

Given the possibility that different seeds might have induced tauK18 aggregation, we decided to couple RT-QuIC technique with biochemical and structural evaluations of final reaction products to assess if they might have acquired different conformations. In particular, final tauK18 RT-QuIC products of reactions seeded by PSP, CBD and AD OM samples were subjected to preliminary structural studies by means of TEM, AFM and FTIR analysis. Thanks to these assessments we have observed that final aggregates were characterized by different structural features when seeded by CBD, PSP and PD OM. Similarly, it was possible to identify morphological differences in tauK18 seeded by different PFFs. If this will be confirmed, structural and biochemical evaluations of tauK18 final RT-QuIC products may be helpful for identifying different seeding-competent tau strains and help for the stratification of patients in the early stages of the disease. This, in turn, will lead to lay the foundation for a precision medicine which is directed against individual pathological processes.

The low specificity and sensitivity of our assay in detecting tau seeding activity in OM from patients with tauopathies moved us to the analysis of body fluids, such as urine. Given that urine contains a lot of metabolic products, we decided to isolate exosomes as they have been shown to potentially contain protein aggregates and to participate in misfolding progression in patients with NDs. RT-QuIC analysis of urinary exosomes showed improved results: indeed, urine exosomes collected from patients with Alzheimer's disease showed higher tauK18 seeding activity if compared to CBD, PSP and control samples. By applying a threshold to distinguish samples characterized by a higher seeding activity (considered as "positive") from those who triggered tauK18 aggregation with less efficiency (considered as "negative), we were able to identify as positive 4/5 primary

tauopathies (3/3 FTD and 1/1 CBD) and 8/8 AD samples. Only one out of four HC samples was considered positive. Additional studies with a higher number of samples are required to validate such results, however, these findings suggested that exosomes isolated from body fluids may represent a suitable source of misfolded protein circulating in the periphery. Given that tau accumulates inside the cell in brain of patients with tauopathies, exosomes might actively contribute to tau pathology spreading in body fluids.

To further evaluate the potential applicability of our tauK18 RT-QuIC assay, we decide to analyze CSF samples collected from AD patients. We found that tauK18 aggregation was accelerated from all the AD CSF tested, but also from some NDP CSF samples. Similarly to what we hypothesized in the previous analysis, CSF might contain proteins or molecules able to promote tauK18 aggregation. Additional studies with a higher number of samples are required to further optimize RT-QuIC analysis of CSF collected from patients with AD and to apply this technology to the analysis of CSF samples from other tauopathies.

These studies represent a fundamental step forward in the field of NDs since it demonstrates that CSF, olfactory mucosa and urine collected from patients at different stages of disease might be exploited for formulating a definitive diagnosis of many NDs without the need of autoptic confirmatory tests. Moreover, these results could be achieved by simple analyses of easily collectable peripheral tissues without the use of invasive procedures. As consequence, it will (1) limit the need of other costly and time consuming clinical, laboratory or instrumental tests, (2) reduce the number of specialist consultations, (3) reduce the length of waiting lists to access specialist clinics while (4) improving selection of patients to be enrolled in clinical trials. The possibility to collect samples at different stages of the disease will enable the monitoring of the effects that specific drugs exert on DSB concentration or in modifying their biochemical and structural features. In addition, since RT-QuIC mimics the same process of protein misfolding which occurs *in vivo*, it might be used to study how therapeutic compounds block the molecular events which lead to dementia, thus focusing the analysis on *molecular* rather than *symptomatic* aspects.

REFERENCES

1.   Heemels, M.T., *Neurodegenerative diseases.* Nature, 2016. **539**(7628): p. 179.
2.   Piaceri, I., B. Nacmias, and S. Sorbi, *Genetics of familial and sporadic Alzheimer's disease.* Front Biosci (Elite Ed), 2013. **5**: p. 167-77.
3.   Tsuang, D.W., L. DiGiacomo, and T.D. Bird, *Familial occurrence of dementia with Lewy bodies.* Am J Geriatr Psychiatry, 2004. **12**(2): p. 179-88.
4.   Ingram, E.M. and M.G. Spillantini, *Tau gene mutations: dissecting the pathogenesis of FTDP-17.* Trends Mol Med, 2002. **8**(12): p. 555-62.
5.   Rabinovici, G.D. and B.L. Miller, *Frontotemporal lobar degeneration: epidemiology, pathophysiology, diagnosis and management.* CNS Drugs, 2010. **24**(5): p. 375-98.
6.   Klein, C. and A. Westenberger, *Genetics of Parkinson's disease.* Cold Spring Harb Perspect Med, 2012. **2**(1): p. a008888.
7.   Inzelberg, R., et al., *Onset and progression of disease in familial and sporadic Parkinson's disease.* Am J Med Genet A, 2004. **124A**(3): p. 255-8.
8.   Levin, J., et al., *The Differential Diagnosis and Treatment of Atypical Parkinsonism.* Dtsch Arztebl Int, 2016. **113**(5): p. 61-9.
9.   Misiak, B., et al., *European studies on the prevalence of dementia in the elderly: time for a step towards a methodological consensus.* Int J Geriatr Psychiatry, 2013. **28**(12): p. 1211-21.
10.   Stroo, E., et al., *Cellular Regulation of Amyloid Formation in Aging and Disease.* Front Neurosci, 2017. **11**: p. 64.
11.   Prusiner, S.B., *Biology and genetics of prions causing neurodegeneration.* Annu Rev Genet, 2013. **47**: p. 601-23.
12.   Kovacs, G.G., *Concepts and classification of neurodegenerative diseases.* Handb Clin Neurol, 2017. **145**: p. 301-307.
13.   Lill, C.M. and L. Bertram, *Towards unveiling the genetics of neurodegenerative diseases.* Semin Neurol, 2011. **31**(5): p. 531-41.
14.   Seeley, W.W., et al., *Neurodegenerative diseases target large-scale human brain networks.* Neuron, 2009. **62**(1): p. 42-52.
15.   Matilla-Duenas, A., et al., *Rare Neurodegenerative Diseases: Clinical and Genetic Update.* Adv Exp Med Biol, 2017. **1031**: p. 443-496.
16.   Soto, C., *Unfolding the role of protein misfolding in neurodegenerative diseases.* Nat Rev Neurosci, 2003. **4**(1): p. 49-60.
17.   Carrell, R.W. and D.A. Lomas, *Conformational disease.* Lancet, 1997. **350**(9071): p. 134-8.
18.   Bayer, T.A., *Proteinopathies, a core concept for understanding and ultimately treating degenerative disorders?* Eur Neuropsychopharmacol, 2015. **25**(5): p. 713-24.
19.   Paulson, H.L., *Protein fate in neurodegenerative proteinopathies: polyglutamine diseases join the (mis)fold.* Am J Hum Genet, 1999. **64**(2): p. 339-45.
20.   Kovacs, G.G., *Molecular Pathological Classification of Neurodegenerative Diseases: Turning towards Precision Medicine.* Int J Mol Sci, 2016. **17**(2).
21.   Lucas-Carrasco, R., et al., *Using the WHOQOL-DIS to measure quality of life in persons with physical disabilities caused by neurodegenerative disorders.* Neurodegener Dis, 2011. **8**(4): p. 178-86.
22.   Agrawal, M. and A. Biswas, *Molecular diagnostics of neurodegenerative disorders.* Front Mol Biosci, 2015. **2**: p. 54.
23.   Duckett, S. and J. Stern, *Origins of the Creutzfeldt and Jakob concept.* J Hist Neurosci, 1999. **8**(1): p. 21-34.
24.   Forstl, H., *The Lewy body variant of Alzheimer's disease: clinical, pathophysiological and conceptual issues.* Eur Arch Psychiatry Clin Neurosci, 1999. **249 Suppl 3**: p. 64-7.
25.   Graeber, M.B., et al., *Rediscovery of the case described by Alois Alzheimer in 1911: historical, histological and molecular genetic analysis.* Neurogenetics, 1997. **1**(1): p. 73-80.

26. Armstrong, R.A., *On the 'classification' of neurodegenerative disorders: discrete entities, overlap or continuum?* Folia Neuropathol, 2012. **50**(3): p. 201-8.

27. Irwin, D.J., *Tauopathies as clinicopathological entities.* Parkinsonism Relat Disord, 2016. **22 Suppl 1**: p. S29-33.

28. Lee, V.M., M. Goedert, and J.Q. Trojanowski, *Neurodegenerative tauopathies.* Annu Rev Neurosci, 2001. **24**: p. 1121-59.

29. Kovacs, G.G., *Tauopathies.* Handb Clin Neurol, 2017. **145**: p. 355-368.

30. Rascovsky, K., et al., *Sensitivity of revised diagnostic criteria for the behavioural variant of frontotemporal dementia.* Brain, 2011. **134**(Pt 9): p. 2456-77.

31. Gorno-Tempini, M.L., et al., *Classification of primary progressive aphasia and its variants.* Neurology, 2011. **76**(11): p. 1006-14.

32. Ghetti, B., et al., *Invited review: Frontotemporal dementia caused by microtubule-associated protein tau gene (MAPT) mutations: a chameleon for neuropathology and neuroimaging.* Neuropathol Appl Neurobiol, 2015. **41**(1): p. 24-46.

33. McKee, A.C., et al., *The spectrum of disease in chronic traumatic encephalopathy.* Brain, 2013. **136**(Pt 1): p. 43-64.

34. Varkey, J., et al., *Membrane curvature induction and tubulation are common features of synucleins and apolipoproteins.* J Biol Chem, 2010. **285**(42): p. 32486-93.

35. Peng, C., R.J. Gathagan, and V.M. Lee, *Distinct alpha-Synuclein strains and implications for heterogeneity among alpha-Synucleinopathies.* Neurobiol Dis, 2018. **109**(Pt B): p. 209-218.

36. Arai, K., et al., *Pure autonomic failure in association with human alpha-synucleinopathy.* Neurosci Lett, 2000. **296**(2-3): p. 171-3.

37. Cohen, T.J., V.M. Lee, and J.Q. Trojanowski, *TDP-43 functions and pathogenic mechanisms implicated in TDP-43 proteinopathies.* Trends Mol Med, 2011. **17**(11): p. 659-67.

38. Mackenzie, I.R., et al., *A harmonized classification system for FTLD-TDP pathology.* Acta Neuropathol, 2011. **122**(1): p. 111-3.

39. Bolton, D.C., M.P. McKinley, and S.B. Prusiner, *Identification of a protein that purifies with the scrapie prion.* Science, 1982. **218**(4579): p. 1309-11.

40. Prusiner, S.B., *Novel proteinaceous infectious particles cause scrapie.* Science, 1982. **216**(4542): p. 136-44.

41. Liemann, S. and R. Glockshuber, *Transmissible spongiform encephalopathies.* Biochem Biophys Res Commun, 1998. **250**(2): p. 187-93.

42. Lanson, N.A., Jr. and U.B. Pandey, *FUS-related proteinopathies: lessons from animal models.* Brain Res, 2012. **1462**: p. 44-60.

43. Neumann, M., et al., *A new subtype of frontotemporal lobar degeneration with FUS pathology.* Brain, 2009. **132**(Pt 11): p. 2922-31.

44. Munoz, D.G., et al., *FUS pathology in basophilic inclusion body disease.* Acta Neuropathol, 2009. **118**(5): p. 617-27.

45. Devys, D., et al., *Pathological mechanisms in polyglutamine expansion diseases.* Adv Exp Med Biol, 2001. **487**: p. 199-210.

46. Lomas, D.A. and R.W. Carrell, *Serpinopathies and the conformational dementias.* Nat Rev Genet, 2002. **3**(10): p. 759-68.

47. Davis, R.L., et al., *Familial dementia caused by polymerization of mutant neuroserpin.* Nature, 1999. **401**(6751): p. 376-9.

48. Dyson, H.J. and P.E. Wright, *Intrinsically unstructured proteins and their functions.* Nat Rev Mol Cell Biol, 2005. **6**(3): p. 197-208.

49. Chiti, F. and C.M. Dobson, *Protein misfolding, functional amyloid, and human disease.* Annu Rev Biochem, 2006. **75**: p. 333-66.

50. Uversky, V.N., *Amyloidogenesis of natively unfolded proteins.* Curr Alzheimer Res, 2008. **5**(3): p. 260-87.

51. Upadhyay, A., *Structure of proteins: Evolution with unsolved mysteries.* Prog Biophys Mol Biol, 2019.

52. Chen, B., et al., *Cellular strategies of protein quality control.* Cold Spring Harb Perspect Biol, 2011. **3**(8): p. a004374.

53. Rambaran, R.N. and L.C. Serpell, *Amyloid fibrils: abnormal protein assembly.* Prion, 2008. **2**(3): p. 112-7.

54. Soto, C. and S. Pritzkow, *Protein misfolding, aggregation, and conformational strains in neurodegenerative diseases.* Nat Neurosci, 2018. **21**(10): p. 1332-1340.

55. Pihlstrom, L., S. Wiethoff, and H. Houlden, *Genetics of neurodegenerative diseases: an overview.* Handb Clin Neurol, 2017. **145**: p. 309-323.

56. Campioni, S., et al., *A causative link between the structure of aberrant protein oligomers and their toxicity.* Nat Chem Biol, 2010. **6**(2): p. 140-7.

57. Lindberg, I., et al., *Chaperones in Neurodegeneration.* J Neurosci, 2015. **35**(41): p. 13853-9.

58. Glabe, C.G. and R. Kayed, *Common structure and toxic function of amyloid oligomers implies a common mechanism of pathogenesis.* Neurology, 2006. **66**(2 Suppl 1): p. S74-8.

59. Glabe, C.G., *Common mechanisms of amyloid oligomer pathogenesis in degenerative disease.* Neurobiol Aging, 2006. **27**(4): p. 570-5.

60. Dohm, C.P., P. Kermer, and M. Bahr, *Aggregopathy in neurodegenerative diseases: mechanisms and therapeutic implication.* Neurodegener Dis, 2008. **5**(6): p. 321-38.

61. Jarrett, J.T. and P.T. Lansbury, Jr., *Seeding "one-dimensional crystallization" of amyloid: a pathogenic mechanism in Alzheimer's disease and scrapie?* Cell, 1993. **73**(6): p. 1055-8.

62. Soto, C., L. Estrada, and J. Castilla, *Amyloids, prions and the inherent infectious nature of misfolded protein aggregates.* Trends Biochem Sci, 2006. **31**(3): p. 150-5.

63. Guo, J.L. and V.M. Lee, *Cell-to-cell transmission of pathogenic proteins in neurodegenerative diseases.* Nat Med, 2014. **20**(2): p. 130-8.

64. Vaquer-Alicea, J. and M.I. Diamond, *Propagation of Protein Aggregation in Neurodegenerative Diseases.* Annu Rev Biochem, 2019. **88**: p. 785-810.

65. Holmes, B.B., et al., *Heparan sulfate proteoglycans mediate internalization and propagation of specific proteopathic seeds.* Proc Natl Acad Sci U S A, 2013. **110**(33): p. E3138-47.

66. Lim, Y.J. and S.J. Lee, *Are exosomes the vehicle for protein aggregate propagation in neurodegenerative diseases?* Acta Neuropathol Commun, 2017. **5**(1): p. 64.

67. Yanez-Mo, M., et al., *Biological properties of extracellular vesicles and their physiological functions.* J Extracell Vesicles, 2015. **4**: p. 27066.

68. Moore, R.A., I. Vorberg, and S.A. Priola, *Species barriers in prion diseases--brief review.* Arch Virol Suppl, 2005(19): p. 187-202.

69. Moreno-Gonzalez, I. and C. Soto, *Misfolded protein aggregates: mechanisms, structures and potential for disease transmission.* Semin Cell Dev Biol, 2011. **22**(5): p. 482-7.

70. Baker, H.F., et al., *Evidence for the experimental transmission of cerebral beta-amyloidosis to primates.* Int J Exp Pathol, 1993. **74**(5): p. 441-54.

71. Rosen, R.F., et al., *Exogenous seeding of cerebral beta-amyloid deposition in betaAPP-transgenic rats.* J Neurochem, 2012. **120**(5): p. 660-6.

72. Guo, J.L. and V.M. Lee, *Neurofibrillary tangle-like tau pathology induced by synthetic tau fibrils in primary neurons over-expressing mutant tau.* FEBS Lett, 2013. **587**(6): p. 717-23.

73. Iba, M., et al., *Synthetic tau fibrils mediate transmission of neurofibrillary tangles in a transgenic mouse model of Alzheimer's-like tauopathy.* J Neurosci, 2013. **33**(3): p. 1024-37.

74. Clavaguera, F., et al., *Transmission and spreading of tauopathy in transgenic mouse brain.* Nat Cell Biol, 2009. **11**(7): p. 909-13.

75. Clavaguera, F., et al., *"Prion-like" templated misfolding in tauopathies.* Brain Pathol, 2013. **23**(3): p. 342-9.

76. Lasagna-Reeves, C.A., et al., *Alzheimer brain-derived tau oligomers propagate pathology from endogenous tau.* Sci Rep, 2012. **2**: p. 700.

77. Clavaguera, F., et al., *Brain homogenates from human tauopathies induce tau inclusions in mouse brain.* Proc Natl Acad Sci U S A, 2013. **110**(23): p. 9535-40.

78. Mougenot, A.L., et al., *Prion-like acceleration of a synucleinopathy in a transgenic mouse model.* Neurobiol Aging, 2012. **33**(9): p. 2225-8.

79. Luk, K.C., et al., *Intracerebral inoculation of pathological alpha-synuclein initiates a rapidly progressive neurodegenerative alpha-synucleinopathy in mice.* J Exp Med, 2012. **209**(5): p. 975-86.

80. Guo, J.L., et al., *Distinct alpha-synuclein strains differentially promote tau inclusions in neurons.* Cell, 2013. **154**(1): p. 103-17.

81. Morales, R., I. Moreno-Gonzalez, and C. Soto, *Cross-seeding of misfolded proteins: implications for etiology and pathogenesis of protein misfolding diseases.* PLoS Pathog, 2013. **9**(9): p. e1003537.

82. Mandal, P.K., et al., *Interaction between Abeta peptide and alpha synuclein: molecular mechanisms in overlapping pathology of Alzheimer's and Parkinson's in dementia with Lewy body disease.* Neurochem Res, 2006. **31**(9): p. 1153-62.

83. Guo, J.P., et al., *Abeta and tau form soluble complexes that may promote self aggregation of both into the insoluble forms observed in Alzheimer's disease.* Proc Natl Acad Sci U S A, 2006. **103**(6): p. 1953-8.

84. Clinton, L.K., et al., *Synergistic Interactions between Abeta, tau, and alpha-synuclein: acceleration of neuropathology and cognitive decline.* J Neurosci, 2010. **30**(21): p. 7281-9.

85. Hamilton, R.L., *Lewy bodies in Alzheimer's disease: a neuropathological review of 145 cases using alpha-synuclein immunohistochemistry.* Brain Pathol, 2000. **10**(3): p. 378-84.

86. Sanders, D.W., et al., *Distinct tau prion strains propagate in cells and mice and define different tauopathies.* Neuron, 2014. **82**(6): p. 1271-88.

87. Kaufman, S.K., et al., *Tau Prion Strains Dictate Patterns of Cell Pathology, Progression Rate, and Regional Vulnerability In Vivo.* Neuron, 2016. **92**(4): p. 796-812.

88. Audouard, E., et al., *High-Molecular-Weight Paired Helical Filaments from Alzheimer Brain Induces Seeding of Wild-Type Mouse Tau into an Argyrophilic 4R Tau Pathology in Vivo.* Am J Pathol, 2016. **186**(10): p. 2709-22.

89. Narasimhan, S., et al., *Pathological Tau Strains from Human Brains Recapitulate the Diversity of Tauopathies in Nontransgenic Mouse Brain.* J Neurosci, 2017. **37**(47): p. 11406-11423.

90. Watts, J.C., et al., *Serial propagation of distinct strains of Abeta prions from Alzheimer's disease patients.* Proc Natl Acad Sci U S A, 2014. **111**(28): p. 10323-8.

91. Stohr, J., et al., *Distinct synthetic Abeta prion strains producing different amyloid deposits in bigenic mice.* Proc Natl Acad Sci U S A, 2014. **111**(28): p. 10329-34.

92. Masuda-Suzukake, M., et al., *Prion-like spreading of pathological alpha-synuclein in brain.* Brain, 2013. **136**(Pt 4): p. 1128-38.

93. Prusiner, S.B., et al., *Evidence for alpha-synuclein prions causing multiple system atrophy in humans with parkinsonism.* Proc Natl Acad Sci U S A, 2015. **112**(38): p. E5308-17.

94. Woerman, A.L., et al., *Propagation of prions causing synucleinopathies in cultured cells.* Proc Natl Acad Sci U S A, 2015. **112**(35): p. E4949-58.

95. Wasmer, C., et al., *Amyloid fibrils of the HET-s(218-289) prion form a beta solenoid with a triangular hydrophobic core.* Science, 2008. **319**(5869): p. 1523-6.

96. Guerrero-Ferreira, R., et al., *Cryo-EM structure of alpha-synuclein fibrils.* Elife, 2018. **7**.

97. Gremer, L., et al., *Fibril structure of amyloid-beta(1-42) by cryo-electron microscopy.* Science, 2017. **358**(6359): p. 116-119.

98. Fitzpatrick, A.W., et al., *4D cryo-electron microscopy of proteins.* J Am Chem Soc, 2013. **135**(51): p. 19123-6.

99. Fitzpatrick, A.W.P., et al., *Cryo-EM structures of tau filaments from Alzheimer's disease.* Nature, 2017. **547**(7662): p. 185-190.

100. Falcon, B., et al., *Structures of filaments from Pick's disease reveal a novel tau protein fold.* Nature, 2018. **561**(7721): p. 137-140.

101. Sunde, M., et al., *Common core structure of amyloid fibrils by synchrotron X-ray diffraction.* J Mol Biol, 1997. **273**(3): p. 729-39.

102. Fandrich, M. and C.M. Dobson, *The behaviour of polyamino acids reveals an inverse side chain effect in amyloid structure formation.* EMBO J, 2002. **21**(21): p. 5682-90.

103. Kajava, A.V. and A.C. Steven, *Beta-rolls, beta-helices, and other beta-solenoid proteins.* Adv Protein Chem, 2006. **73**: p. 55-96.
104. Wright, C.F., et al., *The importance of sequence diversity in the aggregation and evolution of proteins.* Nature, 2005. **438**(7069): p. 878-81.
105. Alarcon, P., et al., *Spatio-temporal and risk factor analysis of alleles related to Scrapie resistance in sheep in Great Britain before, during and after a national breeding program.* Prev Vet Med, 2018. **159**: p. 12-21.
106. Petkova, A.T., et al., *Self-propagating, molecular-level polymorphism in Alzheimer's beta-amyloid fibrils.* Science, 2005. **307**(5707): p. 262-5.
107. Meisl, G., et al., *Differences in nucleation behavior underlie the contrasting aggregation kinetics of the Abeta40 and Abeta42 peptides.* Proc Natl Acad Sci U S A, 2014. **111**(26): p. 9384-9.
108. Baldwin, A.J., et al., *Metastability of native proteins and the phenomenon of amyloid formation.* J Am Chem Soc, 2011. **133**(36): p. 14160-3.
109. Peelaerts, W., et al., *alpha-Synuclein strains cause distinct synucleinopathies after local and systemic administration.* Nature, 2015. **522**(7556): p. 340-4.
110. Andreadis, A., *Misregulation of tau alternative splicing in neurodegeneration and dementia.* Prog Mol Subcell Biol, 2006. **44**: p. 89-107.
111. Caillet-Boudin, M.L., et al., *Regulation of human MAPT gene expression.* Mol Neurodegener, 2015. **10**: p. 28.
112. Sergeant, N., A. Delacourte, and L. Buee, *Tau protein as a differential biomarker of tauopathies.* Biochim Biophys Acta, 2005. **1739**(2-3): p. 179-97.
113. Kahlson, M.A. and K.J. Colodner, *Glial Tau Pathology in Tauopathies: Functional Consequences.* J Exp Neurosci, 2015. **9**(Suppl 2): p. 43-50.
114. !!! INVALID CITATION !!! [60].
115. Schoenfeld, T.A. and R.A. Obar, *Diverse distribution and function of fibrous microtubule-associated proteins in the nervous system.* Int Rev Cytol, 1994. **151**: p. 67-137.
116. Tucker, R.P., *The roles of microtubule-associated proteins in brain morphogenesis: a review.* Brain Res Brain Res Rev, 1990. **15**(2): p. 101-20.
117. Dugger, B.N., et al., *The Presence of Select Tau Species in Human Peripheral Tissues and Their Relation to Alzheimer's Disease.* J Alzheimers Dis, 2016. **51**(2): p. 345-56.
118. Wang, Y. and E. Mandelkow, *Tau in physiology and pathology.* Nat Rev Neurosci, 2016. **17**(1): p. 5-21.
119. Goedert, M., et al., *Multiple isoforms of human microtubule-associated protein tau: sequences and localization in neurofibrillary tangles of Alzheimer's disease.* Neuron, 1989. **3**(4): p. 519-26.
120. Goedert, M., et al., *Cloning and sequencing of the cDNA encoding an isoform of microtubule-associated protein tau containing four tandem repeats: differential expression of tau protein mRNAs in human brain.* EMBO J, 1989. **8**(2): p. 393-9.
121. Kosik, K.S., C.L. Joachim, and D.J. Selkoe, *Microtubule-associated protein tau (tau) is a major antigenic component of paired helical filaments in Alzheimer disease.* Proc Natl Acad Sci U S A, 1986. **83**(11): p. 4044-8.
122. Gustke, N., et al., *Domains of tau protein and interactions with microtubules.* Biochemistry, 1994. **33**(32): p. 9511-22.
123. Drechsel, D.N., et al., *Modulation of the dynamic instability of tubulin assembly by the microtubule-associated protein tau.* Mol Biol Cell, 1992. **3**(10): p. 1141-54.
124. Jeganathan, S., et al., *The natively unfolded character of tau and its aggregation to Alzheimer-like paired helical filaments.* Biochemistry, 2008. **47**(40): p. 10526-39.
125. Buee, L., et al., *Tau protein isoforms, phosphorylation and role in neurodegenerative disorders.* Brain Res Brain Res Rev, 2000. **33**(1): p. 95-130.
126. Sontag, E., et al., *Molecular interactions among protein phosphatase 2A, tau, and microtubules. Implications for the regulation of tau phosphorylation and the development of tauopathies.* J Biol Chem, 1999. **274**(36): p. 25490-8.

127. Takashima, A., et al., *Presenilin 1 associates with glycogen synthase kinase-3beta and its substrate tau.* Proc Natl Acad Sci U S A, 1998. **95**(16): p. 9637-41.
128. Barghorn, S. and E. Mandelkow, *Toward a unified scheme for the aggregation of tau into Alzheimer paired helical filaments.* Biochemistry, 2002. **41**(50): p. 14885-96.
129. Lim, S., et al., *Cell-based Models To Investigate Tau Aggregation.* Comput Struct Biotechnol J, 2014. **12**(20-21): p. 7-13.
130. Janke, C., et al., *Phylogenetic diversity of the expression of the microtubule-associated protein tau: implications for neurodegenerative disorders.* Brain Res Mol Brain Res, 1999. **68**(1-2): p. 119-28.
131. Iqbal, K., et al., *Tau in Alzheimer disease and related tauopathies.* Curr Alzheimer Res, 2010. **7**(8): p. 656-64.
132. Guo, T., W. Noble, and D.P. Hanger, *Roles of tau protein in health and disease.* Acta Neuropathol, 2017. **133**(5): p. 665-704.
133. Dickson, D.W., et al., *Neuropathology of frontotemporal lobar degeneration-tau (FTLD-tau).* J Mol Neurosci, 2011. **45**(3): p. 384-9.
134. Goedert, M., et al., *Tau proteins of Alzheimer paired helical filaments: abnormal phosphorylation of all six brain isoforms.* Neuron, 1992. **8**(1): p. 159-68.
135. Goedert, M., et al., *Epitope mapping of monoclonal antibodies to the paired helical filaments of Alzheimer's disease: identification of phosphorylation sites in tau protein.* Biochem J, 1994. **301 (Pt 3)**: p. 871-7.
136. Mailliot, C., et al., *Phosphorylation of specific sets of tau isoforms reflects different neurofibrillary degeneration processes.* FEBS Lett, 1998. **433**(3): p. 201-4.
137. Reitz, C., C. Brayne, and R. Mayeux, *Epidemiology of Alzheimer disease.* Nat Rev Neurol, 2011. **7**(3): p. 137-52.
138. Masters, C.L., et al., *Alzheimer's disease.* Nat Rev Dis Primers, 2015. **1**: p. 15056.
139. Karch, C.M. and A.M. Goate, *Alzheimer's disease risk genes and mechanisms of disease pathogenesis.* Biol Psychiatry, 2015. **77**(1): p. 43-51.
140. Bateman, R.J., et al., *Autosomal-dominant Alzheimer's disease: a review and proposal for the prevention of Alzheimer's disease.* Alzheimers Res Ther, 2011. **3**(1): p. 1.
141. Schneider, J.A., et al., *The neuropathology of probable Alzheimer disease and mild cognitive impairment.* Ann Neurol, 2009. **66**(2): p. 200-8.
142. Jost, B.C. and G.T. Grossberg, *The evolution of psychiatric symptoms in Alzheimer's disease: a natural history study.* J Am Geriatr Soc, 1996. **44**(9): p. 1078-81.
143. Jost, B.C. and G.T. Grossberg, *The natural history of Alzheimer's disease: a brain bank study.* J Am Geriatr Soc, 1995. **43**(11): p. 1248-55.
144. Serrano-Pozo, A., et al., *Neuropathological alterations in Alzheimer disease.* Cold Spring Harb Perspect Med, 2011. **1**(1): p. a006189.
145. Garai, K. and C. Frieden, *Quantitative analysis of the time course of Abeta oligomerization and subsequent growth steps using tetramethylrhodamine-labeled Abeta.* Proc Natl Acad Sci U S A, 2013. **110**(9): p. 3321-6.
146. Braak, H. and E. Braak, *Neuropathological stageing of Alzheimer-related changes.* Acta Neuropathol, 1991. **82**(4): p. 239-59.
147. Crowther, R.A., *Straight and paired helical filaments in Alzheimer disease have a common structural unit.* Proc Natl Acad Sci U S A, 1991. **88**(6): p. 2288-92.
148. Braak, H. and E. Braak, *Morphological criteria for the recognition of Alzheimer's disease and the distribution pattern of cortical changes related to this disorder.* Neurobiol Aging, 1994. **15**(3): p. 355-6; discussion 379-80.
149. Williams, D.R., et al., *Characteristics of two distinct clinical phenotypes in pathologically proven progressive supranuclear palsy: Richardson's syndrome and PSP-parkinsonism.* Brain, 2005. **128**: p. 1247-1258.
150. Bigio, E.H., D.F. Brown, and C.L. White, 3rd, *Progressive supranuclear palsy with dementia: cortical pathology.* J Neuropathol Exp Neurol, 1999. **58**(4): p. 359-64.
151. Hauw, J.J., et al., *Preliminary NINDS neuropathologic criteria for Steele-Richardson-Olszewski syndrome (progressive supranuclear palsy).* Neurology, 1994. **44**(11): p. 2015-9.

152. Tsuboi, Y., et al., *Atrophy of superior cerebellar peduncle in progressive supranuclear palsy.* Neurology, 2003. **60**(11): p. 1766-9.
153. Nishimura, M., et al., *Glial fibrillary tangles with straight tubules in the brains of patients with progressive supranuclear palsy.* Neurosci Lett, 1992. **143**(1-2): p. 35-8.
154. Komori, T., et al., *Astrocytic plaques and tufts of abnormal fibers do not coexist in corticobasal degeneration and progressive supranuclear palsy.* Acta Neuropathol, 1998. **96**(4): p. 401-8.
155. Arima, K., et al., *Ultrastructural characterization of the tau-immunoreactive tubules in the oligodendroglial perikarya and their inner loop processes in progressive supranuclear palsy.* Acta Neuropathol, 1997. **93**(6): p. 558-66.
156. Dickson, D.W., et al., *Neuropathology of variants of progressive supranuclear palsy.* Curr Opin Neurol, 2010. **23**(4): p. 394-400.
157. Litvan, I., D.A. Grimes, and A.E. Lang, *Phenotypes and prognosis: clinicopathologic studies of corticobasal degeneration.* Adv Neurol, 2000. **82**: p. 183-96.
158. Bak, T.H. and J.R. Hodges, *Corticobasal degeneration: clinical aspects.* Handb Clin Neurol, 2008. **89**: p. 509-21.
159. Bergeron, C., et al., *Unusual clinical presentations of cortical-basal ganglionic degeneration.* Ann Neurol, 1996. **40**(6): p. 893-900.
160. Ikeda, K., et al., *Corticobasal degeneration with primary progressive aphasia and accentuated cortical lesion in superior temporal gyrus: case report and review.* Acta Neuropathol, 1996. **92**(5): p. 534-9.
161. Feany, M.B. and D.W. Dickson, *Widespread cytoskeletal pathology characterizes corticobasal degeneration.* Am J Pathol, 1995. **146**(6): p. 1388-96.
162. Komori, T., *Tau-positive glial inclusions in progressive supranuclear palsy, corticobasal degeneration and Pick's disease.* Brain Pathol, 1999. **9**(4): p. 663-79.
163. Dickson, D.W., *Neuropathologic differentiation of progressive supranuclear palsy and corticobasal degeneration.* J Neurol, 1999. **246 Suppl 2**: p. II6-15.
164. Foster, N.L., et al., *Frontotemporal dementia and parkinsonism linked to chromosome 17: a consensus conference. Conference Participants.* Ann Neurol, 1997. **41**(6): p. 706-15.
165. Tsuboi, Y., et al., *Clinical and genetic studies of families with the tau N279K mutation (FTDP-17).* Neurology, 2002. **59**(11): p. 1791-3.
166. Goedert, M., B. Ghetti, and M.G. Spillantini, *Frontotemporal dementia: implications for understanding Alzheimer disease.* Cold Spring Harb Perspect Med, 2012. **2**(2): p. a006254.
167. Wszolek, Z.K., et al., *Frontotemporal dementia and parkinsonism linked to chromosome 17 (FTDP-17).* Orphanet J Rare Dis, 2006. **1**: p. 30.
168. Yen, S., et al., *FTDP-17 tau mutations decrease the susceptibility of tau to calpain I digestion.* FEBS Lett, 1999. **461**(1-2): p. 91-5.
169. Spillantini, M.G., et al., *Familial multiple system tauopathy with presenile dementia: a disease with abundant neuronal and glial tau filaments.* Proc Natl Acad Sci U S A, 1997. **94**(8): p. 4113-8.
170. Sumi, S.M., et al., *Familial presenile dementia with psychosis associated with cortical neurofibrillary tangles and degeneration of the amygdala.* Neurology, 1992. **42**(1): p. 120-7.
171. Spillantini, M.G., T.D. Bird, and B. Ghetti, *Frontotemporal dementia and Parkinsonism linked to chromosome 17: a new group of tauopathies.* Brain Pathol, 1998. **8**(2): p. 387-402.
172. Lashuel, H.A., et al., *The many faces of alpha-synuclein: from structure and toxicity to therapeutic target.* Nat Rev Neurosci, 2013. **14**(1): p. 38-48.
173. George, J.M., *The synucleins.* Genome Biol, 2002. **3**(1): p. REVIEWS3002.
174. Giasson, B.I., et al., *A hydrophobic stretch of 12 amino acid residues in the middle of alpha-synuclein is essential for filament assembly.* J Biol Chem, 2001. **276**(4): p. 2380-6.
175. Bartels, T., J.G. Choi, and D.J. Selkoe, *alpha-Synuclein occurs physiologically as a helically folded tetramer that resists aggregation.* Nature, 2011. **477**(7362): p. 107-10.
176. Burre, J., et al., *Alpha-synuclein promotes SNARE-complex assembly in vivo and in vitro.* Science, 2010. **329**(5999): p. 1663-7.

177. Lee, A.C., et al., *Dopamine and the representation of the upper visual field: evidence from vertical bisection errors in unilateral Parkinson's disease.* Neuropsychologia, 2002. **40**(12): p. 2023-9.
178. Allen Reish, H.E. and D.G. Standaert, *Role of alpha-synuclein in inducing innate and adaptive immunity in Parkinson disease.* J Parkinsons Dis, 2015. **5**(1): p. 1-19.
179. Polymeropoulos, M.H., et al., *Mutation in the alpha-synuclein gene identified in families with Parkinson's disease.* Science, 1997. **276**(5321): p. 2045-7.
180. Dehay, B., et al., *Targeting alpha-synuclein for treatment of Parkinson's disease: mechanistic and therapeutic considerations.* Lancet Neurol, 2015. **14**(8): p. 855-866.
181. de Lau, L.M. and M.M. Breteler, *Epidemiology of Parkinson's disease.* Lancet Neurol, 2006. **5**(6): p. 525-35.
182. Kumar, K.R., K. Lohmann, and C. Klein, *Genetics of Parkinson disease and other movement disorders.* Curr Opin Neurol, 2012. **25**(4): p. 466-74.
183. Dickson, D.W., *Neuropathology of Parkinson disease.* Parkinsonism Relat Disord, 2018. **46 Suppl 1**: p. S30-S33.
184. Dickson, D.W., *Parkinson's disease and parkinsonism: neuropathology.* Cold Spring Harb Perspect Med, 2012. **2**(8).
185. Salat, D. and E. Tolosa, *Levodopa in the treatment of Parkinson's disease: current status and new developments.* J Parkinsons Dis, 2013. **3**(3): p. 255-69.
186. Wakabayashi, K., et al., *NACP/alpha-synuclein-positive filamentous inclusions in astrocytes and oligodendrocytes of Parkinson's disease brains.* Acta Neuropathol, 2000. **99**(1): p. 14-20.
187. Cykowski, M.D., et al., *Expanding the spectrum of neuronal pathology in multiple system atrophy.* Brain, 2015. **138**(Pt 8): p. 2293-309.
188. Dickson, D.W., et al., *Evidence in favor of Braak staging of Parkinson's disease.* Mov Disord, 2010. **25 Suppl 1**: p. S78-82.
189. Braak, H., et al., *Staging of brain pathology related to sporadic Parkinson's disease.* Neurobiol Aging, 2003. **24**(2): p. 197-211.
190. Fanciulli, A. and G.K. Wenning, *Multiple-system atrophy.* N Engl J Med, 2015. **372**(3): p. 249-63.
191. Kollensperger, M., et al., *Red flags for multiple system atrophy.* Mov Disord, 2008. **23**(8): p. 1093-9.
192. Papp, M.I., J.E. Kahn, and P.L. Lantos, *Glial cytoplasmic inclusions in the CNS of patients with multiple system atrophy (striatonigral degeneration, olivopontocerebellar atrophy and Shy-Drager syndrome).* J Neurol Sci, 1989. **94**(1-3): p. 79-100.
193. Nakamura, K., et al., *Filamentous aggregations of phosphorylated alpha-synuclein in Schwann cells (Schwann cell cytoplasmic inclusions) in multiple system atrophy.* Acta Neuropathol Commun, 2015. **3**: p. 29.
194. Galasko, D., *Lewy Body Disorders.* Neurol Clin, 2017. **35**(2): p. 325-338.
195. McKeith, I.G., et al., *Diagnosis and management of dementia with Lewy bodies: third report of the DLB Consortium.* Neurology, 2005. **65**(12): p. 1863-72.
196. Karantzoulis, S. and J.E. Galvin, *Distinguishing Alzheimer's disease from other major forms of dementia.* Expert Rev Neurother, 2011. **11**(11): p. 1579-91.
197. Geser, F., et al., *How to diagnose dementia with Lewy bodies: state of the art.* Mov Disord, 2005. **20 Suppl 12**: p. S11-20.
198. Harding, A.J. and G.M. Halliday, *Cortical Lewy body pathology in the diagnosis of dementia.* Acta Neuropathol, 2001. **102**(4): p. 355-63.
199. Gomperts, S.N., *Lewy Body Dementias: Dementia With Lewy Bodies and Parkinson Disease Dementia.* Continuum (Minneap Minn), 2016. **22**(2 Dementia): p. 435-63.
200. Rachakonda, V., T.H. Pan, and W.D. Le, *Biomarkers of neurodegenerative disorders: how good are they?* Cell Res, 2004. **14**(5): p. 347-58.
201. Husain, M., *How far can biomarkers take us in neurodegenerative disorders?* Brain, 2017. **140**(12): p. 3067-3068.

202. Mulder, C., et al., *Genetic and biochemical markers for Alzheimer's disease: recent developments.* Ann Clin Biochem, 2000. **37 (Pt 5)**: p. 593-607.
203. Simon, R., *Sensitivity, Specificity, PPV, and NPV for Predictive Biomarkers.* J Natl Cancer Inst, 2015. **107**(8).
204. Yerushalmy, J., *Statistical problems in assessing methods of medical diagnosis, with special reference to X-ray techniques.* Public Health Rep, 1947. **62**(40): p. 1432-49.
205. Brower, V., *Biomarkers: Portents of malignancy.* Nature, 2011. **471**(7339): p. S19-21.
206. Parnetti, L. and D. Chiasserini, *Role of CSF biomarkers in the diagnosis of prodromal Alzheimer's disease.* Biomark Med, 2011. **5**(4): p. 479-84.
207. Coughlin, D. and D.J. Irwin, *Emerging Diagnostic and Therapeutic Strategies for Tauopathies.* Curr Neurol Neurosci Rep, 2017. **17**(9): p. 72.
208. Whitwell, J.L. and K.A. Josephs, *Neuroimaging in frontotemporal lobar degeneration-- predicting molecular pathology.* Nat Rev Neurol, 2012. **8**(3): p. 131-42.
209. Chien, D.T., et al., *Early clinical PET imaging results with the novel PHF-tau radioligand [F18]-T808.* J Alzheimers Dis, 2014. **38**(1): p. 171-84.
210. Lowe, V.J., et al., *An autoradiographic evaluation of AV-1451 Tau PET in dementia.* Acta Neuropathol Commun, 2016. **4**(1): p. 58.
211. Oeckl, P., et al., *Neurochemical biomarkers in the diagnosis of frontotemporal lobar degeneration: an update.* J Neurochem, 2016. **138 Suppl 1**: p. 184-92.
212. Shaw, L.M., et al., *Cerebrospinal fluid biomarker signature in Alzheimer's disease neuroimaging initiative subjects.* Ann Neurol, 2009. **65**(4): p. 403-13.
213. Irwin, D.J., et al., *Comparison of cerebrospinal fluid levels of tau and Abeta 1-42 in Alzheimer disease and frontotemporal degeneration using 2 analytical platforms.* Arch Neurol, 2012. **69**(8): p. 1018-25.
214. Saunders, A.M., et al., *Association of apolipoprotein E allele epsilon 4 with late-onset familial and sporadic Alzheimer's disease.* Neurology, 1993. **43**(8): p. 1467-72.
215. Mayeux, R., et al., *Utility of the apolipoprotein E genotype in the diagnosis of Alzheimer's disease. Alzheimer's Disease Centers Consortium on Apolipoprotein E and Alzheimer's Disease.* N Engl J Med, 1998. **338**(8): p. 506-11.
216. McKhann, G.M., et al., *The diagnosis of dementia due to Alzheimer's disease: recommendations from the National Institute on Aging-Alzheimer's Association workgroups on diagnostic guidelines for Alzheimer's disease.* Alzheimers Dement, 2011. **7**(3): p. 263-9.
217. Kovacs, G.G. and H. Budka, *Current concepts of neuropathological diagnostics in practice: neurodegenerative diseases.* Clin Neuropathol, 2010. **29**(5): p. 271-88.
218. Sabbagh, M.N., et al., *Increasing Precision of Clinical Diagnosis of Alzheimer's Disease Using a Combined Algorithm Incorporating Clinical and Novel Biomarker Data.* Neurol Ther, 2017. **6**(Suppl 1): p. 83-95.
219. Beach, T.G., et al., *Accuracy of the clinical diagnosis of Alzheimer disease at National Institute on Aging Alzheimer Disease Centers, 2005-2010.* J Neuropathol Exp Neurol, 2012. **71**(4): p. 266-73.
220. Adler, C.H., et al., *Low clinical diagnostic accuracy of early vs advanced Parkinson disease: clinicopathologic study.* Neurology, 2014. **83**(5): p. 406-12.
221. McKeith, I.G., et al., *Prospective validation of consensus criteria for the diagnosis of dementia with Lewy bodies.* Neurology, 2000. **54**(5): p. 1050-8.
222. Merdes, A.R., et al., *Influence of Alzheimer pathology on clinical diagnostic accuracy in dementia with Lewy bodies.* Neurology, 2003. **60**(10): p. 1586-90.
223. Montine, T.J., et al., *National Institute on Aging-Alzheimer's Association guidelines for the neuropathologic assessment of Alzheimer's disease: a practical approach.* Acta Neuropathol, 2012. **123**(1): p. 1-11.
224. Lee, G. and C.J. Leugers, *Tau and tauopathies.* Prog Mol Biol Transl Sci, 2012. **107**: p. 263-93.
225. Cairns, N.J., et al., *Neuropathologic diagnostic and nosologic criteria for frontotemporal lobar degeneration: consensus of the Consortium for Frontotemporal Lobar Degeneration.* Acta Neuropathol, 2007. **114**(1): p. 5-22.

226. Campbell, B.C., et al., *The solubility of alpha-synuclein in multiple system atrophy differs from that of dementia with Lewy bodies and Parkinson's disease.* J Neurochem, 2001. **76**(1): p. 87-96.
227. Walker, L.C. and M. Jucker, *Neurodegenerative diseases: expanding the prion concept.* Annu Rev Neurosci, 2015. **38**: p. 87-103.
228. Soto, C., G.P. Saborio, and L. Anderes, *Cyclic amplification of protein misfolding: application to prion-related disorders and beyond.* Trends Neurosci, 2002. **25**(8): p. 390-4.
229. Barria, M.A., D. Gonzalez-Romero, and C. Soto, *Cyclic amplification of prion protein misfolding.* Methods Mol Biol, 2012. **849**: p. 199-212.
230. Saa, P., J. Castilla, and C. Soto, *Ultra-efficient replication of infectious prions by automated protein misfolding cyclic amplification.* J Biol Chem, 2006. **281**(46): p. 35245-52.
231. Castilla, J., et al., *In vitro generation of infectious scrapie prions.* Cell, 2005. **121**(2): p. 195-206.
232. Castilla, J., et al., *Crossing the species barrier by PrP(Sc) replication in vitro generates unique infectious prions.* Cell, 2008. **134**(5): p. 757-68.
233. Xue, C., et al., *Thioflavin T as an amyloid dye: fibril quantification, optimal concentration and effect on aggregation.* R Soc Open Sci, 2017. **4**(1): p. 160696.
234. Atarashi, R., et al., *Ultrasensitive human prion detection in cerebrospinal fluid by real-time quaking-induced conversion.* Nat Med, 2011. **17**(2): p. 175-8.
235. Castilla, J., P. Saa, and C. Soto, *Detection of prions in blood.* Nat Med, 2005. **11**(9): p. 982-5.
236. Saa, P., J. Castilla, and C. Soto, *Presymptomatic detection of prions in blood.* Science, 2006. **313**(5783): p. 92-4.
237. Bougard, D., et al., *Detection of prions in the plasma of presymptomatic and symptomatic patients with variant Creutzfeldt-Jakob disease.* Sci Transl Med, 2016. **8**(370): p. 370ra182.
238. Concha-Marambio, L., et al., *Detection of prions in blood from patients with variant Creutzfeldt-Jakob disease.* Sci Transl Med, 2016. **8**(370): p. 370ra183.
239. Moda, F., et al., *Prions in the urine of patients with variant Creutzfeldt-Jakob disease.* N Engl J Med, 2014. **371**(6): p. 530-9.
240. Barria, M.A., et al., *Rapid amplification of prions from variant Creutzfeldt-Jakob disease cerebrospinal fluid.* J Pathol Clin Res, 2018. **4**(2): p. 86-92.
241. Rubenstein, R. and B. Chang, *Re-assessment of PrP(Sc) distribution in sporadic and variant CJD.* PLoS One, 2013. **8**(7): p. e66352.
242. McGuire, L.I., et al., *Real time quaking-induced conversion analysis of cerebrospinal fluid in sporadic Creutzfeldt-Jakob disease.* Ann Neurol, 2012. **72**(2): p. 278-85.
243. Zanusso, G., et al., *Advanced tests for early and accurate diagnosis of Creutzfeldt-Jakob disease.* Nat Rev Neurol, 2016. **12**(7): p. 427.
244. Franceschini, A., et al., *High diagnostic value of second generation CSF RT-QuIC across the wide spectrum of CJD prions.* Sci Rep, 2017. **7**(1): p. 10655.
245. Orru, C.D., et al., *Rapid and sensitive RT-QuIC detection of human Creutzfeldt-Jakob disease using cerebrospinal fluid.* MBio, 2015. **6**(1).
246. Salvadores, N., et al., *Detection of misfolded Abeta oligomers for sensitive biochemical diagnosis of Alzheimer's disease.* Cell Rep, 2014. **7**(1): p. 261-8.
247. Saijo, E., et al., *Ultrasensitive and selective detection of 3-repeat tau seeding activity in Pick disease brain and cerebrospinal fluid.* Acta Neuropathol, 2017. **133**(5): p. 751-765.
248. Fairfoul, G., et al., *Alpha-synuclein RT-QuIC in the CSF of patients with alpha-synucleinopathies.* Ann Clin Transl Neurol, 2016. **3**(10): p. 812-818.
249. Shahnawaz, M., et al., *Development of a Biochemical Diagnosis of Parkinson Disease by Detection of alpha-Synuclein Misfolded Aggregates in Cerebrospinal Fluid.* JAMA Neurol, 2017. **74**(2): p. 163-172.
250. Groveman, B.R., et al., *Rapid and ultra-sensitive quantitation of disease-associated alpha-synuclein seeds in brain and cerebrospinal fluid by alphaSyn RT-QuIC.* Acta Neuropathol Commun, 2018. **6**(1): p. 7.

251.   De Luca, C.M.G., et al., *Efficient RT-QuIC seeding activity for alpha-synuclein in olfactory mucosa samples of patients with Parkinson's disease and multiple system atrophy.* Transl Neurodegener, 2019. **8**: p. 24.

252.   Zanusso, G., et al., *Detection of pathologic prion protein in the olfactory epithelium in sporadic Creutzfeldt-Jakob disease.* N Engl J Med, 2003. **348**(8): p. 711-9.

253.   Orru, C.D., et al., *A test for Creutzfeldt-Jakob disease using nasal brushings.* N Engl J Med, 2014. **371**(6): p. 519-29.

254.   Redaelli, V., et al., *Detection of prion seeding activity in the olfactory mucosa of patients with Fatal Familial Insomnia.* Sci Rep, 2017. **7**: p. 46269.

255.   Schmitz, M., et al., *Application of an in vitro-amplification assay as a novel pre-screening test for compounds inhibiting the aggregation of prion protein scrapie.* Sci Rep, 2016. **6**: p. 28711.

256.   Herva, M.E., et al., *Anti-amyloid compounds inhibit alpha-synuclein aggregation induced by protein misfolding cyclic amplification (PMCA).* J Biol Chem, 2014. **289**(17): p. 11897-905.

257.   Gandini, A., et al., *Tau-Centric Multitarget Approach for Alzheimer's Disease: Development of First-in-Class Dual Glycogen Synthase Kinase 3beta and Tau-Aggregation Inhibitors.* J Med Chem, 2018. **61**(17): p. 7640-7656.

258.   Sucheta, S. Tahlan, and P.K. Verma, *Biological potential of thiazolidinedione derivatives of synthetic origin.* Chem Cent J, 2017. **11**(1): p. 130.

259.   Sartiani, L., et al., *Biochemical and Electrophysiological Modification of Amyloid Transthyretin on Cardiomyocytes.* Biophys J, 2016. **111**(9): p. 2024-2038.

260.   Adams, S.J., et al., *Three repeat isoforms of tau inhibit assembly of four repeat tau filaments.* PLoS One, 2010. **5**(5): p. e10810.

261.   Molinuevo, J.L., et al., *White matter changes in preclinical Alzheimer's disease: a magnetic resonance imaging-diffusion tensor imaging study on cognitively normal older people with positive amyloid beta protein 42 levels.* Neurobiol Aging, 2014. **35**(12): p. 2671-2680.

262.   Tsartsalis, S., et al., *Early Alzheimer-type lesions in cognitively normal subjects.* Neurobiol Aging, 2018. **62**: p. 34-44.

263.   Elobeid, A., et al., *Altered Proteins in the Aging Brain.* J Neuropathol Exp Neurol, 2016. **75**(4): p. 316-25.

264.   Moussaud, S., et al., *Alpha-synuclein and tau: teammates in neurodegeneration?* Mol Neurodegener, 2014. **9**: p. 43.

265.   Hoover, C.E., et al., *Endogenous Brain Lipids Inhibit Prion Amyloid Formation In Vitro.* J Virol, 2017. **91**(9).

266.   Hardy, J.A. and G.A. Higgins, *Alzheimer's disease: the amyloid cascade hypothesis.* Science, 1992. **256**(5054): p. 184-5.

267.   Arnold, S.E., et al., *Olfactory epithelium amyloid-beta and paired helical filament-tau pathology in Alzheimer disease.* Ann Neurol, 2010. **67**(4): p. 462-9.

268.   McEwen, D.P., P.M. Jenkins, and J.R. Martens, *Olfactory cilia: our direct neuronal connection to the external world.* Curr Top Dev Biol, 2008. **85**: p. 333-70.

269.   Uchihara, T. and B.I. Giasson, *Propagation of alpha-synuclein pathology: hypotheses, discoveries, and yet unresolved questions from experimental and human brain studies.* Acta Neuropathol, 2016. **131**(1): p. 49-73.

270.   Giasson, B.I., et al., *Biochemical and pathological characterization of Lrrk2.* Ann Neurol, 2006. **59**(2): p. 315-22.

271.   Schoch, G., et al., *Analysis of prion strains by PrPSc profiling in sporadic Creutzfeldt-Jakob disease.* PLoS Med, 2006. **3**(2): p. e14.

272.   Puoti, G., et al., *Sporadic Creutzfeldt-Jakob disease: co-occurrence of different types of PrP(Sc) in the same brain.* Neurology, 1999. **53**(9): p. 2173-6.